Quantitative and dynamic analysis of the focused-ultrasound induced blood-brain barrier opening *in vivo* for drug delivery

Gesthimani Samiotaki

Submitted in partial fulfillment of the

requirements for the degree

of Doctor of Philosophy

In the Graduate School of Arts and Sciences

COLUMBIA UNIVERSITY

2015

ABSTRACT

Quantitative analysis of the focused-ultrasound induced blood-brain barrier opening in vivo for drug delivery for the treatment of neurodegenerative diseases

Gesthimani Samiotaki

The rate limiting factor for the treatment of neurodegenerative diseases is the blood-brain barrier (BBB), which protects the brain microenvironment from the efflux of large molecules, and thus it constitutes a major obstacle in therapeutic drug delivery. All state-of-the-art strategies to circumvent the BBB are invasive or non-localized, include side-effects and limited distribution of the molecule of interest to the brain. Focused Ultrasound (FUS) in conjunction with microbubbles has been shown to open the BBB non-invasively, locally and transiently to allow large molecules diffusion in rodents and non-human primates. This thesis entails a quantitative analysis of the FUS-induced BBB opening in vivo for drug delivery in neurodegenerative diseases. First, quantitative analysis and modeling of the physiologic changes of the BBB opening, such as permeability changes, volume of opening, and reversibility timeline, were studied in wild-type mice, in brain areas related to Alzheimer's and Parkinson's disease. This study provided in vivo tools for BBB opening analysis, as well as the design of a FUS method with optimized parameters for efficient and safe drug delivery. Second, the neurotrophic factor Neurturin, which has been shown to have neuroregenerative and neuroprotective effects in dopaminergic neurons was successfully delivered in wild-type mice and MPTP-lesion parkinsonism model mice. It was shown that FUS enhanced the delivery of Neurturin to the entire regions of interest associated with the disease, downstream signaling for neuronal proliferation was also detected, and finally neuroregeneration was observed in the FUS-treated side compared to the contralateral side. In the third part of this thesis, a pre-clinical translation of the pharmacodynamic analysis was designed and analyzed in non-human primates. The permeability changes, the volume of opening separately in grey and white matter, as well as the concentration of an MR-contrast agent were measured *in vivo* for the first time. The interaction of FUS with the inhomogeneous primate brain

was investigated and the drug delivery efficiency of the FUS technique for BBB opening was measured non-invasively; rather critical findings for safe and optimal drug delivery using FUS in a pre-clinical setting.

Table of Contents

LIST OF GRAPHS, IMAGES, AND ILLUSTRATIONS

ABBREVIATIONS

AD: Alzheimer's disease

BBB: blood brain barrier

CED: Convection-enhanced delivery

CNS: central nervous system

CP: Caudate-putamen

DA: dopaminergic

DCE-MRI: Dynamic Contrast Enhanced Magnetic Resonance Imaging

EES: extravascular extracellular space

FUS: focused ultrasound

GM: grey matter

K_{trans}: permeability transfer rate from blood plasma to extravascular extracellular space

IDD: Intranasal Drug Delivery

IHC: immunohistochemistry

i.v.: intravenous

i.p.: intraperitoneal

MPTP: 1-methyl-4-phenyl-1,2,3,6-tetrahydropyridine neurotoxin precursor

MRI: Magnetic Resonance Imaging

NHP: non-human primate

NTN: Neurturin

PD: Parkinson's Disease

PNP: peak negative pressure

PL: pulse length

SN: Substantia Nigra

s.c.: subcutaneous

SWI: susceptibility weighted imaging

TH: tyrosine hydroxylase

TH-IR: tyrosine hydroxylase immunoreactive

V_{BBB}: Volume of BBB opening

VFA: variable flip angle

WM: white matter

ACKNOWLEDGEMENTS

Having spent almost 6 years at Columbia University and having dedicated all this time towards the completion of this Thesis, there are several people I would like to acknowledge for helping me go through this journey. It was tough, yet one of my life dreams which finally is true after effort and devotion. And yet, I enjoyed it much!

I would first like to thank Babak and James who inspired me with their work ethic and passion and I would like to thank them for believing in me. I would like to thank Fotis who stood by me in the first years and shared his knowledge. Several lab mates, Ronny, Gary, Kirsten, Ethan and Jason made the long days in the lab enjoyable and unique. I would like to thank Shutao for his help and knowledge. Marilena joined the lab and my friends' list later in my PhD, and I would like to thank her for her support, and so many more things.

On a personal level, I would like to thank Christos, who is the one person that shared this experience with me, stood by me through thick and thin, and gave me all the support I needed. I would also like to thank my friend Dimitris who encouraged me to apply for this PhD program while I was still studying in Greece.

Most importantly, I would like to acknowledge Dr. Sachin Jambawalikar and Dr. Serge Przedborski for their invaluable contribution and scientific input throughout my studies, without which none of this progress could have been achieved.

Finally, my advisor Elisa, not only for being an excellent advisor, but for being a role model for me, an inspiration, a woman to look up to.

INTRODUCTION:

Quantitative analysis of the focused-ultrasound induced blood-brain barrier opening in vivo for drug delivery for neurodegenerative diseases

Brain diseases, including neurodegenerative diseases, are among the most common diseases worldwide, however, there are no effective treatments, and current techniques are limited to symptomatic relief. It is rather challenging to design therapeutic treatments or agents for the brain, due to the skull, which makes surgical access difficult and impractical, as well as due to the blood-brain barrier. The blood-brain barrier (BBB), which normally helps maintain the brain homeostasis, constitutes a major obstacle in brain drug delivery and is the rate-limiting factor in the treatment of the central nervous system (CNS) [1], [2]. The BBB is a physical and metabolic barrier lining cerebral micro-vessels and hinders the flux of molecules from the blood plasma to the brain parenchyma [3],[4]. Focused Ultrasound (FUS) in conjunction with systemically administered microbubbles is currently the only non-invasive and localized method to transiently disrupt the BBB in vivo [5]–[8], while the feasibility of delivery of various pharmacologically relevant agents [9]–[23] and molecules thereafter has been shown in small animals and non-human primates. These findings suggest the strong potential of FUS as a CNS therapeutic mediator, especially since neurodegenerative diseases typically affect specific regions in the brain, especially at their early stages.

In order to achieve optimal and efficient drug delivery through the FUS-induced BBB opening, it is first necessary to develop methods to quantitatively assess and analyze the BBB opening's physiological characteristics, such as the volume of opening (V_{BBB}), the permeability (K_{trans}) and the reversibility timeline, and investigate their correlation. This correlation can provide further insight into selecting the appropriate FUS parameters for safe and controlled BBB opening according to the therapeutic needs. Second, the design and the application of such a FUS treatment for drug delivery in a disease animal-model, and the quantitative analysis of the drug's trans-BBB bioavailability, bioactivity and therapeutic effects is a critical pre-clinical step.

The objective of this dissertation is the quantitative and pharmacodynamic analysis of BBB opening in vivo in wild-type and disease-model rodents and non-human primates (NHP) for the design of efficient drug delivery using FUS in a pre-clinical setting. Even though several few groups have studied BBB opening's physiological characteristics [24]–[27] and their dependence on acoustic parameters, such as the applied peak pressure [28]–[30], a more thorough investigation and quantitative analysis of the correlation between such characteristics, i.e. V_{BBB}, K_{trans} and reversibility timeline, in distinct brain structures was designed and studied [31], [32] in vivo in rodents using Magnetic Resonance Imaging (MRI). For this analysis, their dependence on

some acoustic parameters, such as the acoustic pressure and the acoustic pulse length (PL), as well as the microbubble size was studied. Moreover, a FUS-induced BBB-opening for the efficient and safe drug delivery of Neurturin, a neurotrophic factor which has been shown to have therapeutic potential in Parkinson's disease (PD) when administered with invasive techniques [33]–[35], was designed, implemented and assessed in wild-type and a PD mouse-model (MPTP). Immunostaining results confirmed the localized delivery to brain structures affected in PD, i.e. the Caudate Putamen (CP) and the Substantia Nigra (SN), followed by downstream signaling to the neuronal nuclei. Neuro-regeneration was also investigated and quantified in the MPTP model of PD, emphasizing the potential of the technique for the reversibility of PD phenotype. Finally, thus far, T1-weighted MRI is being used for the detection of opening in NHP [26], [36], as well as for the quantification of V_{BBB} and the reversibility timeline [37] as a pre-clinical translation and evaluation of the technique. In this dissertation, MR relaxivity mapping, i.e. T_1 relaxation times and $\Delta R1$ mapping, were used as a more sensitive tool to depict BBB opening, while data-processing helped generate gadolinium concentration maps, for further drug delivery efficiency evaluation. Moreover, K_{trans} was measured in NHP for the first time, revealing the effect of FUS-induced opening in BBB's permeability, and its correlation with the acoustic pressure and the underlying brain structures inhomogeneity.

CHAPTER ONE:
Specific Aims

Section 1.1: Specific Aims

This thesis has three specific aims, as shown in the schematic in **Figure 1**. The first specific aim entails the design of an efficient and safe technique for non-invasive, localized, and transient FUS-induced BBB opening in a small animal model, i.e. mice. The second specific aim constitutes an actual drug delivery and treatment study in a small animal PD disease model using the optimized parameters identified in specific aim 1. The third specific aim entails the translation of the technique to non-human primates, performing pharmacodynamic analysis in vivo in order to achieve efficient and safe drug delivery in a pre-clinical setting.

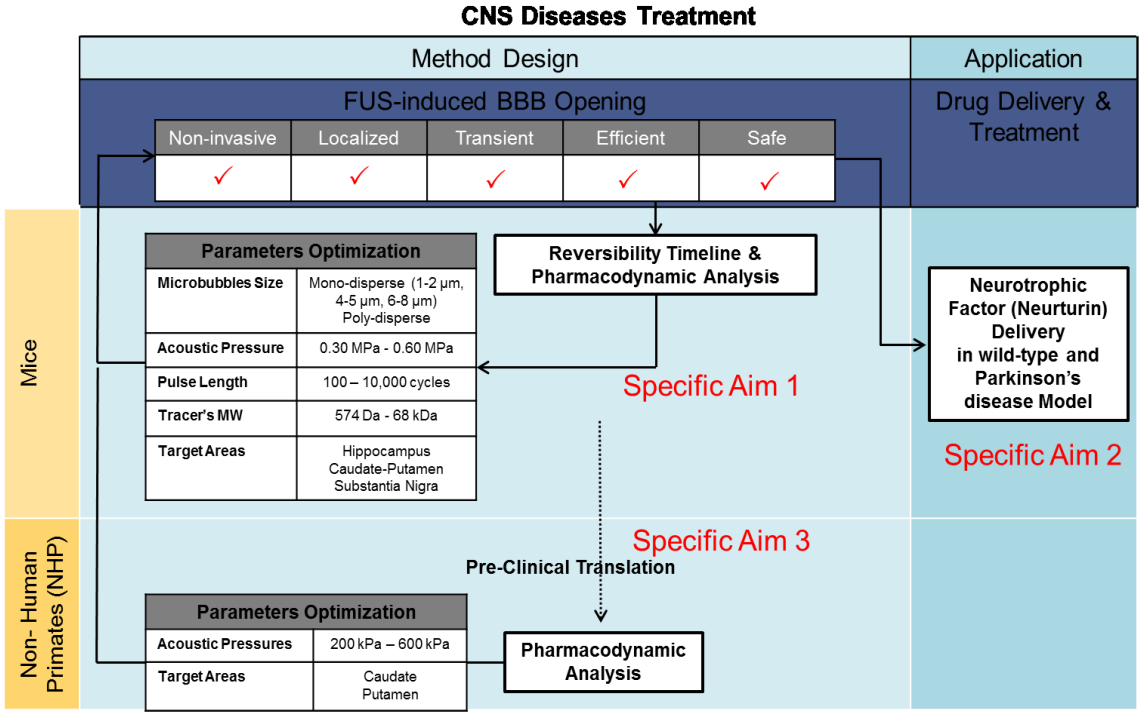

Figure 1. Specific aims

Section 1.2: MRI-based quantification and analysis of FUS-induced BBB opening's physiological characteristics in wild-type mice (Specific Aim 1, Chapter Three)

The purpose of this aim is to investigate and quantify the focused ultrasound- induced BBB opening's physical characteristics, i.e. permeability, volume of opening, reversibility timeline using Magnetic Resonance Imaging and their dependence on the:

a) Microbubble size and acoustic pressure
b) Pulse length and acoustic pressure

As part of this specific aim, the hypothesis that BBB-opening characteristics depend on the acoustic parameters and the microbubbles was tested, and it was shown that their combination could allow designing studies according to the objective at hand [9]–[11]. For example, depending on the disease and the brain region affected, the FUS treatment could be designed in such a way that it affects only that brain region. Moreover, quantitative correlation of the changes of the physiologic characteristics of the BBB after opening with the time required for closing, showed not only that under safe parameters the BBB can be reinstated, but also that the timeline could be predicted and controlled.

Section 1.3: Quantitative assessment of the delivery of the Neurturin (NTN) neurotrophic factor to specific murine brain targets and potential reversibility of Parkinson's disease phenotype (Specific Aim 2, Chapter Four)

The purpose of this aim is the design and implementation of a FUS-induced BBB opening for efficient and safe drug delivery of NTN, which is shown to have therapeutic potential, in PD animal-model disease. The study was divided and will be studied as follows:

a) Optimization of acoustic parameters and design of a FUS treatment in the CP and SN for delivery of a protein of 23.6 kDa
b) Localized delivery of NTN using FUS in wild-type mice; detection and quantification of bioavailability and bioactivity in CP and SN
c) Neuroregenetation study following NTN in the MPTP mouse-model of Parkinson's disease

For specific sub-aims (a) and (b), it was found that BBB could be safely and reversibly disrupted in the ipsilateral CP and SN allowing the penetration of a 23.6 kDa molecule. NTN was also shown to be successfully and independently delivered to both CP and SN, while downstream activation from its receptor to the neuronal nuclei was confirmed, and no effects were detected in the contralateral control (non-sonicated) side. NTN's bioavailability using FUS and IV administration was found to be significantly increased compared to the conventional invasive method of direct injection (D.I.). Also, using invasive techniques it was shown that NTN has neuroprotective and neuroregenerative effects in rodent and NHP animal-models of PD disease, such as the MPTP or 6-OHDA PD models[12]–[14].

Therefore, the hypothesis in sub-aim (c) was that in MPTP-lesioned mice, NTN would induce neuroregenerative effects following IV administration after FUS-induced BBB-opening in the ipsilateral CP and SN. Results shown that neuroregeneration was possible, significantly depended on the targeting accuracy of the CP.

Section 1.4: Pharmacodynamic analysis of FUS-induced BBB opening in non-human primates using MRI (Specific Aim 3, Chapter Five)

The objective of this specific aim was the investigation of the physiologic properties of BBB opening, including safety, in non-human primates (NHP) using MRI. Pre- and post-contrast high resolution T1-weighted imaging, relaxometry imaging, dynamic contrast enhanced (DCE-MRI) and T2-weighted and Susceptibility Weighted Imaging (SWI) were performed. Diffusion of Gadolinium (Gd-DTPA-BMA) into the brain parenchyma, which otherwise does not cross the BBB, was used as a tracer to depict the BBB-opened areas in NHP. Quantitative analysis of T1 and ΔR1 maps was performed to detect and quantify the volume of opening separately in the grey and white matter, and contrast agent (CA) concentration maps were also generated for pharmacodynamic analysis, and finally, permeability mapping.

a) Design and optimization of MRI sequence for variable flip angle (VFA) based T1 relaxivity mapping

b) Generation of ΔR1 and Gadolinium concentration (C_{Gd}) maps, and quantification of V_{BBB} and integrated C_{Gd}

c) Design and optimization of a Dynamic Contrast Enhanced (DCE) MRI sequence for permeability mapping

d) Correlation with edema and/or hemorrhage detection in T2-weighted and Susceptibility Weighted Imaging (SWI)

The hypotheses were that T_1 mapping could provide more sensitive BBB-opening detection, while pharmacodynamic analysis through gadolinium concentration (C_{Gd}) maps, permeability (K_{trans}) maps and V_{BBB} quantification, were conducted for the first time in NHP, and were shown to serve as sensitive *in vivo* tools for safe and optimal drug delivery. These methods also provided further insight to this pre-clinical application of FUS treatment. Finally, the correlation with edema or hemorrhage was investigated.

CHAPTER TWO:
Background and Motivation

Section 2.1: The Blood-Brain Barrier

The blood-brain barrier (BBB) is a specialized vascular system lining the cerebral microvessels, consisting of endothelial cells connected together by tight junctions, under the inductive influence of the the cells within the "neurovascular unit" (NVU)[15], i.e. astrocytes, neurons, microglia and pericytes [3], [4] as shown in Figure 2. BBB's main role is to control the flow of nutrients from the lumen to the parenchyma in order to maintain the proper brain homeostasis for neuron firing [2]. The BBB is a physical and metabolic barrier which constrains the passage of molecules to the brain, either through paracellular or transcellular pathways [3], unless they are both lipid-soluble and of a molecular weight (MW) less than 400 Da.

Even though the brain is extremely vascularized, allowing each neuron to be near a capillary at a distance of 8-20 μm [16], [17], the selective permeability of the BBB regulates the homeostasis within the CNS, protecting the delicate nerve tissue from insult due to the entrance of foreign material. The BBB serves to regulate nutrient delivery and ion concentration. Only small lipophilic compounds, such as O_2, CO_2 and H_2O are able to diffuse across the BBB along their concentration gradient [18].

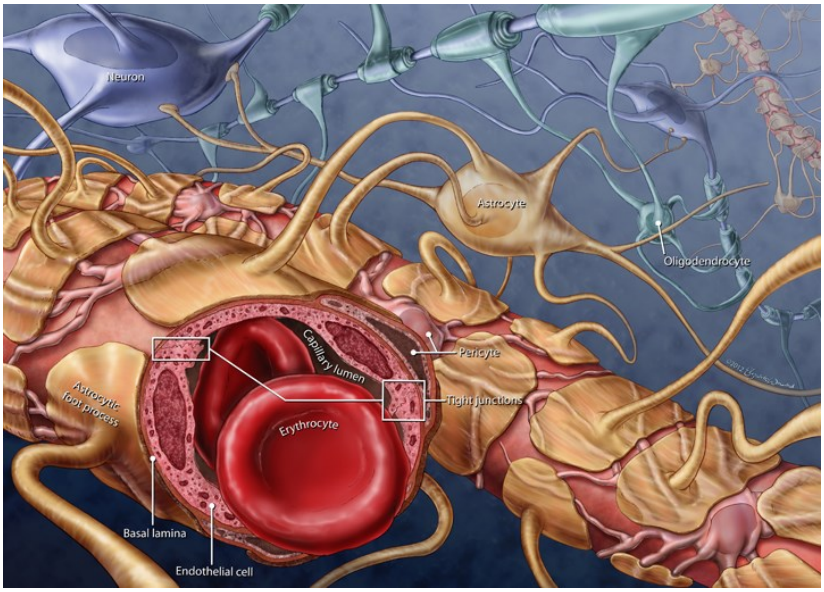

Figure 2. The Blood-Brain Barrier (Source: Lu KW et al. 2013 Biphys Soc 57th Annual Meeting)

The BBB constitutes a major obstacle in drug delivery to the CNS because the same physiological characteristics which regulate the environment within the CNS also prevent the

delivery of therapeutic compounds to the CNS. The BBB, among the rest of the biological membranes, has uniquely restrictive permeability properties and effectively excludes 98% of small-molecule drugs and 100% of all large molecule drugs and neurotherapeutic agents [1], [19], including proteins, enzymes, antibodies etc. The BBB is the rate-limiting factor for the treatment of the central nervous system (CNS) diseases since drugs, when intravenously-administered, cannot be transported across to the brain parenchyma and reach their end-targets as mandated.

To overcome the challenges associated with delivery of therapeutics to the CNS, multiple strategies have been developed aiming at increasing effective active drug delivery. All the strategies for drug delivery through the BBB utilize the transport mechanisms shown in Figure 3.

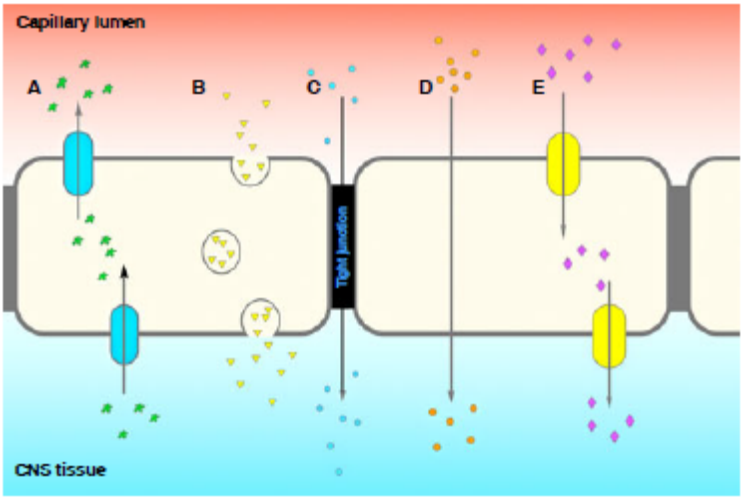

Figure 3. Multiple transport mechanisms for the passage of molecules through the BBB. (A) Efflux pumps such as P-glycoprotein (P-gp) remove unwanted material from the CNS. (B) Endocytosis mechanisms, such as GLUT1-mediated endocytosis, mediate transport of large molecules such as glucose. (C) Paracellular transport is passive diffusion of small molecules that are permeable through the tight junctions between capillary endothelial cells. (D) Transcellular passive diffusion also exists for small lipophilic molecules. (E) Receptor-mediated transport, for example insulin receptor-mediated transport, are a major mechanism of the transport of molecules across the BBB (source: **[20]**)

Section 2.2: Central Nervous System diseases

Central nervous system (CNS) diseases affect the brain and/or the spinal cord. Different CNS diseases have different signs and symptoms. CNS diseases that implicate neurons per se are called “Neurodegenerative diseases” and neurodegeneration is their common marker. Not all CNS diseases are considered neurodegenerative diseases if they are not primarily neuronal diseases, and neurons die as the results of another cause such as hypoxia, poison, metabolic defects or infections. Effectively, neurodegenerative diseases are characterized by a large and

heterogeneous spectrum of clinical and pathological expressions, affecting specific functional anatomic systems, while they arise for unknown reasons and progress in a relentless manner[21]. Currently, the most common neurodegenerative diseases include Alzheimer's disease (AD), Parkinson's disease (PD), Huntington's disease (HD) and amyotrophic lateral sclerosis (ALS).

The impact of neurodegenerative diseases focusing on AD and PD, as shown in Table 1, is very significant due to their high prevalence and mortality. More importantly, there is a increasing magnitude of the emotional, physical and financial burden on patients as well as their caregivers, and the cost to the nation. The most consistent risk factor for developing a neurodegenerative disorder is increasing age, in industrialized countries the growth rate of the population aged 65 and beyond has far exceeded that of the population as a whole. Recent statistics showed that there were 26.6 million people worldwide with AD and it is predicted to affect 1 in 85 people globally by 2050. At the same time, PD affects also younger people, with 4% of the patients under the age of 50, significantly deteriorating their quality of life and often forcing them to quit the work-force much earlier than expected.

There is no treatment for neurodegenerative diseases to date, only drugs that are limited to symptomatic relief. These drugs alleviate symptoms but their chronic use is often associated with debilitating side effects, while none of them seems to stop the progression of the degenerative processes. Given the growing effect of CNS diseases, the development of effective preventive or protective therapies is urgent.

Alzheimer's Disease	Parkinson's Disease
Prevalence and Mortality	
• 5.2 million in the U.S. in 2014 • **200,000 under the age of 65** • 500,000 senior's deaths each year	• 1 million in the US, 10,000 millions worldwide (60,000 new patients/year) • **4% is under the age of 50**
Impact on Caregivers/Patients	
• In 2013, 15.5 million family and friends provided 17.7 billion hours of unpaid care to those with Alzheimer's and other dementias – care valued at **$220.2 billion**	• Medication costs $6,000 year/patient • Therapeutic surgery **$100,000 per patient** • Institutional care/assisted-living facility/ nursing home: **$100,000 per person annually**
Cost to the nation	
• The most expensive condition • In 2014, was estimated **$214 billion**, including **$150 billion** in costs to Medicare and Medicaid. • Alzheimer's will cost an estimated $**1.2 trillion** (in today's dollars) in 2050	• **$25 billion** per year in the US combined direct and indirect cost including treatment, social security payments and lost income from inability to work

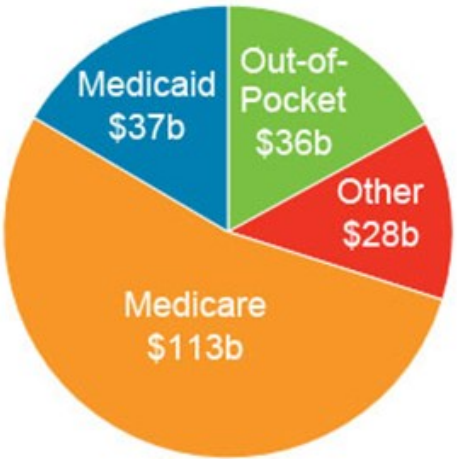

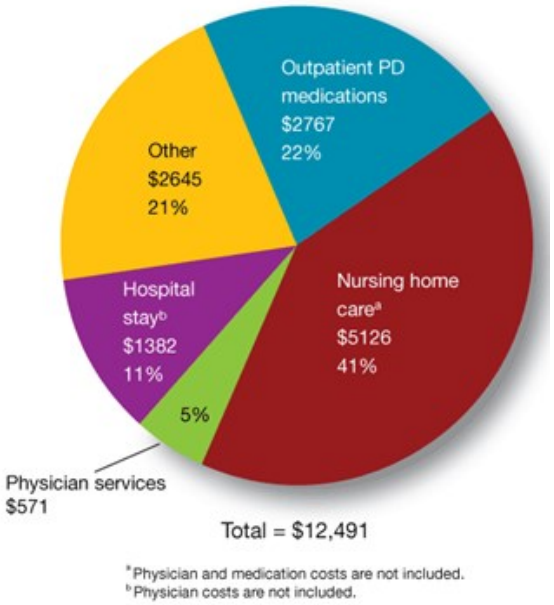

Table 1. Prelevance and costs associated with Alzheimer's and Parkinson's Disease (sources: National Institute on Aging http://www.nia.nih.gov/, Alzheimer's Association http://www.alz.org/, National Institute of Neurological Disorders and Stroke http://www.ninds.nih.gov/

Section 2.3: State of the art strategies for CNS drug delivery

Currently, drug delivery to the CNS is limited even though various strategies have been developed. The main two broad categories are invasive and non-invasive methods. Invasive methods are characterized by direct entering of the therapeutic agent to the CNS or disrupting the BBB [22]. Non-invasive approaches implement endogenous mechanism to enhance drug delivery to the CNS [23].

2.3.1. Non-invasive drug delivery techniques

Non-invasive drug delivery techniques aim at entering or bypassing the BBB utilizing endogenous transport mechanisms [23]. They are not inherently risky since they do not require surgery or hospitalization; however, a major drawback is that they are not as efficient in the treatment of chronic disorders requiring long-term intervention, such as neurodegenerative diseases [24].

Chemical approaches

Molecular weight, solubility and permeability are some characteristics of drugs that can be easily modified in order for them to cross the BBB. The most common chemical modification of CNS drugs is the “lipidization” of the drug by converting non-polar functional groups into polar groups which makes it lipophilic [25]. Drugs with increased lipophilicity should have improved permeability across the BBB, but on the other hand, site-specificity still remains a challenge and, therefore, the poor tissue selectivity results in side effects. Another common chemical modification of drugs is to modify them to target endogenous transporters in order to achieve site-specific transport [26]. Receptor-mediated transport (RMT) and carrier-mediated transport (CMT) are the main two methods used as endogenous transport for CBS delivery. They are limited to a number of molecules. For example, certain large peptides and proteins are good candidates for utilizing RMT across the BBB and the endocytic process, by binding to the insulin receptor (INSR), transferrin receptor (TFR) and insulin-like growth factor receptors (IGF1R, IGF2R). CMT on the other hand, is more suitable for the transport of small molecules (MW< 600Da), and it is normally designed to transport nutrients, vitamins and hormones into the CNS [25]. Drugs which are chemically modified to be transported through the CMT system have a pseudo-nutrient structure or they are conjugated into a nutrient substrate. Some CMT examples expressed in the BBB are the carriers for neutral amino acid (LAT1) and glucose (GLUT1) [27], [28].

Intranasal drug delivery

Intranasal drug delivery (IDD) is another method that bypasses the BBB [29], through direct transmission of the therapeutic agent into the CNS through the olfactory epithelium in the nasal cavity. Once the drug passes through the olfactory and trigeminal nerve, then gets

distributed to the brain in bulk flow via perivascular channels [30], where it may have an effect within minutes. Intranasal delivery presents a safe and effective drug delivery technique and is promising in the treatment for chronic CNS diseases, therefore, may clinical applications have been found or being researched preclinically [30]. For example, insulin administration via the nasal epithelium was shown in clinical trials to improve cognitive functioning and was able to increase insulin levels within the CNS to normal levels from the deficiency levels in Alzheimer's patients [24], [31]. The main advantages of IDD is the easy and safe administration, increasing patient compliance and monitoring in an outpatient setting [32]. The disadvantage and major limitation of this technique though is that only a number of molecules are able to diffuse through the olfactory epithelium, making this the major limitation of IDD [29].

Biological approaches

Biological approaches for non-invasive BBB disruption include nanoparticles and cell-penetrating peptides. Nanoparticles are manufactured with the use of nanotechnology, and can be so small that they are able to pass through the BBB and diffuse into the target cells inside the CNS[33]. In this type of drug modification, the drug is loaded into a nanocarrier at higher therapeutic concentration than it would previously have[34]. Manipulation of the nanocarrier's structure can be done in order to improve the selectivity and permeability of the loaded drug and targeting toward specific receptors [35], followed by trancytosis and, therefore, delivery across the BBB [33]. Drugs, oligonucleotides, contrast agents, and genes can been potentially delivered to a target site in the CNS with few to no systemic effects and minimal damage to the BBB with the use of nanocarriers [34]. Various types of nanoparticles have been tested for diagnostic and therapeutic purposes, such as polymeric, lipid-based, magnetic, and dendritic nanocarriers. There are several other types including micelles, nanogels, nanoemulsions, nanosuspensions, ceramic, and metal-based nanocarriers [36]. Nanoparticles development and delivery constitute a relative new field, and only a small number of nanoparticles are currently available for clinical use. Currently, because of their ability to cross the BBB efficiently and provide targeted drug therapy, there are a number of clinical trials proceeding to test the safety and efficacy of certain nanoparticles as drug carriers in human treatments. Concerns regarding adverse effects associated with nanoparticles include poor biodegradation causing accumulation in tissue, which may lead to chronic inflammatory reactions [36]. Some nanoparticles, especially cationic nanoparticles, have been known to cause increased blood clotting and hemolysis. Studies have shown that they can cause an increase in reactive oxygen species, resulting in increased damage to mitochondria and the nucleus. They may also have an adverse effect on neurotransmitter release in the brain, reduced cell viability and increased cell death, and up-regulation of pro-inflammatory molecules [33]. It is important to note that nanotechnology is still in

early developing state and requires much more research to prove their safety and efficacy before widespread use.

Cell-penetrating peptides are short sequences of amino acids with the ability to pass through the lipid bilayers of a cell membrane and reach the intracellular space. They are rich in positively charged amino acids and are highly lipid-soluble hydrophobic compounds. This method of delivery is ideal for substances such as drugs, large proteins, and substances vital for cellular function [38], [39]. Cell-penetrating peptides are non-toxic and highly effective without the need for cell-surface receptor attachment [39], and are therefore ideal for the delivery of various biologically active molecules [38]. However, there are limitations and adverse effects associated with the use of cell-penetrating peptides should their clinical applicability be considered. When their size is increased their capacity for successful entry into the cell through the plasma membrane is decreased. Moreover, the size of the entity, surface hydrophobicity, surface charge, morphology of the surface, and the sequence of the amino acids in the peptide and nucleic acid complex can affect the immunogenicity of the molecule and cause an immune response [40]. Also, they are non-localized and the lack of specificity renders all different types of cells to be targeted by them, which can lower the dose to the target site and causes toxic effects at other sites. Finally, the in vivo applications of cell-penetrating peptides can also be limited by enzymes that easily break down these peptide molecules [41].

2.3.2. Invasive drug delivery techniques

Invasive strategies involve the direct administration of the therapeutic agent into the target site within the CNS, and are usually aggressive in order to maximize the amount that reaches the site with minimal exposure to the surrounding healthy tissue. Invasive strategies are usually localized, and exclude drugs from entering systemic circulation, therefore reducing and eliminating peripheral adverse effects [20].

Transcranial direct injection

Transcranial direct injections are the golden standard for invasive drug delivery techniques to the BBB, and are either intracerebral or intracerebroventricular. The advantage of this technique is the infusion of the drug directly and only to the target site, so it is localized. However, the results are highly dependent on the diffusion of the molecule of interest, and the treatment area may remain rather small limited to few millimeters around the injection site [20].

Convection-enhanced Drug Delivery

Convection-enhanced delivery (CED) is an invasive drug delivery technique in which BBB is bypassed via direct intracerebral injection of the drug with the use of positive hydrostatic pressure during direct infusion [42] which causes the drug to penetrate farther into the target

tissue. It has been shown that the amount of drugs delivered to the target site matches the amount which was infused, and therefore CED achieves increased delivery efficiency. Additionally, CED causes minimal structural damage to the brain, except for the catheter insertion track. Even though CED has been shown as a feasible method for intracerebral drug delivery and it has been used in both preclinical and clinical studies, it is still a surgical procedure with all the associated risks involved, while, when large areas need to be treated multiple insertion points might be needed which is increases the complication risks. Finally, the damage along the catheter track would be more extensive when trying to reach more ventral or medial structures in the brain, adding to the challenges of this method.

Optical modulation of vascular permeability

Increased BBB permeability can be also achieved with the minimally invasive technique of optical modulation, i.e. laser irradiation. In this technique, a femtosecond near-infrared pulsed laser is used for deep-tissue penetration with minimal scattering and localized nonlinear absorption [43]. The technique has been successfully used for cell permeabilization and enables minimally invasive optical modulation of cells in along the targeted blood vessels which fully recover with no damage to the integrity of the BBB. As the drug is present in the systemic circulation, the leaky BBB allows the unmodified molecules to pass through it and enter the CNS.

The main limitation of this technique is the low tissue penetration of the laser, which is approximately 1 mm as of now [44]. Moreover, a problematic side effect is the fact that near-infrared laser can evoke the generation of reactive oxygen species leading to membrane dysfunction, DNA fragmentation and apoptosis [45].

2.3.3. Motivation and current short-comings for drug delivery to the CNS

As indicated in section 2.3, none of the techniques currently used for drug delivery to the CNS is simultaneously non-invasive and localized as shown in the chart below in Figure 4. It should be noted here though, that the fact that a technique might not be non-invasive or localized is not the only limitation, nor the most critical. For example, in the localized techniques, the common limitation is that, even though the drug can be administrated in a large enough dose in order to be efficient, it becomes hard to reach the entire region of interest due to the brain's tortuosity and the diffusion coefficient of the molecule in the brain parenchyma. On the other hand, in the non-localized techniques, where the drug can reach by definition the entire region and in most cases the entire brain, the amount of the drug delivered might be inefficient and the risk of adverse systemic effects is a major obstacle.

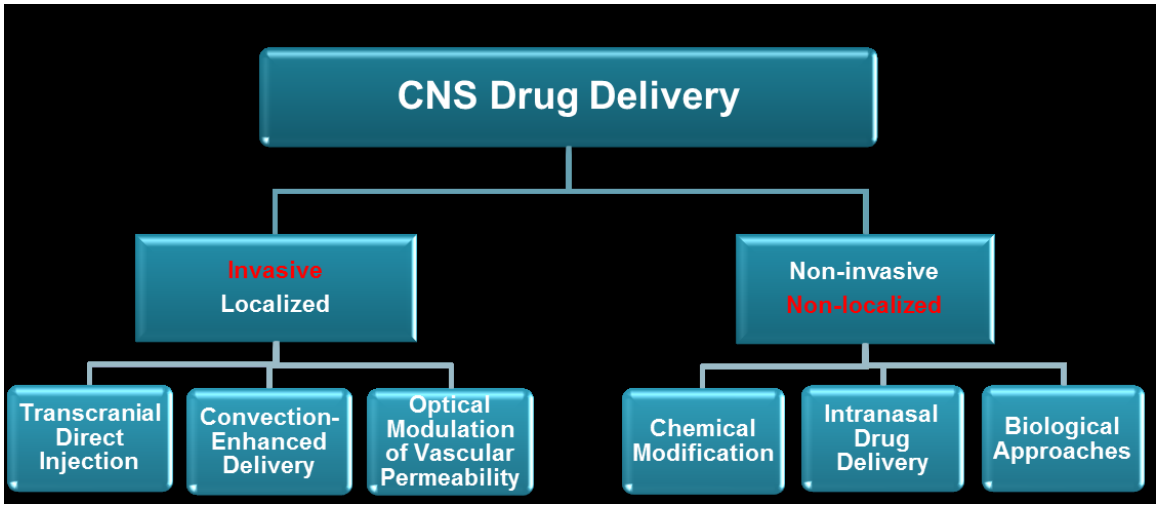

Figure 4. Current CNS drug delivery techniques

At the same time there are several drugs that have significant therapeutic potential for neurodegenerative diseases, which are currently shelved due to the fact that there is no efficient modality at the moment to validate their efficiency.

Section 2.4: Focused Ultrasound

2.4.1. Focused Ultrasound (FUS) in conjunction with microbubbles for BBB opening

The use of focused ultrasound (FUS) in conjunction with microbubbles has been demonstrated by several groups to successfully induce BBB opening noninvasively, locally and reversibly [5], [6], [8], [46], by increasing the BBB permeability and therefore aiding in drug delivery to the brain. With this technique, systemically administered microbubbles act as cavitation nuclei when they are in the focal zone of the FUS beam, which propagates through intact skin and skull. The focal zone is the area of highest energy and is contained within a small region at a targeted distance from the transducer surface, and it varies with the transducer's characteristics and geometry as shown in **Figure 5.** The acoustic transducer is a piezoelectric element and when electric energy is applied to drive it, an acoustic pressure wave is generated, which longitudinally propagates through the scalp, skull and tissue. The focal spot overlaps with a localized brain area, and the focal size increases when the center frequency of the acoustic transducer decreases, while the attenuation decreases. For this reason, different center frequencies are used for different application. In this thesis for example, the transducer used for the small animals is driven at 1.5 MHz, while the transducer used for the non-human primates is driven at 500 kHz.

Passive cavitation detection of the acoustic emissions of the FUS-driven microbubbles has also shown that acoustic cavitation, non-inertial at lower pressures or inertial at higher pressures, plays a key role in BBB opening [47]–[49]. During cavitation the bubbles may exert forces to the surrounding capillary walls, while microsteaming and shock waves due to fragmentation may occur [50], [51].

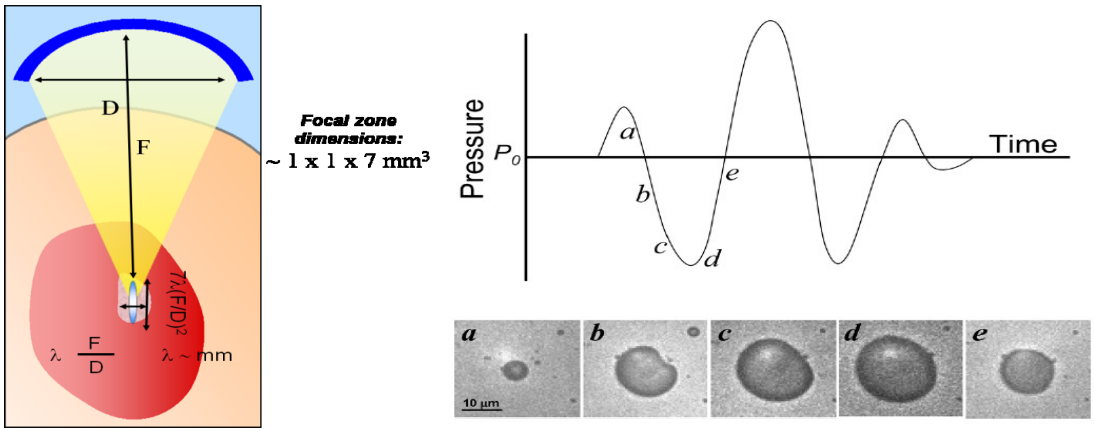

Figure 5. Left: Schematic of a FUS transducer (blue), and the acoustic beam which is focused in an area at distance F from the transducer surface. The length of the focal zone is $7\lambda(F/D)^2$ and the focal width is $\lambda F/D$, where D is the transducer's diameter and λ the wavelength the center frequency. Right: Volumetric oscillations of microbubbles during ultrasound; bubble compression and expansion occur during high- and low- acoustic pressure phases respectively. **[52]**

2.4.2. Detection and quantitative assessment of BBB opening in vivo

One challenging aspect of FUS-induced BBB opening is the detection and monitoring of its properties, its safety, and also its recovery. Thus far, Magnetic Resonance Imaging (MRI) is the only imaging modality that can detect and characterize the BBB opening *in vivo*, providing good spatial and temporal resolution. T1-weighted (T1-w) imaging after injection of MRI contrast agents, which do not normally cross the BBB and are used as tracers, can be used to quantify several properties. T2-weighted and T2*-weighted or Susceptibility-Weighted Imaging (SWI) can also be used for the detection of edema and/or hemorrhage respectively. MRI has been used by several groups [6], [53]–[58], in rodents, rabbits and non-human primates, for the aforementioned purposes and results have shown its strong potential for the quantification of several BBB opening physical characteristics, which will be further exploited in this research dissertation. Other modalities, such as SPECT/CT [59] and microscopy [60] have also been used for the study of BBB opening, however, they lack in spatial resolution or imaging penetration depth, and while

these techniques may have increased sensitivity in signal detection, they provide less anatomical and functional information than MRI.

Several particles within a wide size range, e.g. small agents such as Omniscan® (MW: 574 Da) [53] to viruses [19] and neural stem cells [20] (MW in the order of 1 MDa and higher) have been shown to pass the FUS-disrupted BBB, into various deep brain structures selectively. BBB opening's reversibility was also shown but the timeline varied among different studies with the variation of the parameters used, between 3 h to 48 h [63]–[68].

2.4.3. Cellular Mechanisms of FUS-induced BBB opening

The mechanism is not yet known. However, it has been shown that after FUS-induced BBB opening molecules of various sizes can reach the brain parenchyma via transcytosis, fenestrations and channel formation, tight junction opening as well as passage through injured endothelium [66], [69], [70]. The effect is due to the interaction of the cavitating bubbles with the walls of the cerebral capillaries, but the precise mechanism is still unclear.

Trans-cellular passage of tracer molecules has been detected with the use of electron microscopy[66], [69], [70] . It was shown that there were cytoplasmic channels and an increased number of vesicles in the endothelial cells of the BBB following FUS, suggesting endocytosis. In another study, it was also shown with the use of high resolution microscopy and ultra-high frame-rate recordings that the microbubble oscillations in the ultrasound field causes deformation of the endothelial cells. Fluorescent dye uptake was found to occur in only deformed cells, thus suggesting that the oscillation of the microbubbles lead to pore formation in the cell membrane and thereafter, drug uptake [71]. Moreover, active uptake of drugs has also been demonstrated through electron microscopy identifying the existence of gold particles and labeled IgG within the endothelia cells caveolae[69].

Para-cellular transport of drugs has also been shown, and has been hypothesized to be due occur via stretching the tight junctions and spatial or temporal rearrangement of the tight junction proteins, and in some case by injury to the endothelial lining [72]. Again, using electron microscopy, the widening of tight junctions has been shown, while the transmembrane proteins, i.e. occluding, claudin 1 and claudin 5, were shown to be down regulated post-FUS [66], [67]. Moreover, the gap junction proteins connexin 36 and 43 were shown to be reorganized post-FUS [74]. They normally interact with the tight junction protein zonula occludens, therefore, their redistribution might be one cause for increased permeability through tight junction stretching. Especially marcromolecules are thought to enter the brain parenchyma post sonication via the para-cellular route rathen than the trans-cellular.

2.4.4. Drug Delivery through FUS-induced BBB opening

FUS in conjunction with systemically administered microbubbles has been shown to allow the penetration of several molecules to the brain including anti-cancer therapeutic drugs (Doxorobucin [74]–[77], Cytarabine [78], Trastuzumab[79]), therapeutic antibodies (Herceptin[80], Anti-αβ antibodies [81], endogenous antibodies[82]), nanoparticles[83], [84], neurotrophic factors (BDNF[85], GDNF[86]), Adeno-Associated Virus (AAV[62], AAV serotype) and neural stem cells [61]. These findings suggest the strong potential of FUS as a CNS therapeutic means, since CNS diseases affect profoundly different regions in the brain, which will be further exploited in this dissertation.

2.4.5. Advantages of FUS-induced BBB opening

Overall FUS has many advantages to address the limitation of the current CNS drug delivery techniques:

- **Non-invasive**

Ultrasound propagates through intact skin and skull, and no surgical procedure is required. The only requirement is the intravenous injection of microbubbles, which have a half-life circulation of few minutes and can be administered multiple times should it be necessary.

- **Targeted and localized**

FUS can be applied to a specific brain area as small as the size of the focal spot, and it can also independently be aimed at different structures in the brain, to induce opening in multiple sonication locations.

- **Transient**

It has been shown that the BBB opening is reversible and fully closed as early as 4 h post FUS [10], if a safe regimen of acoustic parameters is used. It has also been shown that it can remain open up to several days and normally recover eventually.

- **Efficient**

It has been shown is a few cases that drug delivery through the FUS-induced BBB opening can be efficient for therapeutic applications. In brain tumor models, drug delivery increased the median survival time significantly in rats, or decreased the tumor growth along with improving animal survival [64], [80], [87]. Most recently, it was shown that FUS alone reduced the phenotype of AD pathology through reduction in amyloid plaque size and number, with the hypothesis that it enhances the reuptake of endogenous antibodies[88].

- **Safe**

As mentioned previously, there is a safe regimen of acoustic parameters, which have been shown to cause no histological damage or hemorrhage. However, some minor extravasations following BBB disruptions can be cleared by glial cells with no effect on the neuronal population [89]. Behavioral, cognitive and motor tests have shown that FUS has also no adverse effects is small and large animals.

CHAPTER THREE:
MRI-based quantification and analysis of FUS-induced BBB opening's physiological characteristics in wild-type mice

As described earlier, the first aim of this thesis is the design of a method for efficient and safe BBB opening in mice, since it has already been shown that it is non-invasive, localized and transient as shown in

Figure **6**.

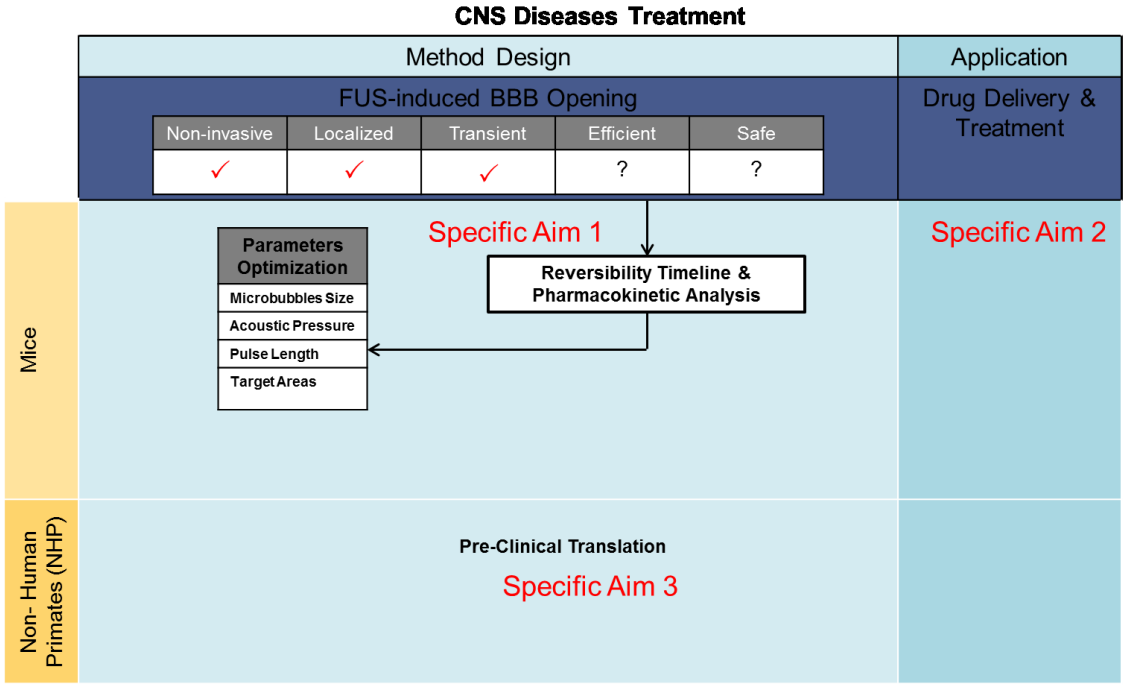

Figure 6. The rationale of the Specific Aim 1

In order to achieve this first milestone, a reversibility timeline and a pharmacokinetic analysis needed to be performed, in parallel with a parameters optimization which would allow for such a method design. These analyses were separated into two sets of studies as described below.

Section 3.1: Opening volume and reversibility timeline using different microbubble-sizes and acoustic pressures

3.1.1. Abstract

Focused Ultrasound (FUS) in conjunction with the systemic administration of microbubbles has been shown to open the blood-brain barrier (BBB) selectively, non-invasively and reversibly. In this study, we investigate the dependence of the BBB opening's reversibility on the peak-rarefactional pressure (PRP) (0.30 MPa - 0.60 MPa) as well as the microbubble size (diameters of 1-2, 4-5 or 6-8 microns) in mice using contrast-enhanced T1-weighted (CE-T1) MR images (9.4 T). Volumetric measurements of the diffusion of Gd-DTPA-BMA into the brain parenchyma were used for the quantification of the BBB-opened region on the day of sonication and up to five days thereafter. The volume of opening was found to increase with both pressure and microbubble diameter. The duration required for closing was found to be proportional to the volume of opening on the day of opening, and ranged from 24 hours, for the smaller microbubbles, to 5 days for high PRPs. Overall, larger bubbles did not show significant differences. Also, the extent of BBB opening decreased radially towards the focal region until BBB's integrity was restored. In the cases where histological damage was detected, it was found to be highly correlated with hyperintensity in the pre-contrast T1 images.

3.1.2. Introduction and study design

The use of focused ultrasound (FUS) in conjunction with microbubbles has been demonstrated by several groups [5], [6], [8], [46] to successfully induce BBB opening non-invasively, locally and reversibly. The FUS–induced BBB opening has been shown by our group to allow molecules of various molecular weights into the murine brain, such as Gd-DTPA-BMA (MW 574 Da)[5], and fluorescent dextrans (MW 3kDa and 70kDa) [90]. Several particles within a wide size range have also been shown to pass through the disrupted BBB, e.g.,MRI contrast agents such as Magnevist ® (MW: 938 Da) and MION (MW: 10,000 Da) [91], Trypan blue (MW: 961), horseradish peroxidase (MW: 40,000 Da) [63] and antibodies (MW: 150,000 Da) [64]. In this study, the MRI contrast agent was used as a tracer to depict the area of opening quantitatively.

Reversibility of the BBB opening in several animal models has previously been shown, but the timeline varied among different studies, together with the variation of parameters used. Using Optison (mean diameter of 2-4.5 μm) and a 260-kHz transducer at 0.40 MPa, or a 0.69 MHz transducer at pressure amplitudes of 0.8 MPa and 1 MPa [63], contrast-enhanced fast spin-echo T1-weighted images using intravenously administered Magnevist ® revealed that the BBB was closed 5h after sonication in rabbits [91]. Using Sonovue (mean diameter of 2.5 μm) at

1.1 MHz, T1-weighted fast spin-echo images (1.5 T) showed that the BBB signal enhancement in the opened region, following Magnevist® injection, returned in its initial state 8 h after sonication in rabbits [65], whereas using a 1.63 MHz transducer and varying the acoustic pressures from 1 MPa up to 4.7 MPa, the BBB closed within 24-48 h [6]. In rats, with the use of Optison, at 1.5 MHz and 1.1 MPa, immunoelectron microscopy showed that the BBB was shown permeable to Horseradish Peroxidase Passage (HRP) and Lanthanum Passage up to 6 hrs after sonication, and remained impermeable 24h later, while immunoelectron microscopy showed that tight junctions appeared disintegrated only up to 4h after FUS and were later restored [66]. Using Definity (mean diameter 1.1-3.3 μm) and an unfocused single-element transducer at 2.15 MHz, T1 spin-echo images (7 T), the BBB was shown to recover within 4-27 h [92]. In Alzheimer's disease-model mice, using Sonovue at 1.525 MHz, and PRP of 0.50 MPa, the enhancement due to Gd-DTPA-BMA (Omniscan) in CE-T1 images (9.4 T) revealed that the BBB opening was a transient phenomenon, closing within 24 h [68]. In large animals, i.e., pigs, using lipid or albumin coated microbubbles at 2 MHz transducer and 2.0 W/cm^2, Evans blue color spectromorphometry as well as contrast-enhanced T1-weighted spin-echo echo planar images (1.5 T) revealed differences between the treated and untreated sides of the brain indicating altered BBB permeability, lasting up to 3h after sonication [93].

Even though the mechanism of FUS-induced BBB opening is not yet known, overall it has been shown to be affected by acoustic parameters of the ultrasound beam, such as the applied peak rarefactional pressure [5],[6], [46], [47], [94], [95] which we further investigated in this study by longitudinally monitoring the BBB self-repairing characteristics. The interaction of intravenous administered microbubbles with the ultrasound beam generates a range of biological effects [96]. At low acoustic pressures, stable cavitation of the gas-filled microbubbles, microstreaming and acoustic radiation force may lead to shear stress exerted by the microbubbles onto the vessel endothelial cells and these effects can activate the mechanosensitive ion channels [97] or deforms the vascular endothelium [98] yielding BBB opening. At higher acoustic pressure levels, or when oscillating near a boundary, microbubbles can collapse and produce shock waves and high-velocity jets [51], [99], [100], a phenomenon referred to as inertial cavitation. The BBB has been shown to open in the presence of inertial cavitation, but without it being a necessary condition [95], [101].

Most studies so far have been utilizing poly-dispersed ultrasound contrast agents (UCAs) (i.e. Definity, Sonovue and Optison). The duration of the microbbubles interaction with the vessel wall has been found to increase with the microbubble diameter [102]. It has been well established that the microbubble diameter dictates its resonance frequency [103], [104], expansion ratio [102], lifetime of stable cavitation [102], [105], pressure threshold for inertial

cavitation [102], [105], and damage to the brain parenchyma [105]. Choi et al. [94]used mono-dispersed microbubbles of 1-2μm and 4-5μm in diameter with a sorting method developed by Feshitan et al. [106] and 3-kDa fluorescent dextran. They showed that the FUS-induced BBB opening was dependent on both the size distribution and injected microbubble volume, together with different pressure dependence for the opening threshold at each diameter size. Vlachos et al. 2011[107] also showed that the exchange rate between the blood plasma and the brain tissue is proportional to the microbubble size and PRP, and that it increases and then reaches a plateau, for larger mono-dispersed microbubbles (4-5 μm and 6-8 μm) and higher PRPs, but is significantly lower for smaller bubbles (1-2 μm).

In this study, we investigated the dependence of both the spatial extent and the duration of FUS-induced BBB opening in vivo with different microbubble sizes and PRPs. Gd-DTPA-BMA retention in the brain parenchyma was used as a signature of the area of BBB opening. Volumetric quantification of the region of BBB opening was assessed by measuring the diffusion volume of Gd-DTPA-BMA in the sonicated region of the brain, i.e., the right hippocampus, detected by the longitudinal signal enhancement. Starting with the day of sonication and continuing up to five days following sonication, pre- and post- contrast enhancement T1-weighted high resolution MR images were consecutively acquired at each time-point. The objective of this study was to provide a more thorough insight into, as well as a control over, the self-repairing characteristic of the BBB after FUS opening and its closing timeline, when different PRPs and microbubble sizes are used. It could also contribute to the optimization of the parameters used, and to a more efficient drug delivery, i.e., repeated drug administration over an extended time period.

The specific aim of this study was to investigate the dependence of both the spatial extent and the duration of FUS-induced BBB opening in vivo on different acoustic pressures and monodisperse microbubble sizes as shown in **Table 2**. Starting on the day of sonication and continuing up to 5 days following sonication, pre- and post-contrast high resolution T1-weighted images were acquired as shown in Table 3.

FUS and Microbubbles	
FUS Parameter	Value
Frequency	1.5 MHz
Focus Size	7.5 mm length 1 mm width
Pressures (peak rarefractional)	**0.30 MPa** **0.45 MPa** **0.60 MPa**
Monodispersed Microbubbles Diameters [1]	**1-2 µm** **4-5 µm** **6-8 µm**

Table 2 Study Design

MRI	
Parameter	Value
System	9.4 T
Contrast Agent	Omniscan (MW:574 D)
Volume	6 mmol/kg IP
Imaging	T1-weighted FLASH 2D
Resolution	86 x 86 μm^2
Slice Thickness	500 µm
Slices	23

Table 3 MRI parameters

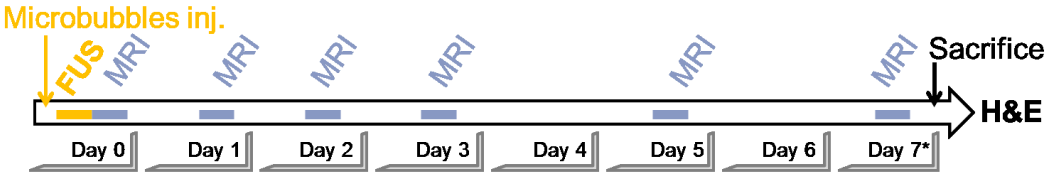

Figure 7. Experimental Timeline

3.1.3. Materials and methods

Ultrasound Setup

The acoustic waves used were generated by a single-element, spherical-segment FUS transducer (center frequency: 1.525 MHz, focal depth: 90mm, radius: 30mm; Imasonic, France), which was driven by a function generator (Agilent, Palo Alto, CA, USA) through a 50-dB power amplifier (E&I, Rochester, NY, USA) (Fig.1(a)). A central-void (radius: 11.2mm) of the therapeutic transducer held a pulse-echo ultrasound transducer (center frequency: 7.5MHz, focal length: 60mm), which was used for imaging, with their two foci aligned. The imaging transducer was driven by a pulser-receiver (Olympus, Waltham, MA, USA) connected to a digitizer (Gage Applied Technologies, Inc., Lachine, QC, Canada). A cone filled with degassed and distilled water was mounted onto the transducer system and was fitted with a polyurethane membrane (Trojan; Church & Dwight Co., Inc., Princeton, NJ, USA). The transducers were attached to a computer-controlled 3D positioning system (Velmex Inc., Lachine, QC, Canada). The targeting procedure has been described elsewhere [5]. Briefly, the FUS transducer was moved 3 mm laterally of the sagittal suture and 2 mm anterior of the lambdoid suture [5]. A needle hydrophone (Precision Acoustics Ltd., Dorchester, Dorset, UK, needle diameter: 0.2 mm) was used to measure the three-dimensional pressure field in a degassed water-tank prior to the in vivo application. The FUS focal spot overlapped with the right hippocampus and the latter portion of the thalamus, since the axial and lateral full-width at half-maximum intensities of the beam were 7.5 mm and 1 mm respectively. The left hippocampus fissure was used as a control, and was not sonicated. Pulsed FUS was emitted for 60 s, with a burst rate of 10 Hz, 100 burst cycles, at acoustic pressures adjusted to correspond to 0.30 MPa, 0.45 MPa and 0.60 MPa (peak-rarefractional), after accounting for 18% murine skull attenuation. These pressures were obtained experimentally in degassed water [5]. The mice were anesthetized using 1.25-2.50% isoflurane (SurgiVet, Smiths Medical PM, Inc., Winsconsin, USA) mixed with oxygen during FUS.

Size Isolated Microbubbles

The microbubbles used for this study were manufactured in-house, and they were size-isolated from a polydispersed microbubble distribution using differential centrifugation (34). The bubbles had a 1,2-disearoyl-sn-glycero-3-phosphocholine (DSPC) and polyoxyethylene-40 stearate (PEG40S) lipid shell and perfluorobutane (PFB) core. After the centrifugation and resuspension processes were repeated several times, three desired ranges of 1-2 μm, 4-5 μm

and 6-8 μm in diameter were isolated. A bolus of 1μl/g at a concentration of 107/ml was injected intravenously through the tail vein immediately preceding the sonication.

Magnetic Resonance Imaging

BBB opening in the murine hippocampus was confirmed using a 9.4T system (Bruker Medical; Boston, MA, USA). All mice were anesthetized orally using 1-2% of isoflurane mixed with oxygen and were placed inside the vertical-bore, having a fixed position in a plastic tube with a 3.0 cm diameter birdcage coil. Vital signals were monitored and respiration rate was approximately 55 breaths/min. Each MRI session included a pre- and a post-contrast enhancement, T1-weighted 2D FLASH acquisition (TR/TE: 230/3.3ms, flip angle: 70^{o}, NEX: 18, resolution 86μm x 86μm, slice thickness: 500μm, 23 slices, F.O.V.: 22 mm x 16.5 mm, matrix size 256 x 192, receiver bandwidth: 50 kHz), obtained respectively 15 min after sonication and 55 min after injection of the MRI contrast agent (Gd-DTPA-BMA). Based on prior experience, signal enhancement in the area of the sonicated hippocampus reaches a peak approximately 1 hour after IP injection. Therefore, the CE-T1 images were acquired 55 min following the injection. OmniscanTM (Gd-DTPA-BMA) was used to enhance the MR contrast in the murine brain, and as a tracer for the BBB opening since it diffuses into the brain parenchyma following BBB's altered permeability in the targeted area. Gd-DTPA-BMA was admninistered intraperitoneally (IP) at a dose of 6 mmol/kg. As previously reported, an IP bolus provides more temporally consistent and sustained MR enhancement as an IV bolus and is logistically simpler [92]. Preliminary work on the IP bolus dosage indicated that the 6 mmol/ kg low enough so as to avoid the signal decrease which is observed when, due to excessive Gd-DTPA-BMA, the T2 relaxivity dominates the T1 relaxivity. The same MRI session was repeated daily starting from the day of the BBB opening (day 0) and lasting up to five days. In the five cases where significant signal enhancement was detected on Day 5, MRI sessions were repeated on Day 7.

Animal preparation

All procedures used in this study involving animals were approved by the Columbia University Institutional Animal Care and Use Committee. A total of forty-two (n=42) wild-type mice, (strain C57BL/6, mass: 20-25g, sex: male, Harlan, Indianapolis, IN, USA) was used for the purposes of this study, separated into ten groups. Each mouse in the first nine groups was sonicated with a different set of PRP, i.e., 0.30 MPa, 0.45 MPa or 0.60 MPa, and a microbubble diameter, i.e., 1-2 μm, 4-5 μm or 6-8 μm. These mice underwent MRI for several days after FUS. The sham group had three (n=3) mice, for which the whole procedure was repeated without FUS, i.e., anesthesia, injection of microbubbles, and MRI sessions for up to 5 days.

Histology and Imaging

On day 7 after FUS-induced BBB opening, all mice were euthanized and transcardially perfused with 30mL PBS and 60mL 4% paraformaldehyde. Brains were soaked in paraformaldehyde for 24h. Skulls were removed, and the brains were fixed again in 4% paraformaldehyde for 6 days, followed by conventional post-fixation procedures. The paraffin-embedded specimens were sectioned horizontally at a thickness of 6 μm. 24 sections were stained and examined for each brain. Sections were stained with hematoxylin and eosin and then examined for red blood cell extravasations into the brain parenchyma as well as cell loss.

Image Processing and Volumetric measurements

The enhancement in CE-T1 MR images was quantified in elliptic cylindrical VOIs encompassing the hippocampal formation, at two contralateral regions, in the right (sonicated) and the left (control) hemisphere, on each brain for each day. The major diameter of the elliptic cylinders was 4.3 mm, the minor diameter 3.4 mm, and the height 4.5 mm, covering an area of approximately 14,000 voxels from a total of 9 consecutive horizontal slices, on each side. Therefore, the total volume on each cylinder was approximately 52 mm3. In order to quantify the BBB opening volume at the sonicated side, an intensity threshold was determined and the contrast-enhancened pixels in the vessels and ventricles were excluded. To address these issues, the signal intensity was averaged over a small circular region of 1mm in diameter, centered around the non-sonicated contralateral side close to the hippocampus and used as a reference. The number of voxels in the right (sonicated) and left (control) VOI at an intensity of 2.5 standard deviations (S.D.) or above the reference were counted. The total number of these voxels in the left VOI was then subtracted from the respective total number of voxels in the right VOI, to exclude volume contrast-enhancement in the vessels and ventricles (

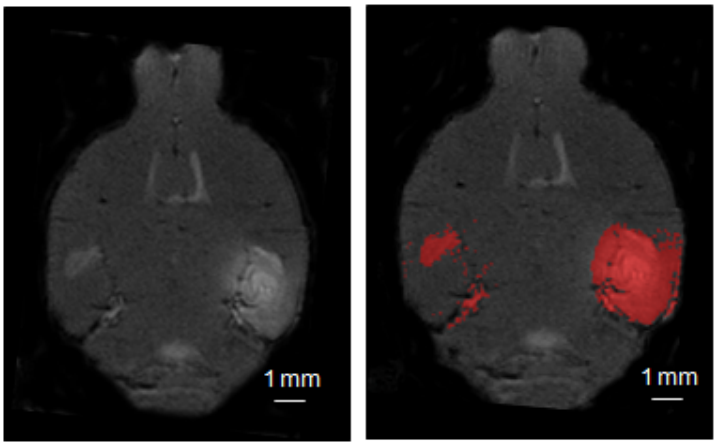

Figure 8). Pre-contrast images were used for the detection of any hyperintense areas before Gd-DTPA-BMA injection, and were not co-registered with the post-contrast.

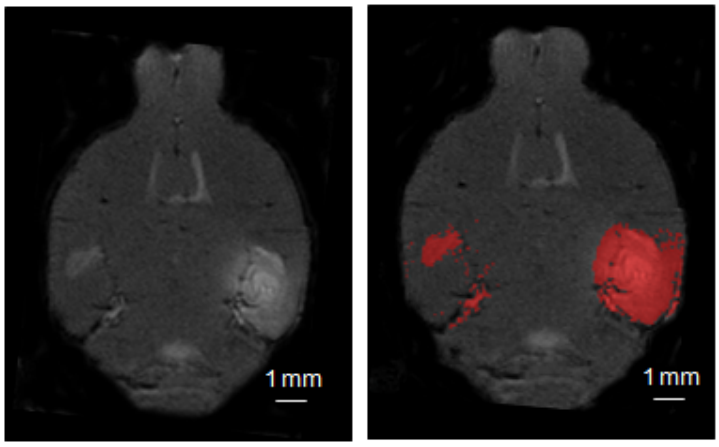

Figure 8. Horizontal CE-T1 image, where Gd-DTPA-BMA has diffused and signal enhancement is shown on the right hippocampus. (c) Thresholded voxels at the left and right VOIs of the original image in Fig.1 (b) are overlaid in red. On the left hemisphere (control side) only the voxels of the ventricles and the vasculature are above the threshold. On the right (sonicated) side voxels of the BBB opened area are also above the threshold. By subtracting the voxels of the left from the right, the effect of the vasculature and ventricles is reduced.

Statistical analysis

The measurements in the sham group were used as the baseline, denoting that the integrity of the BBB was fully restored. Following the calculation of the mean and standard deviation (S.D.) of the volumetric measurements for each group, i.e., mice sonicated at the same PRP and microbubble size, a two-tailed Student's t-test was performed, and if no statistically significant difference compared to the control baseline was observed ($p>0.05$), then the BBB was considered to have closed. In other words, the closing criterion was tested if met on each day by each group and not by each measurement individually. All groups met the closing criterion by day 5. For the five individual cases where signal enhancement was significant on day 5, MRI was repeated on day 7. These cases however, did not belong all in the same group, and the groups they belonged to could still meet the closing criterion based on the statistical analysis.

In order to investigate the differences in the timeline for closing between microbubble sizes and pressures, a statistical analysis was performed on the volume of diffusion of Gd-DTPA-BMA on Day 0. To evaluate the effect of the microbubble size, a two-tailed Student's t-test was performed for each PRP, i.e., between 1-2 μm and 4-5 μm, between 1-2 μm and 6-8 μm, as well as between 4-5 μm and 6-8 μm. The purpose was to examine any statistically significant differences between the different groups regarding the volume of BBB opening and the time required for the opened BBB to be reinstated.

3.1.4. Results

An example of the volume quantification is shown in **Figure 9**. The VOIs were manually traced to overlap with the right and left hippocampi. On both sides, voxels with an intensity 2.5 S.D. or above the reference intensity are overlaid in red. As shown in these images, when there is no diffusion of Gd-DPTA-BMA from the vasculature to the brain parenchyma, e.g., on the control side, only the vessels and the ventricles have CE-T1 intensity above the threshold. However, when the permeability of the BBB is altered on the right hippocampus as a result of the FUS, Gd-DTPA-BMA diffuses in that region and the area of opening is overlaid in red. The example in Fig. 2 shows the same brain in multiple 2D slices where 6-8-μm bubbles at a PRP of 0.30 MPa were used. The volume of opening was reduced radially towards the focal region over several subsequent days, until no trans-BBB diffusion was detected on day 3, signifying that the BBB was successfully reinstated.

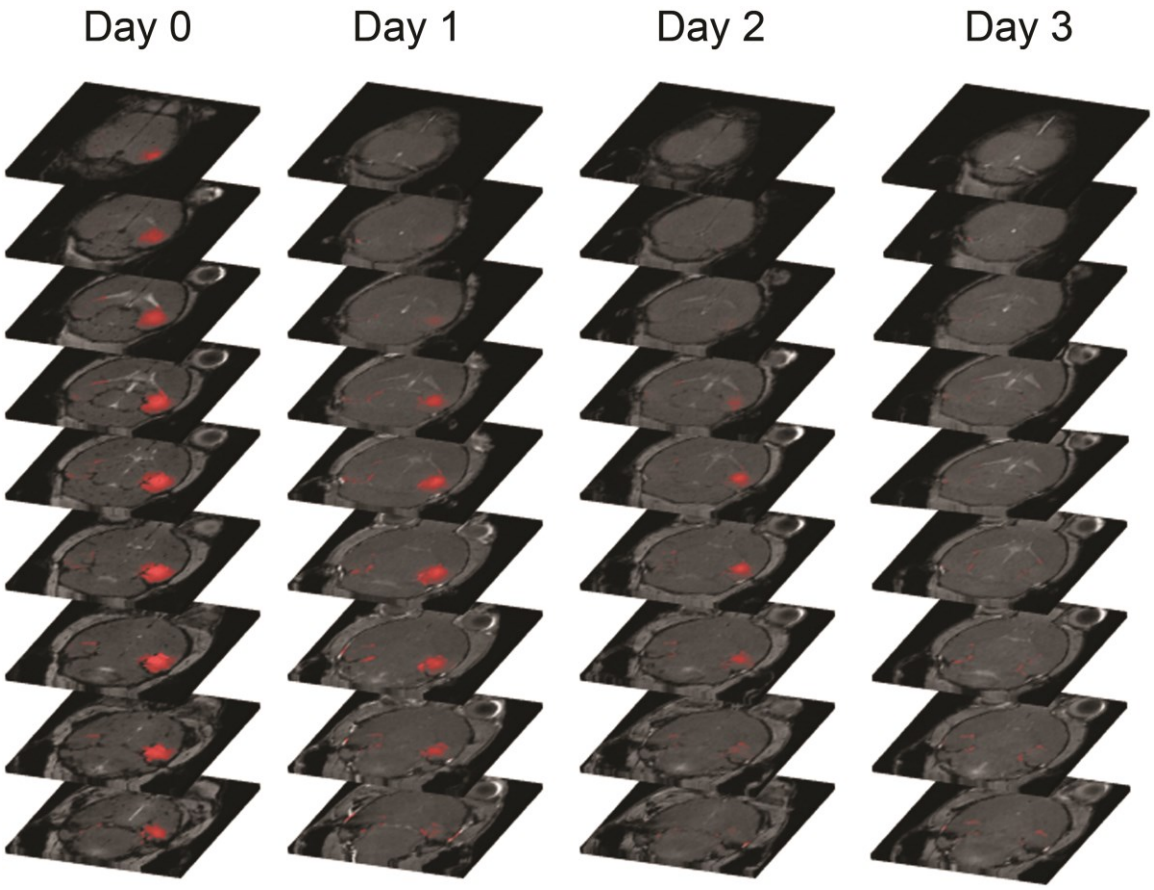

Figure 9. Horizontal consecutive CE-T1 images (500 μm thickness, dorsal on top, ventral on bottom) from Day 0 up to Day 3 for a 6-8 μm /0.30 MPa case. The BBB opening reduced radially towards the center of the FUS beam over time, until closing was detected in Day 3, when no Gd-DTPA-BMA diffused from the vasculature to the brain parenchyma.

For all cases of microbubble sizes and pressures studied, the BBB was found to be reinstated by day 5, and the duration of opening depended on the microbubble diameter and PRP used. In **Figure 10**, there are reconstructions of the horizontal planes, sliced coronally at the level of the hippocampal formation, at all pressures and microbubble sizes. In Figure 10, it is also shown that the area of Gd-DTPA-BMA diffusion in the brain and its spatial characteristics depend on the microbubble size and pressure used. The BBB permeability to Gd-DTPA-BMA appears to occur dorsally in the brain only in the cases when larger microbubbles were used, i.e., not in the 1-2 μm case, where diffusion of the contrast agent Gd-DTPA-BMA was observed mainly ventrally in the brain near the vasculature. This effect becomes more apparent in higher PRPs, i.e., 0.60 MPa.

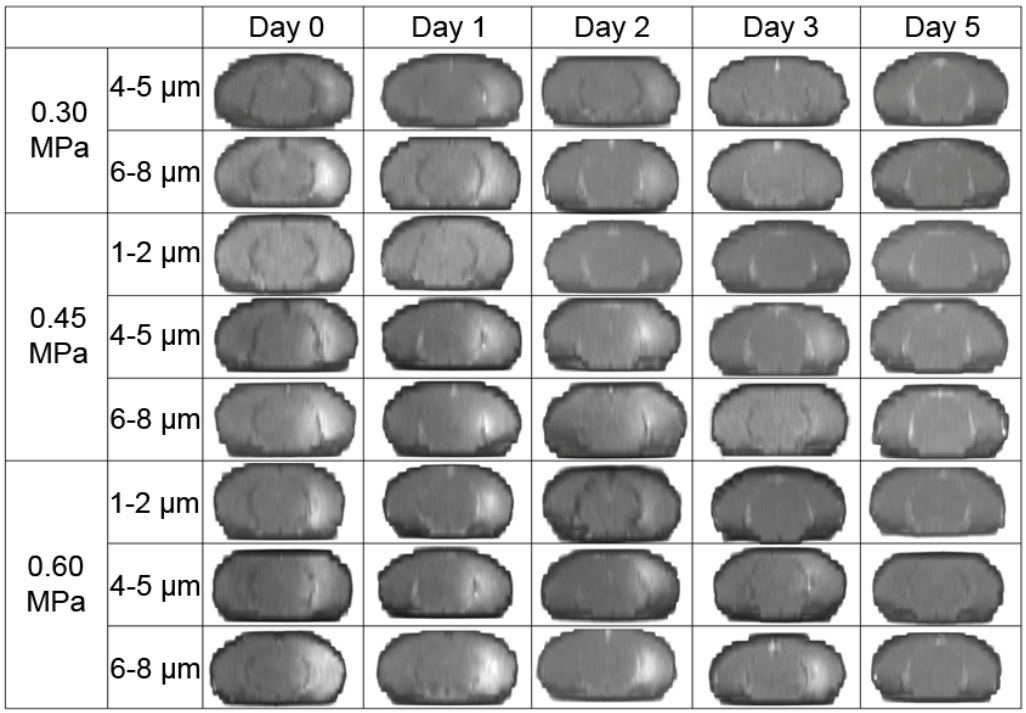

Figure 10. Coronal reconstructions from horizontal CE-T1 images with one example provided in each case of PRP and microbubble size.

Volumetric measurements are shown in **Figure 11**(a),(b) and (c) for the 1-2 µm, 4-5 µm and 6-8 µm microbubble cases. At 0.30 MPa with the 1-2 µm microbubbles no BBB opening was detected. Depending on the microbubble and pressure used, the BBB closing occurred within 24 hours and 5 days after sonication. More specifically, with the 1-2 µm microbubbles (**Figure 11**(a)), closing was found to be closed on Day 1 and Day 2 at 0.45 MPa and 0.60 MPa, respectively. With the 4-5 µm and 6-8 µm microbubbles, the BBB was found to be closed on Day 2 at 0.30 MPa, day 3 at 0.45 MPa and day 5 at 0.60 MPa. A proportional relationship between the volume and the duration of the BBB opening regardless of the PPR and microbubble size used to induce the opening was thus established (**Figure 12**). Linear regression showed a correlation of R2 = 0.72. Excluding Day 0 a logarithmic fit showed a correlation of R^2 = 0.78.

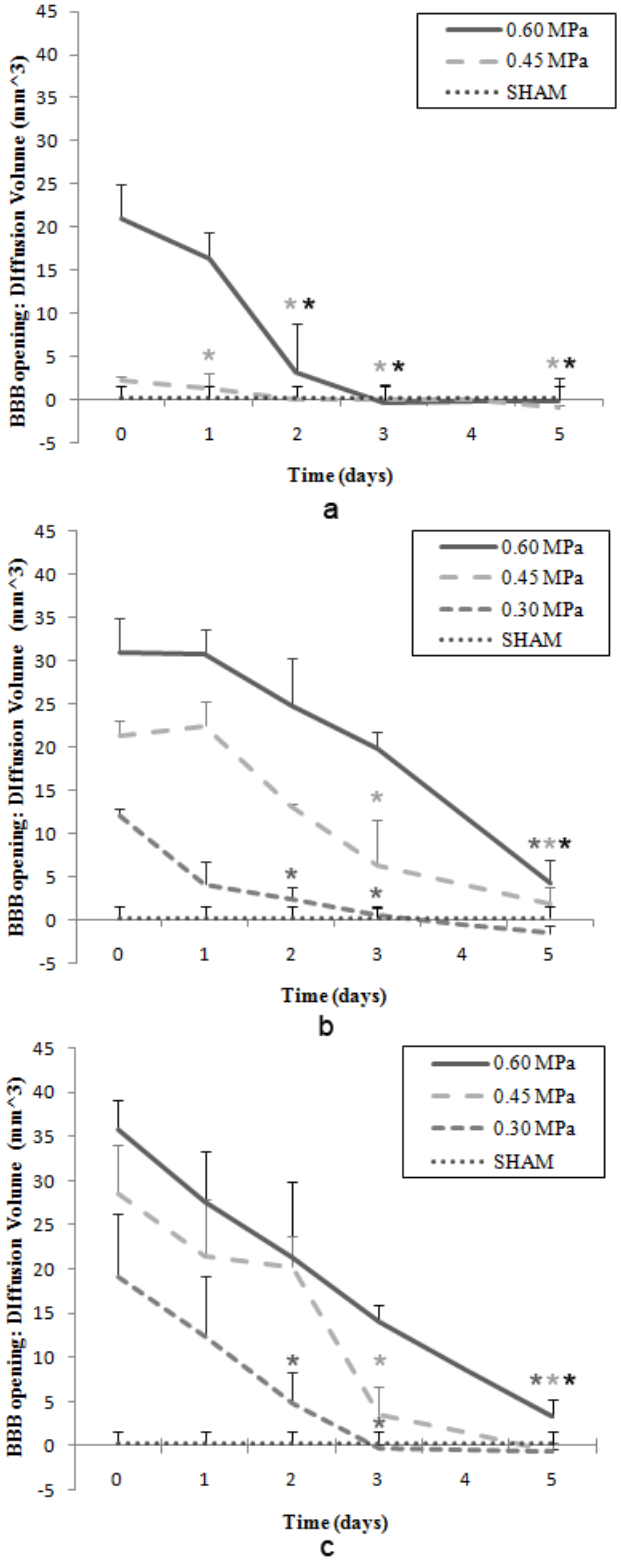

Figure 11. Volume of diffusion of Gd-DTPA-BMA area, depicting BBB opening, for PRP of 0.30 MPa, 0.45 MPa, and 0.60MPa and the sham group with microbubbles of (a) 1-2μm, (b) 4-5μm and (c) 6-8μm in diameter. Error bars correspond to standard deviation and (*) denotes closing.

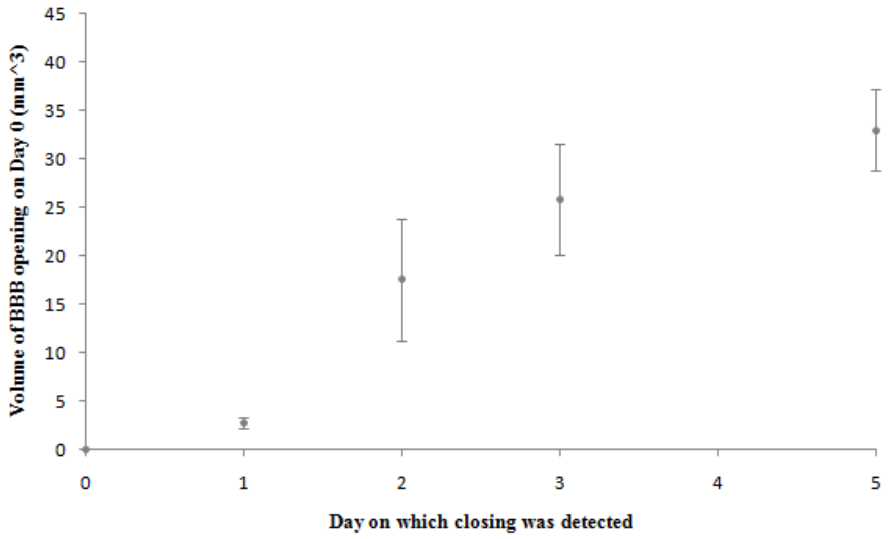

Figure 12. Volume of BBB opening on day 0 versus time to closing, showing that the duration of BBB opening increased monotonically with the volume of opening on Day 0.

The results of the statistical analysis on day 0 are shown in Table 4. At 0.30 MPa, opening was induced only in the 4-5 μm and 6-8 μm cases, with no statistically significant difference ($p>0.05$) between these two diameter ranges (**Table 4**), and the BBB was restored by day 2 in both cases. At 0.45 MPa, the volume of BBB opening induced with 1-2μm microbubbles, was statistically different ($p<0.01$) than that with larger microbubbles (**Table 4)**, and also it occurred within 24 hours, compared to 2-3 days needed in the cases of the larger microbubbles. Finally, in Table 1, it is shown that at 0.60 MPa, there was a statistically significant difference between the 1-2-μm and 6-8-μm bubbles ($p< 0.05$), and at least 2 days were required for the BBB to be reinstated in the 1-2 μm case, as opposed to 4-5 days required for the larger microbubbles.

Day 0		**1-2 μm**	**4-5 μm**
0.30 MPa	**6- 8 μm**	-	$p > 0.05$
0.45 MPa	**6- 8 μm**	$p < 0.01$	$p > 0.05$
	4-5 μm	$p < 0.01$	-
0.60 MPa	**6- 8 μm**	$p < 0.05$	$p > 0.05$
	4-5 μm	$p > 0.05$	-

Table 4 P values from Statistical Analysis on the volume of diffusion of Gd-DTPA-BMA on day 0, comparing different cases of microbubble diameters, per PRP.

Good correlation was also found between all histological damage cases and hyperintensity in the pre-contrast T1-w images. An example is shown in **Figure 13**, where hyperintensity was detected at the sonicated region in the pre-contrast image, and cell loss was detected on the H&E stained slices at the level of the hippocampus. Damage was observed upon histological examination only in five animals, approximately 13% of the total number of animals used, all of which were at higher PRPs.

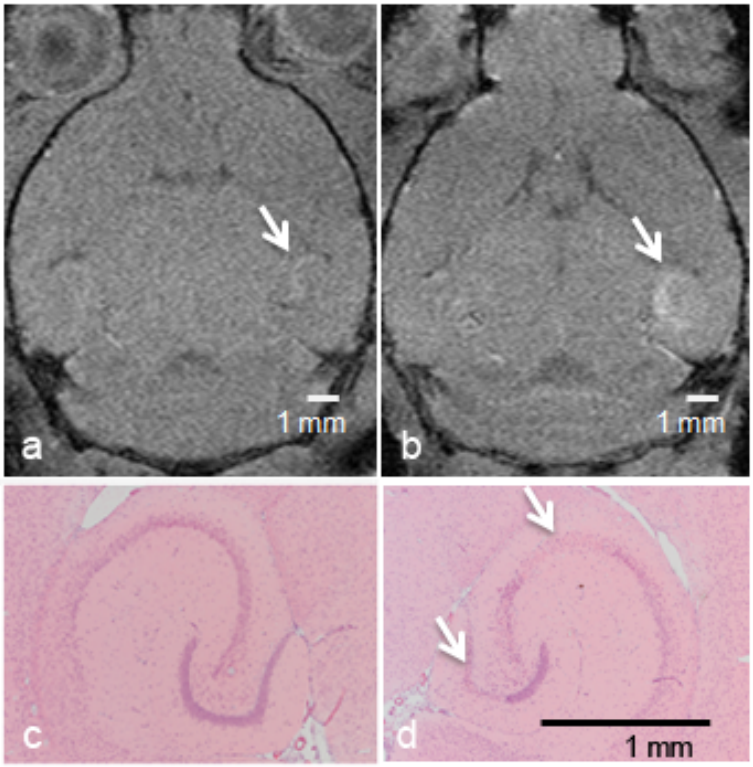

Figure 13. Example of one out of the five cases where damage was detected. (a) and (b) are horizontal pre-contrast T1-weighted images, acquired on Day 0 and Day 7, respectively. Hyperintensity is shown (white arrows) on the sonicated side, more enhanced on Day 7. (c) and (d) are the H&E stained slices, magnified (10x) at the left (control) hippocampus and at the right (sonicated) hippocampus respectively. In (c) cell loss is detected at the dentate gyrus and CA1 area (white arrows).

3.1.5. Discussion

In this longitudinal study, the reversibility of BBB opening was investigated using Gd-DTPA-BMA that cannot cross the BBB when the BBB is reinstated or closed. Spatial (i.e., volume) and temporal (i.e., duration) characteristics of the intact or BBB's altered function were studied, while opening was induced using three different microbubble sizes and three different PRPs. BBB opening induced by FUS has been shown in several studies to be transient but with differing reports on the duration which has indicated the dependence on the acoustic parameters

and bubbles used. Also, several studies have shown that the BBB opening is dependent on the acoustic pressure used as well as the microbubble size. The features of the BBB self-repairing characteristic were studied for the first time here under a combination of different acoustic parameters, and a range of mono-dispersed microbubbles. Our study indicated a proportional relationship between the BBB opening volume and the time required for closing. Therefore, both the BBB opening volume and duration were shown to be dependent on the acoustic pressure and the microbubble size used.

The spatial characteristics of the BBB opening and its reversibility were unveiled as follows. Firstly, as seen in the examples of Figure 9 and Figure 10, the BBB function was reinstated in a reverse direction to that of the diffusion after opening, i.e., closing starts from the outer opened regions and ends at the focal region while also being dependent on the hippocampal vasculature. It has also been shown [55] that the permeability values towards the center of the focal region were higher. A first explanation is that the peak of the acoustic pressure distribution lies at the center of the focal spot which may result in larger BBB openings, hence taking longer to close. Another explanation could be that where the vasculature is denser, there is a higher number of opening sites, requiring thus longer timelines for closing to be completed.

Overall, even though the volume of opening induced by the 6-8-μm bubbles was greater than the volume induced by the 4-5 μm microbubbles, these two microbubble sizes did not differ significantly in this study(
Table 4) and the days required for closing were also similar (**Figure 11**(b) and (c)). According to these observations, several conclusions can be drawn. First, it could be assumed that their differences were not significant because both 4-5-μm and 6-8-μm bubbles are within the diameter size range of the capillary, i.e., is 4-8μm, and therefore they are both in contact with the capillary wall, exerting forces on it while being acoustically driven. However, the mechanical stress on the capillary walls due to the acoustically driven microbubbles for a specific pressure when induced by the 6-8-μm is larger than when induced by the 4-5-μm bubbles, because the latter would require higher PRP to reach the same size expansion as the 6-8-μm and have the same effect [101] hence the BBB opening volume slightly increased.

Another interesting observation is that the BBB opening volume using 1-2-μm bubbles was significantly lower than for the larger microbubbles (**Table 4)** and the BBB closed significantly faster. Therefore, for more efficient BBB recovery at high pressures, smaller microbubbles may be preferable. The relative expansion of a microbubble is inversely proportional to its resting diameter (31). 1-2-μm bubbles induced no opening at 0.30 MPa, where only stable cavitation is expected (20). This is probably due to the fact that stable oscillations of smaller microbubbles

may not be sufficient to induce the needed repeated stress against the capillary wall at 0.30 MPa, but are adequate at 0.45 MPa, and even more so at 0.60 MPa. It has been also shown that fragmentation occurs more frequently for microbubbles with a small rather than a large resting diameter at a threshold size of 2.5 μm. Below that level, fragmentation occurs [104] and bubbles smaller than 2 μm can be fragmented prior to reaching the endothelium and not interact with the vessel wall [101]. Therefore, it could be concluded that the smaller microbubbles were not capable of inducing opening in sites away from the bigger vessels, because they may have undergone fragmentation at the beginning of the FUS pulse before perfusing the microvasculature. Thereby, the therapeutic efficacy of 1-2 μm bubbles in the capillaries might be decreased, an effect noted in previous studies [108], [109].

In this study, the timeline required for closing is longer than what has been reported by previous studies, i.e., 3-24h ([6],[91],[63],[65],[66],[68], [92], [93]) as previously explained. The discrepancy with the findings presented here could be due to multiple factors. First of all, the microbubble formulation, manufactured in-house, used in this study is different than the commercially available contrast agents used in the other BBB restoration studies, in terms of the combination of shell properties, gas core and diameter size; therefore, this microbubble formulation used here is a parameter that could also induce variations. However, the size range of the commercially available microbubbles used in those studies is closer to the case of the 1-2-μm bubbles used in our study, which are also shown here to induce BBB opening that can close within 24 h. At lower PRPs, we showed that the BBB closes faster, and in most of these studies, the PRPs used were below 0.50 MPa. Moreover, the FUS frequency (1.5 MHz) used in this study might also introduce differences compared to other studies. The resonance frequency decreases with the microbubble radius, and also decreases with decreasing microvessel radius [110]. Therefore, in this study, with the use of a lower frequency for example, which would be closer to the resonance frequency of the microbubbles within the microvessles and capillaries, and the aforementioned effects could be further enhanced. Finally, in other timeline studies, the agents used to cross the BBB for the detection of opening, had larger molecular weights (Magnevist ®: 938Da, HRP: 40 kDa, Evans Blue: 961 Da) while it has been shown that the BBB becomes less permeable at higher molecular weights ([90], 38)). Since we administered Gd-DTPA-BMA , which is a relatively smaller (574 Da) agent and only above the size threshold to cross the BBB (400 Da), our method may have an increased sensitivity regarding the detection of BBB opening, which could contribute to the longer times shown here.

In the five cases where cell loss was detected in the H&E stained brain sections on the sonicated region, hyperintensity was also detected on the pre-contrast MRI images at the corresponding regions. The signal enhancement detected in these areas in the pre-contrast T1-w

images could be therefore due to permanent damage, blood present in the brain or arrested Gd-DTPA-BMA in possibly damaged vasculature, and BBB could not be completely restored. These cases however, did not belong all in the same group, and the groups they belonged to could still meet the closing criterion based on the statistical analysis.

Another interesting finding in this study is that the BBB remained opened over several days in some cases. It was thereafter restored and 87% of the cases showed no detectable damage, while the remaining 13% showed minimal cell loss. In the past, more significant damage has been reported [111] including microvacuolated sites, dark neurons and sites with extravasated erythrocytes, when the BBB opening was induced in mice at similar PRPs, with Definity microbubbles (mean diameter: 1.1 – 3.3 μm) and the same PRF (10 Hz) but longer burst lengths (20ms) than the one used here. Also, in that study [111], survival time periods were 30 min and 5 h, whereas in this study it was 7 days. It could therefore be concluded that, first, at shorter burst lengths opening is induced [112] with less damage, and second, that the self-repairing mechanism of the BBB could restore certain types of injury induced to the brain after FUS provided sufficient time is allowed.

There are certain limitations in this study that should be acknowledged and addressed. Firstly, BBB may have been disrupted longer than what could be detected by the sensitivity the MRI system used and the resolution of the images acquired. Another limitation is that the first acquisition or post-contrast T1-w images was 1 h after FUS, and within this time it is possible that some cases with very small BBB opening might have not been detected. Finally, it was assumed that the circulation times and persistence of all the different sizes of microbubbles were similar for the 10-20 sec interval between injection and FUS, however, it must be taken into consideration that any differences could have had an impact on our results.

In this longitudinal study we showed dependence of the volume of BBB opening and the time required for the BBB to be reinstated on the microbubble size and the acoustic pressure. In addition, the time required for closing was found to be proportional to the volume of opening induced by FUS, and BBB was shown to recover its functionality between 24 h and 5 days after. The BBB opening volume was shown to decrease radially towards the center of the focal spot over time. At lower acoustic pressures, the microbubble size becomes more important, with smaller microbubble diameters inducing a lower volume of BBB opening and the closing timeline being significantly different than with larger microbubbles. As the PRP increases, the differences in BBB opening and closing between the different microbubble sizes become less significant. Overall, the BBB closes faster when small microbubbles are used, while for the 4-5 μm and 6-8 μm the same duration for closing was required. Finally, hyperintensity in the area of BBB opening

was detected in the pre-contrast MR images only in the cases where damage was seen in histology. In conclusion, this study may offer some further insight in the understanding of the FUS-opened BBB self-repairing characteristics, spatially and temporally, and the methodology may be adjusted to fit the pharmacokinetic needs of the administered CNS drugs.

Section 3.2: Permeability, opening volume and reversibility timeline using different pulse-lengths and acoustic pressures

3.2.1. Abstract

The most challenging aspect of intravenously-administered drugs currently developed to treat central nervous system (CNS) diseases is their blood-brain barrier impermeability, which is a specialized vasculature system protecting the brain microenvironment. Focused Ultrasound (FUS) in conjunction with systemically administered microbubbles has been shown to open the blood-brain barrier (BBB) locally, non-invasively and reversibly. The objective of this study was to investigate the effect of the FUS pulse length (PL), ranging here from 67 μs to 6.7 ms, on the physiology of the FUS-induced BBB opening. Dynamic Contrast Enhanced (DCE) and T1-weighted Magnetic Resonance Imaging (MRI) were used to quantify the permeability changes using transfer rate (K_{trans}) mapping, the volume of BBB opening (V_{BBB}) and the reversibility timeline of the FUS-induced BBB opening, with the systemic administration of Definity microbubbles at different acoustic pressures, ranging from 0.30 MPa to 0.60 MPa. Permeability and volume of opening were both found to increase with the acoustic pressure and pulse length. At 67-μs PL, the opening pressure threshold was higher, the maximum K_{trans} was 0.0057 ± 0.0015 min^{-1}, the maximum V_{BBB} was 6.92 ± 5.73 mm^3, and closing occurred within 8 h after opening. At 0.30 MPa, for a 0.67-ms PL measurements yielded K_{trans}=0.0050 ± 0.0013 min^{-1} and V_{BBB}= 1.5 ± 0.5 mm^3 and closing occurred within 8 h, while for a 6.7-ms PL K_{trans} was 0.0092 ± 0.0023 min^{-1} and V_{BBB} was 9.9 ± 5.7 mm^3 and closing occurred within 24 – 48 h. At both 0.45 MPa and 0.60 MPa, for the 0.67- and 6.7-ms PLs, K_{trans} reached similar values ranging from 0.0097 ± 0.0026 min^{-1} to 0.0111 ± 0.0027 min^{-1}, and the corresponding V_{BBB} ranged from 18.3 ± 8.0 mm^3 to 23.9 ± 9.2 mm^3. However, the time required for closing varied between 24 – 48 h for the 0.67-ms PL, and between 48 – 72 h for the 6.7-ms PL. Stacked histograms of the K_{trans} provided further insight to the non-uniform spatial distribution of permeability changes and its relation to closing timeline. Linear regression between K_{trans} and V_{BBB} showed a good correlation fit. Also, the time required for closing linearly increased with V_{BBB}. The volume decay rate was measured to be 11.4 ± 4.0 mm^3 per day suggesting that the closing timeline could be predicted from the initial volume of opening. Finally, no histological damage was detected in any of the cases 7 days post-FUS, indicating the safety of the methodology and parameters used.

3.2.2. Introduction and Study Design

Despite the fact that the mechanism of FUS-induced BBB opening remains unknown, several studies have been conducted aiming at investigating the influence of several acoustic parameters, such as the frequency [8],[9], pulse repetition frequency (PRF) [93], [115], [116], sonication duration [9],[13], microbubble size [9], [94], [107], [118], and pulse length [93], [115], [116]. Moreover, it has been previously reported that the BBB opening can be achieved in short pulse lengths (PL) as low as 33 μs [115] at 0.46 MPa and 10 Hz PRF, or even at 2.3 μs pulses transmitted at the higher PRF of 100 Hz, and higher pressure of 0.51 MPa [116], which were also found to facilitate a more spatially uniform distribution of the delivered fluorescently tagged dextrans. It has also been reported that increased number of cycles within a given pulse length (10 ms) correlated with edema without significantly increasing the enhancement of the tracer delivery [119] . However, the effect of the pulse length on the transfer rate from blood to tissue parenchyma and the corresponding permeability maps as well as the volume and the duration or reversibility of the BBB opening have not been studied thus far.

Recently, some physiologic characteristics of the FUS-induced BBB opening, i.e., the in vivo permeability changes [107], the volume of opening and the reversibility timeline [9], have been investigated with the use of Dynamic Contrast Enhanced MRI (DCE-MRI) and T1-weighted MR images with gadodiamide (MW: 574 Da, Omniscan, Healthcare, GE) as a tracer, and mono-dispersed microbubbles (1-2, 4-5 and 6-8 μm in diameter) at a pulse length of 0.67 ms, showing a dependence on the acoustic pressure and the microbubble size used. Definity microbubbles, which have been widely used in FUS-induced BBB opening studies, are highly polydisperse in size, containing a range of diameters from under 1 μm to 10 μm, but with most of the microbubbles ranging below 2 μm in diameter [120], [121]. The bioeffects of poly-dispersity compared to what has been previously reported for the isolated mono-dispersed microbubbles were also studied here.

The purpose of this study was thus to investigate the effect of FUS *in vivo* on the BBB opening physiology, using a range of pulse lengths, varying from 67 μs to 6.7 ms at a PRF of 10 Hz, while also varying the acoustic pressure between 0.30 MPa and 0.60 MPa, in order to study their effect on the FUS induced BBB opening in vivo. Gadodiamide was used as the tracer to depict BBB opening for the acquisition of DCE-MRI and T1-weighted MR images in order to measure the permeability changes and maps, to quantify the volume of opening and determine the reversibility timeline of BBB opening. Moreover, another objective of this study is to investigate the relation between permeability changes, volume of opening and the time required for BBB closing, aiming at establishing a correlation, which could potentially be used to predict

the time required for closing. Finally, the safety of the procedures and the acoustic parameters used was assessed through histological analysis.

Frequency	1.5 MHz (IMASONIC, France)
Pressure (PRP)	0.30 MPa, 0.45 MPa , 0.60 MPa
Pulse Length (PL)	**67 µs (100 cycles)**
	0.67 ms (1000 cycles)
	6.7 ms (10000 cycles)
Pulse Rate	10 Hz (100 ms)
Total Duration	1 min (600 pulses)
Microbubbles (1 µL / g)	Definity ® (diluted 1:20 in PBS) (mean diameter range 1.1 – 3.3 µm)
Targeting	3 mm below skull Right hippocampus
Focal size	Width: 1mm, Length: 7.5 mm

Table 5 FUS parameters

System	Bruker 9.4 T
Contrast agent	Gd (Omniscan^{TM})
Volume	0.30 mL Intreperitoneal
Imaging Methods	Dynamic Contrast Enhanced T1-weighted Images (**DCE**)[8] using **General Kinetic Model** (130 x 130 x 600 µm^3)
	T1-weighted images (100 x 100 x 400 µm^3)

Table 6 MRI parameters

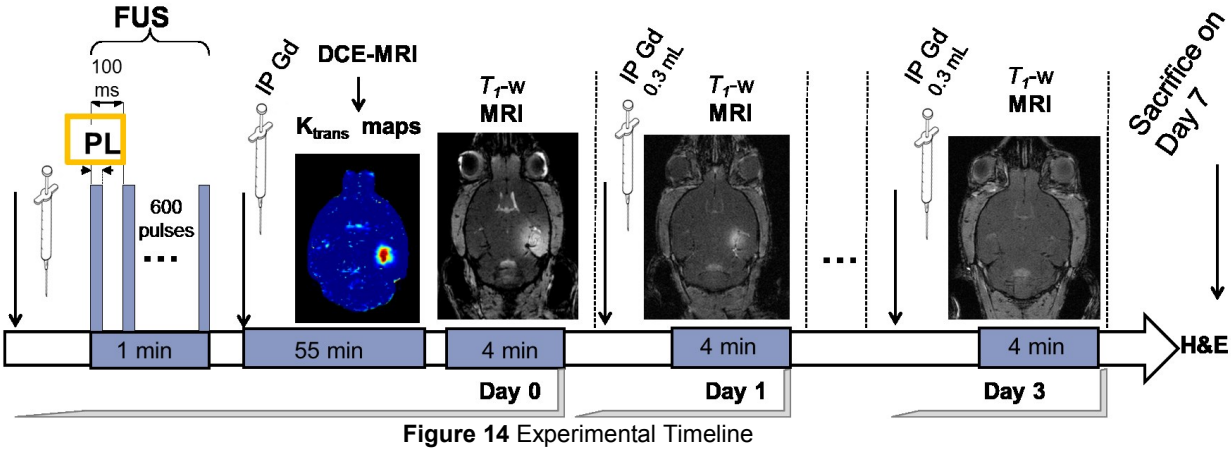

Figure 14 Experimental Timeline

3.2.3. Materials and Methods

A. Ultrasound

A single-element, spherical-segment FUS transducer (center frequency: 1.5 MHz, focal depth: 60mm, radius: 30mm; Imasonic, France), driven by a function generator (Agilent, Palo Alto, CA, USA) through a 50-dB power amplifier (E&I, Rochester, NY, USA). A central void of the therapeutic transducer held a pulse-echo ultrasound transducer (center frequency: 10 MHz) used for imaging, with their two foci aligned. The imaging transducer was driven by a pulser-receiver (Olympus, Waltham, MA, USA) connected to a digitizer (Gage Applied Technologies, Inc., Lachine, QC, Canada). A cone filled with degassed and distilled water was mounted onto the transducer assembly. The transducers were attached to a computer-controlled 3D positioning system (Velmex Inc., Lachine, QC, Canada). The FUS focal spot, axial and lateral full-width at half-maximum intensities were 7.5 mm and 1 mm respectively, overlapped with the right hippocampus and the lateral portion of the thalamus. 1 μl/ g of body mass of Definity® microbubbles, 1:20 diluted in PBS, was intravenously injected immediately preceding the sonication. Thirty-six (n=36) wild-type adult male mice (strain: C57BL/6, Harlan Sprague Dawley, Indianapolis, IN, USA) were sonicated for 60 s, with a pulse rate of 10 Hz, at peak negative acoustic pressures (PNP) of 0.30 MPa, 0.45 MPa and 0.60 MPa, after accounting for 18% murine skull attenuation [122]. A sham group of three mice underwent the whole procedure without FUS. All mouse experiments were carried out in accordance with the Columbia University Institutional Animal Care and Use Committee. The pulse length (PL) tested was equal to 67μs, 0.67 ms or 6.7 ms. The acoustic pressures were obtained experimentally in a degassed water tank. A needle hydrophone (ONDA, Sunnyville, CA) was used for the transducer calibration, which measured the acoustic pressure in a tank filled with degassed water. The mice were anesthetized using 1.25-2.50% isoflurane (SurgiVet, Smiths Medical PM, Inc., Winsconsin, USA) mixed with oxygen during the experiments.

B. Magnetic Resonance Imaging

All mice were imaged using a 9.4 T microimaging MRI system (DRX400, Bruker, Biospin, Billerica, MA, USA). Each mouse was scanned 30-40 min after sonication, using a 30-mm-diameter single resonator. Isoflurane gas (1-2%) was used to keep the mouse anesthetized at 50-70 breaths/min during the entire MRI procedure. On the day of sonication (Day 0) Dynamic Contrast-Enhanced MR imaging (DCE-MRI) was performed using a 2D FLASH T1- weighted sequence (192×128 matrix size, spatial resolution of 130×130 μm^2, slice thickness of 600 μm, TR/TE=230/2.9 ms). During the 3rd acquisition of the dynamic sequence, a 0.30-mL non-diluted bolus of gadodiamide (Omniscan) was injected intraperitoneally (IP) and was used as a tracer to depict the area of opening. This large dose ensured the presence of a bolus peak in the blood circulation in the vasculature, which is required for the arterial input function determination as well

as a sufficient amount for the depiction of the BBB opening. After the completion of DCE-MRI, a post-contrast enhancement, T1-weighted 2D FLASH high resolution acquisition (TR/TE: 230/3.3 ms, resolution 100 μm x 100 μm, slice thickness: 400 μm) was acquired. The scanning time of each DCE and T1-weighted MRI image was 40 min and 4 min respectively. T1-weighted MR imaging was repeated on a daily basis starting from the day of sonication (1 h) and lasting up to 72 h after sonication. Mice with small detectable opening were also imaged 8 h after sonication. The general kinetic model (GKM) was used to measure the BBB permeability in the targeted region as described elsewhere [15], providing maps of K_{trans} (Fig. 2), which denotes the transfer rate from the blood plasma to the extravascular extracellular space of each voxel. The arterial input function (AIF) was determined by averaging the gadodiamide concentration changes in the internal carotid artery from the entire cohort of wild type mice. The average of all K_{trans} values of the voxels in a 3D volume of interest (VOI) of 52 mm^3 overlapping with the targeted area was calculated and was used for the quantitative K_{trans} plot for all groups, as shown in Fig.3. Stacked K_{trans} histograms in the same VOI's were also created to provide more quantitative information on the relative changes in K_{trans} within the VOI as shown in Fig.4. The average K_{trans} was also measured in the non-sonicated contralateral side of the VOI and in the sham group, and was used a reference, i.e. a baseline K_{trans} of the brain tissue around the hippocampal area without any BBB disruption. The volume of opening (V_{BBB}) was quantified by thresholding voxels within the VOI with signal intensity (S.I.) of 2.5 standard deviations or above the S.I. of a reference region in the non-sonicated area, while the volume of contrast-enhanced vasculature was excluded, and those longitudinal measurements are shown in **Figure 18**.

C. Safety assessment

On day 7 after the FUS-induced BBB opening, all mice were euthanized and transcardially perfused with 30 mL PBS and 60 mL 4% paraformaldehyde. Heads were soaked in paraformaldehyde for 24h. Skulls were removed, and the brains were fixed again in 4% paraformaldehyde for 6 days, followed by conventional post-fixation procedures. The paraffin-embedded specimens were sectioned horizontally at a thickness of 6 μm. For each brain, there were 32 sections prepared, with 100 μm spacing between planes. Sections were stained with hematoxylin and eosin and then examined for red blood cell extravasations into the brain parenchyma as well as cell loss.

D. Statistical analysis

The measurements in the sham group were used to determine whether the integrity of BBB was fully restored in the BBB opened cases, as described by Samiotaki et al. 2011 [9]. Following the calculation of the mean and the standard deviation of the volumetric measurements for each group, a two-tailed Student's t-test was performed between the FUS group and the sham

group, and if no statistically significant difference was observed ($p>0.05$), then the BBB was considered to have been restored.

Comparison among different groups that received sonication was also performed, using a two-tailed Student's t-test, to reveal any statistically significant differences ($p<0.05$) as a result of the different acoustic parameters used for both the quantitative measurements of K_{trans} and Volume of opening.

3.2.4. Results

Horizontal MR images overlaid with K_{trans} maps are shown in Figure 15, for all PLs and PNPs used, followed by longitudinal high-resolution T1-weighted MR images showing BBB opening. Yellow frames denote closing, and images following detected closing confirm that BBB remained closed. The K_{trans} maps show the non-uniformity of the spatial distribution in permeability changes in each combination of PL and PNP studied. The progress of BBB opening until closing is shown in the T1-weighted images; signal enhancement due to the diffusion of gadodiamide through the opened BBB depicts the opening area. BBB closing followed a radial inward pattern towards the center of the FUS beam, in agreement with previous findings [16]. At 67-μs PL, 0.30 MPa was found not to be sufficient to induce detectable opening, and for 0.45 MPa and 0.60 MPa closing occurred within 8 h after opening. At 0.67-ms PL closing occurred within 8 h for 0.30 MPa, within 24 h for 0.45 MPa, and within 24h -48h for 0.60 MPa. Finally, at 6.7-ms PL, closing occurred within 24h - 48 h for 0.30 MPa, and within 48 h – 72 h for both 0.45 MPa and 0.60 MPa.

The permeability average K_{trans} values of the 3D VOI which was overlapping with the right hippocampus, as provided by quantitative measurements, are shown in Figure 16. The dotted line represents the average Ktrans of the non-sonicated contralateral side of all the animals used in this study which was measured to be 0.0038 ± 0.001 min^{-1}. At 0.30 MPa, a 67-μs PL did not cause any increase in permeability compared to baseline, a 0.67-ms PL increased Ktrans to 0.0050 ± 0.0013 min-1 and a 6.7-ms PL increased Ktrans to 0.0092 ± 0.0023 $^{min-1}$. At 0.45 MPa, a 67-μs PL increased Ktrans slightly above baseline to 0.0036 ± 0.0008 min1, but 0.67-ms and and 6.7-ms PLs significantly increased Ktrans compared to the shortest PL to 0.0097 ± 0.0026 min^{-1} and 0.0111 ± 0.0027 min^{-1} respectively. At 0.60 MPa, Ktrans was increased to 0.0057 ± 0.0015 min-1 at 6.7-μs PL, and then to 0.0101 ± 0.0017 min-1 and 0.098 ± 0.0119 min-1 for 0.67- and 6.7-ms PL respectively.

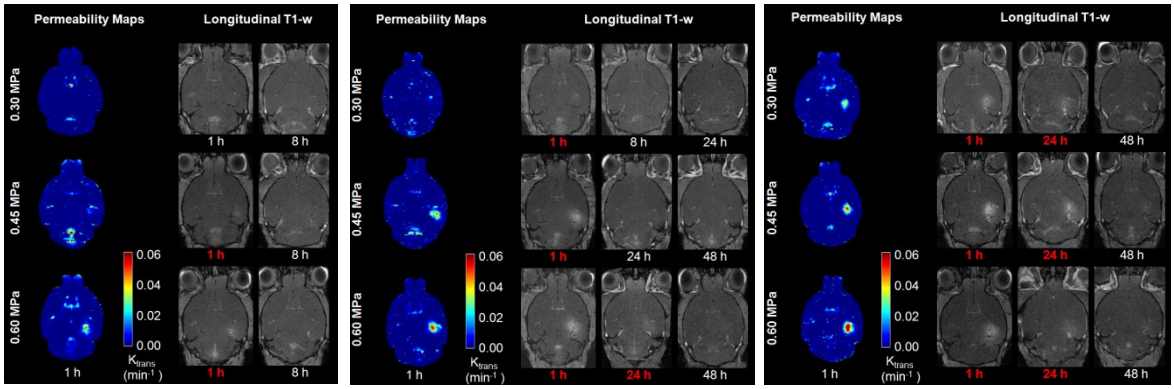

Figure 15. Horizontal permeability maps after FUS followed by longitudinal T1-weighted images showing the reversibility timeline for all opeak negative acoustic pressures and pulse lengths(left: 67 μs, middle: 0.67 ms, right: 6.7 ms). Singal enhancement in the BBB opened region resulting from the diffusion of Gd-DTPA-BMA threough the BB is observed in the sonicated region, which was overlapping with the right hippocampus. Red font denoted that BBB opening was detected, whereas white font denotes closing.

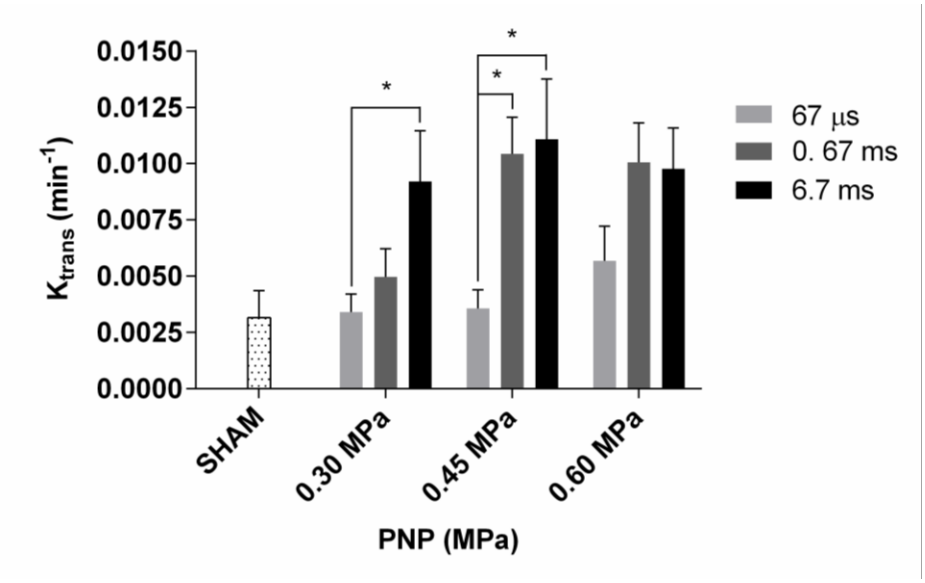

Figure 16 K_{trans} averaged in the whole sonicated area at different PNPs and PLs. Error bars denote standard deviation. The permeability of the sham group is also shown (0.030 ± 0.007 min^{-1})

The relationship between the non-uniform changes in permeability as revealed in the Ktrans maps, PL and PNP was further analyzed in the stacked histograms of Ktrans shown in Figure 17. At 0.30 MPa, the volume of the blue cluster (0.006 – 0.015 min-1) Ktrans as well as

the volume of the green cluster (0.016 – 0.025 min-1) Ktrans were increased 3-fold when PL was 0.67 ms, and 8-fold when it was 6.7 ms, compared to baseline volume, i.e. compared to 67 µs where no opening was detected. There was some increase in the volume of the yellow Ktrans cluster (0.026 – 0.035 min-1) and the orange cluster (0.036 – 0.045 $^{min-1}$) and no difference in the red Ktrans cluster (0.046 – 0.060 $^{min-1}$). At 0.45 MPa, the volume of all permeability clusters increased more linearly with the increase of PL from 67 µs to 0.67 ms and then to 6.7 ms. At 0.60 MPa, there was no difference between 0.67-ms and 6.7-ms PL, which were very similar to the 6.7-ms PL with 0.45-MPa PNP. At 0.60 MPa, the 67-µs PL did not significantly differ from the 67-µs PL at 0.45-MPa PNP or the 0.67-ms PL at 0.30 MPa PNP. The combinations of PL and PNP that were shown to have similar Ktrans histograms had also similar reversibility timelines.

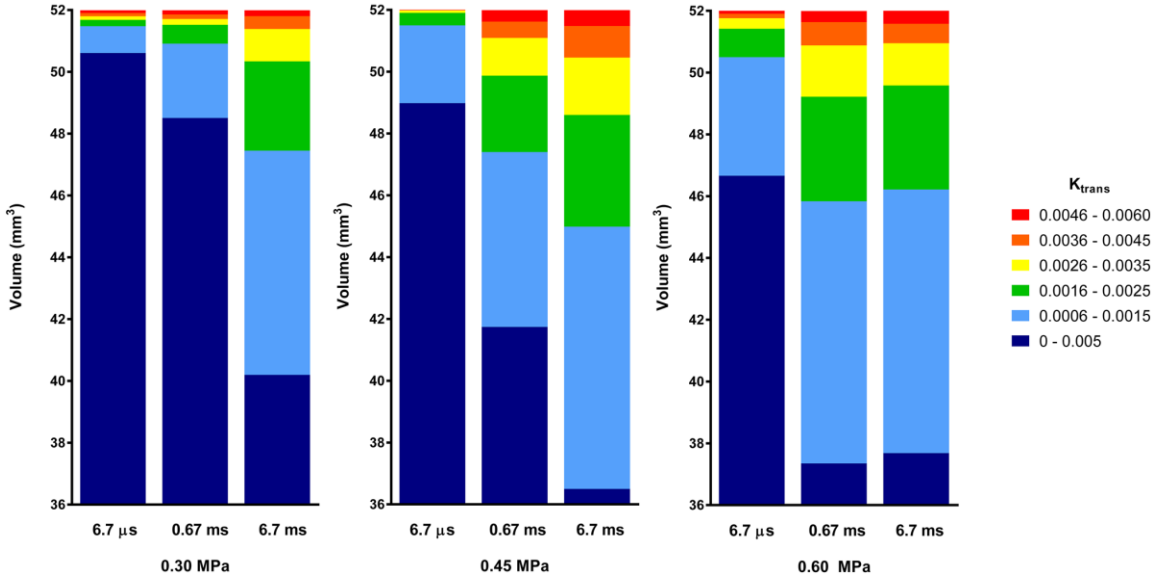

Figure 17. Stacked histograms of K_{trans} values. K_{trans} values of all permeability maps created were grouped into six clusters (i.e. 0- 0.005, 0.006-0.015, 0.016-0.025, 0.026-0.035, 0.036-0.045, 0.046- 0.060 min^{-1}) , and the average volume of each cluster is shown for all PNPs and PLs.

Quantitative volumetric measurements and the BBB opening reversibility timeline are shown in Figure 18 (a), (b) and (c) for 0.30 MPa, 0.45 MPa and 0.60 MPa respectively. More specifically at 67 µs, VBBB of 1.0 ± 1.4 mm3 at 0.30 MPa (not opened – similar to sham) , 2.6 ± 1.6 mm3 at 0.45 MPa and 6.9 ± 5.7 mm3 at 0.60 MPa were induced, while BBB closed within 8 h after opening. At a 0.67 ms pulse length, VBBB initially induced was as low as 1.4 ± 0.5 mm3 at 0.30 MPa and closing occurred within 8 h too, but increased to 18.3 ± 8.0 mm3 at 0.45 MPa and 19.9 ± 5.3 mm3 at 0.60 MPa, while closing occurred within 24 – 48 h for these pressures. At a 6.7 ms pulse length, VBBB initially induced was 9.9 ± 5. 7 mm3 at 0.30 MPa, 23.9 ± 9.2 mm3 at 0.45 MPa and 19.3 ± 5.6 mm3 at 0.60 MPa, and closing occurred within 24 – 48 h at 0.30 MPa, and within 48 – 72 h at the higher pressures. In addition, the volume decay rate was measured to be

11.4 ± 4.0 mm3 per day, while any BBB opening below that value closed within the first 24 h or less.

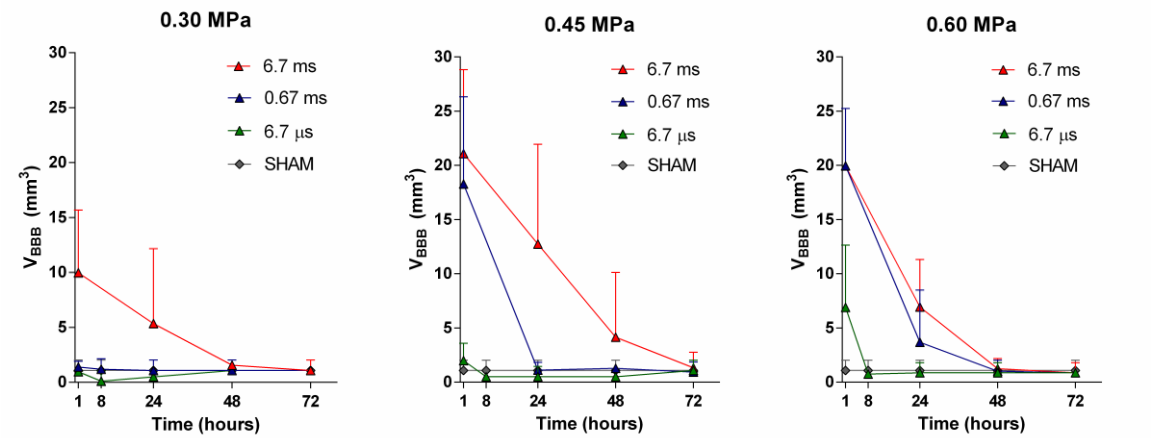

Figure 18. BBB opening volume for each group, with all PLs and PNP of (a) 0.30 MPa, (b) 0.45 MPa and (c) 0.60 MPa. Error bars correspond to standard deviation across different mice (S.D.). There was no opening detected at 67 µs/ 0.30 MPa. Closing occurred within 8 h for the 67 µs/ 0. 45- and 0.60- MPa, as well as for the 0.67 ms/ 0.30 MPa cases. Clossing occurred within 24 h – 48 for the 0.67 ms/ 0.45- and 0.60- MPa, as well as for the 6.7ms/ 0.30 MPa cases. Finally, closing occurred within 48 h – 72 h for the 6.7 ms/ 0.45- and 0.60- MPa cases.

Statistical analysis showed that there was no significant difference within the Ktrans (Figure 3) or the VBBB (Figure 18) as induced by a 67-µs PL/ 0.45-MPa- or 0.60-MPa-PNP and a 0.67-ms-PL/0.30-MPa-PNP. Their closing timeline was also similar (8h) as described earlier. Furthermore, there were no significant differences within the average Ktrans or the VBBB as induced by a 0.67-ms-PL at 0.45 MP, at 0.60 MPa, and a 6.7-ms-PL at all the PNPs tested. However, the distribution of Ktrans changes (i.e. the volume of their Ktrans clusters) for these later groups varied among them, as described previously (Figure 17), and so did the closing timeline; from 24 – 48 h to 48 – 72 h.

The correlation between Ktrans, VBBB and the time required for closing was also investigated and shown in this study. Good correlation between the time required for closing and the VBBB¬ on day 0 of opening is shown in Figure 19. The time required for closing was found to monotonically increase with the volume of BBB opening induced on the day of FUS, and a linear regression fit showed a correlation of R2 = 0.78, suggesting that the time required for closing could be predicted based on the volume of opening initially induced. As may be expected, when the Ktrans and the 1-hour-post-sonication VBBB were averaged within the same 52-mm3 VOI, they were found to be linearly correlated (Figure 20; R^2 = 0.74).

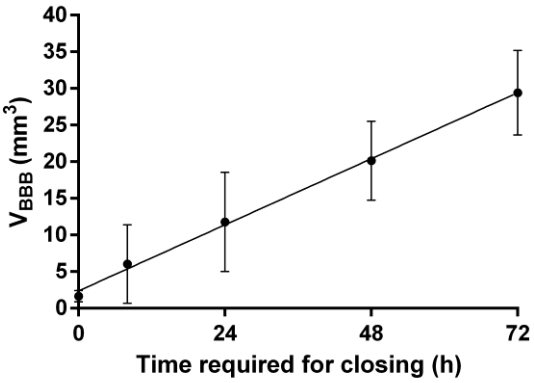

Figure 19. Correlation of the volume of opening (V_{BBB}) 1 h after FUS and the time required for closing. Linear regression shown good correlation (R^2 = 0.77). The reversibility of BBB opening was measured to have a volume decay rate of 11.4 ± 4.0 mm^3 per day.

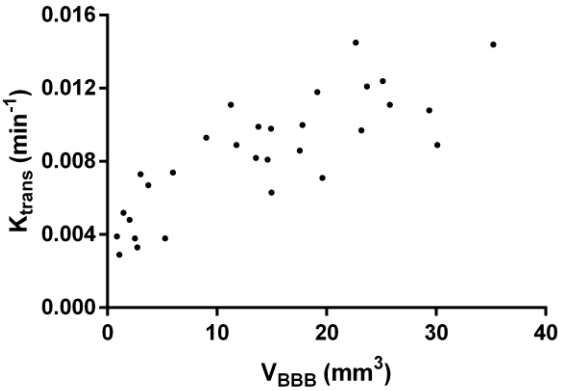

Figure 20. Scatter plot of the Ktrans versus VBBB measured in the same VOI 1h after opening. A linear fit shown a good correlation (R^2 = 0.74).

There was no damage detected under histological examination with H&E indicating that the parameters used were safe. An example is shown in **Figure 21**.

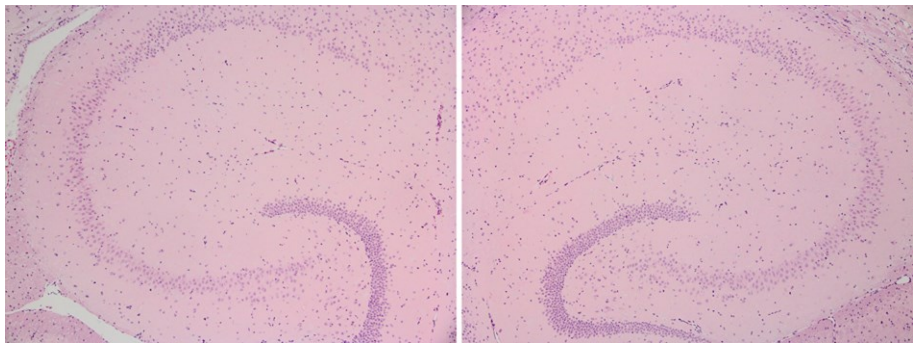

Figure 21 H&E stained horizontal slices of 6 µm thickness magnified (4x) in the area of the (a) left and (b) right hippocampus for a case of 6.7 ms PL and 0.60 MPa, i.e., the highest FUS energy case. No damage was detected in any of the mice in the study.

3.2.5. Discussion

In this study, properties of the FUS-induced BBB opening, i.e. permeability (K_{trans}), volume of opening (VBBB) and the reversibility timeline, were assessed in order to determine the effect of the pulse length (PL) and the acoustic peak negative pressure (PNP) on the restoration of the barrier. Ktrans, VBBB and reversibility timeline were shown to be dependent on the PL and PNP. The PNP threshold for BBB opening was shown here to be dependent on the PL. A PL of 67 μs at 0.45 MPa and 0.60 MPa induced BBB opening with similar Ktrans, VBBB and closing timeline (8h) with that induced by a 0.67-ms-PL at 0.30 MPa. A PL of 6.7 ms at 0.30 MPa induced a BBB opening with similar characteristics to those induced by a 0.67-ms-PL at 0.45 MPa or 0.60 MPa, with a 24 48 h closing timeline. A PL of 6.7 ms at 0.45 MPa and 0.60 MPa also induced BBB opening with similar Ktrans and VBBB and closing timeline varied within 48 – 72 h. The time required for closing increased monotonically with the volume of opening [16], and was shown to follow a decay rate of 11.4 ± 4.0 mm3 per day. The Ktrans averaged in the whole sonicated BBB region was linearly correlated to the VBBB on the day of sonication. Finally, there was no histological damage detected indicating that the parameters tested here are safe.

An interesting finding is that at 0.30 MPa, the BBB opening occurred at the pulse length threshold of 0.67 ms with the BBB opening volume increasing with the pulse length beyond that value. It has been previously shown that inertial cavitation occurs at the pressures of 0.45 MPa and 0.60 MPa but not at 0.30 MPa [21]. At the absence of inertial cavitation, the microbubbles undergo stable oscillations that continue over several cycles possibly leading to bubble growth through rectified diffusion or shrinkage leading to dissolution. The results shown here suggest that at 0.30 MPa with a pulse length of 67 μs emitted at 1.5 MHz and a PRF of 10 Hz was not sufficient to mechanically engage the capillary walls, disrupt the blood-brain barrier and cause diffusion of gadodiamide thereafter. Definity® microbubbles were used in this study, which are poly-dispersed, with a mean diameter of 1.1 – 3.3 μm, which is comparatively smaller than the brain capillary mean diameter (4-10 μm), and thus induced opening only when the pulse length was increased to 0.67 ms and beyond. Therefore, it could be assumed that the duration of mechanical stress exerted on the capillary walls during each pulse need to be sustained over a sufficient period of time to induce BBB opening.

Another interesting finding is that there were no significant differences between 0.45 MPa and 0.60 MPa in the closing timeline, when the PL remained the same (Figure 15 (a), (b), (c)). This finding indicates that, since the effect on the BBB opening volume and duration is not affected by the increase in the acoustic pressure from 0.45 MPa to 0.60 MPa, higher acoustic pressures should be avoided in order to achieve homogeneity of molecular diffusion.

At higher PNPs (0.45 MPa and 0.60 MPa), despite the fact that the BBB opening characteristics (Ktrans, VBBB, closing timeline) were similar between the 0.67-ms and 6.7-ms

PLs, they were entirely different compared to the 67-μs-PL. It has been shown that, at 0.45 MPa and 0.60 MPa, the microbubbles undergo inertial cavitation [21], which means that the microbubbles expand several times to their equilibrium radii and then collapse. This, therefore, implies that due to the inertial cavitation, the microbubble activity and interaction with the capillary walls were significantly enhanced during a PL of 0.67 ms compared to a PL of 6.7 μs while, also, there was not much difference induced compared to 6.7 ms. So, the assumption that can be made here is that inertial cavitation is not fully exploited at very short non burst-ed PL (i.e. 67 μs) and, after 0.67 ms all bubbles would likely be destroyed, with additional cycles becoming redundant.

The results indicated that the effect on the Ktrans, VBBB and closing timeline of the PNP at 0.45-MPa- or 0.60-MPa at 67-μs-PL was similar to the PNP at 0.30MPa and PL of 0.67-ms. The effect of higher PNPs (0.45 MPa and 0.60 MPa) with a PL of 0.67-ms was also similar to that of PNP at 0.30MPa and PL of 0.67-ms. It is also interesting that the Ktrans histograms (Figure 4) among the PL/PNPs combinations that had similar closing timeline were also quite similar. For example, despite the fact that the average K¬trans¬ as shown in Figure 16 is the same among several groups, only the groups that had an increased volume with very high Ktrans (red cluster) required more time for BBB restoration. This finding suggests that the time required for closing, is strongly dependent on the volume of opening that has highly increased permeability after FUS. Also, in the aforementioned cases, the fact that the BBB opening induced with the use of a low PNP with a long PL was similar to that induced by a higher PNP with a shorter PL, suggests that there is a beneficial “complementary” relationship between the elongation of the PL and the decrease of the PNP, and vice versa.

At the longest PL studied (6.7 ms), a PNP of 0.45 MPa induced a BBB with a consistently higher Ktrans and VBBB compared to the case of 0.60 MPa (Figure 16, Figure 18 and Figure 19). One possible explanation is that the effect of inertial cavitation is more pronounced at 0.60 MPa compared to 0.45 MPa [21].

As mentioned above, it has been previously shown that the BBB opening acoustic pressure threshold is pulse-length dependent [10],[11],[12], [18]. However, the underlying BBB characteristics, such as the permeability, volume of opening and reversibility timeline, had not been investigated until now. First, McDannold et al. [10] have also shown that the acoustic threshold pressure for BBB opening is pulse-length dependent. Testing was performed with mainly longer pulse lengths than the ones used here, and more specifically, at 1-Hz PRF (at 0.69 MHz, with Optison), BBB opening threshold was at 0.60, 0.47 and 0.36 MPa for 0.1, 1 and 10 ms pulse lengths respectively. Moreover, using closely-timed short pulses, O’Reilly et al. [18] reported a semi-log relationship between the MR enhancement and the number of burst cycles, with a minimum of a 3-μs burst at 1 Hz (1.18 MHz center frequency, Definity microbbubles) required to induce opening which is in agreement with the results shown in this study.

Furthermore, there was no additional benefit in the outcome when the number of cycles was increased. The volume of opening, the permeability or the reversibility timeline of BBB opening were not assessed in the aforementioned studies, rendering a direct comparison with the aforementioned studies impossible. This study provides further insight in the underlying physiology for a range of acoustic parameters that have been shown to play a critical role in BBB opening.

Using the same center frequency (1.5 MHz) and microbubbles (Definity) as in this study, Choi et al. [11] showed that with a PRF of 10 Hz and an acoustic pressure of 0.46 MPa, 0.1, 0.2, 1.0 and 2.0 ms pulse lengths led to significant increase of the Dextran diffusion compared to the control group. Opening, however, could still be achieved at 33 μs, and pulse lengths of 10, 20 and 30 ms led to a significant increase in the FUS-induced BBB opening compared to 0.033-, 0.1- and 0.2-ms PLs induced, without any significant difference among them. In this study, we showed that both the permeability and volume of opening as induced at 0.45 MPa at 0.67 ms (1000 cycles) PL were significantly higher than at 0.067 ms (100 cycles) PL, but not different from 6.7 ms (10000 cycles) PL; these results are in agreement with what was previously reported in Choi et al. [11]. Choi et al. [12] showed that, if pulses are grouped into bursts, emitted at a certain burst repetition frequency (BRF) allowing intervals between bursts, while increasing the PRF, the disruption of the BBB is possible at a significantly lower number of cycles, i.e. at 100-kHz PRF and 5-Hz BRF, even with 3-cycle PL, BBB can be disrupted. The study of the PL effect using bursts can be challenging with the respect to the resolution when using DCE-MRI due to the inadequate resolution of MRI, typically on the order of 100 μm compared to only a few μm that fluorescent microscopy allows, and therefore was not studied here.

The effect of the poly-dispersity of the bubbles used, compared to what has been previously reported for mono-dispersed microbubbles (1-2, 4-5 and 6-8 μm in diameter) at similar acoustic parameters [15],[16] should be taken into account. First, in those studies, it was shown that only the 4-5μm and 6-8 μm bubbles were capable of inducing physiologic changes (permeability and BBB opening volume) at 100 cycles and 0.30 MPa, whereas the 1-2 μm mono-dispersed microbubbles could not. This could be attributed to the fact that, albeit being highly polydisperse, the Definity mean diameter (1.1- 3.3 μm) falls closer in range of the 1-2 μm bubbles previously studied. Also, when the higher pressures of 0.45 MPa and 0.60 MPa were used, the permeability, the volume of opening, and the reversibility timeline at 6.7 μs with Definity were similar to what has been reported for the 1-2 μm bubbles [15],[16], and significantly lower than what has been reported for the 4-5 μm and 6-8 μm bubbles. These results suggest that the higher range of diameters -larger than 2 μm- contained in the poly-dispersed dose of Definity injected before sonication, were not sufficient to increase the bioeffects and efficacy of Definity above the level that the 1-2 μm mono-dispersed bubbles were shown to, since their effect on the BBB opening permeability, volume and reversibility timeline are quite similar.

In this study, a linear relationship was established between the time required for BBB closing and the volume of opening. It was found that the time required for closing increased monotonically. These results indicate that the duration of the induced BBB opening could be predicted based on the volume of opening in agreement with what was previously reported [16].

In contrast with the previously reported Ktrans measurement methods developed by our group [15], in this study the average Ktrans was estimated over a VOI of 52 mm3 which overlapped with the targeted region, instead of a small circular region of 1 mm in diameter. This method effectively provided a better approximation of the Ktrans because the changes in the whole BBB opened volume were taken into account, avoiding overestimation of the Ktrans due to focusing within a smaller area. Additionally, the stacked histograms showing the volume of each Ktrans cluster (Figure 17) for all the combinations of PL and PNP tested, were found to better illustrate the non-uniform distribution of Ktrans changes within the opened region. It should be noted that the of Ktrans distributions were also highly correlated with the closing timelines.

There are several limitations associated with this study. One limitation could be due to the MR sensitivity resolution. The resolution was optimized but the small BBB disruptions may still remain undetectable. Also, since DCE MR images were acquired there was approximately a 1h interval between the acquisition of the first MRI image and the FUS application, during which the volume of opening could have decreased, especially for the cases of minute disruptions. A similar limitation is associated with the detection of closing. The animals with detectable but small openings were imaged 8 h after sonication. The rest of the animals were imaged in 24-h intervals, i.e., the time that was reported as “time required for closing” could be overestimated within the range of the time interval between the final two consecutive MRI scans. Finally, the detection and characterization of BBB opening, and thus the closing timeline, is dependent on the size of the tracer used. In this study, Ktrans, VBBB and closing timeline were associated with the contrast agent used, i.e. gadodiamide, which has a very low molecular weight (574 Da). Larger MR tracers as tracers may be associated with different timelines than those reported in this paper.

3.2.6. Conclusion

In this longitudinal study, the dependence of the BBB opening permeability, volume and reversibility timeline on the acoustic pulse length and peak rarefactional FUS pressure was established. It was found that, with the use of Definity microbubbles, at relatively low peak rarefactional pressures (0.3 MPa), a longer pulse length was required to induce BBB opening. When higher pressures were used, i.e., 0.45 MPa and 0.60 MPa, short pulse lengths were found to be sufficient for opening while an increase in the pulse length enhanced all BBB opening characteristics. It was also found that the duration of BBB opening was linearly proportional to the initial volume of opening. Finally, there was no histological damage detected in any of the animals studied, indicating that all methodology parameters used here fell within the safety window of the technique.

Section 3.3.: Contribution

In this chapter, a thorough analysis on the reversibility timeline and the pharmacokinetics of the FUS-induced BBB opening was performed along with optimization of parameters to allow the design of a method for safe and efficient BBB opening, focusing on the effect of the microbubble sizes and the pulse length.

The reversibility timeline [6], [63], [65], [66], [91], [92] as well as the pharmacokinetic analysis[55, p. 20], [107] of the BBB had been previously studied. However, the self-repairing, spatially and temporally, characteristic of the BBB was shown and analyzed here for the first time. The correlation of the time required for closing and the physiologic changes after the FUS-induced BBB disruption was also investigated for the first time here. The reversibility timeline was found to be proportional to the volume of opening on the day of opening, while the average permeability changes were found less reliable for closing prediction. This analysis of the safety profile of this technique is of critical importance in order to consider a clinical application.

Following an acoustic parameter optimization set of studies, a trade-off between the acoustic pressure, the microbubble size and the pulse length was shown. The major contribution was therefore the confinement of the combination of these acoustic parameters within a safe and efficient window which can then be used for drug delivery and treatment in mice CNS animal models, and also for the pre-clinical translation of the technique in non-human primates as shown in Figure 22. The results of these studies have been published in peer reviewed scientific journals [9], [10].

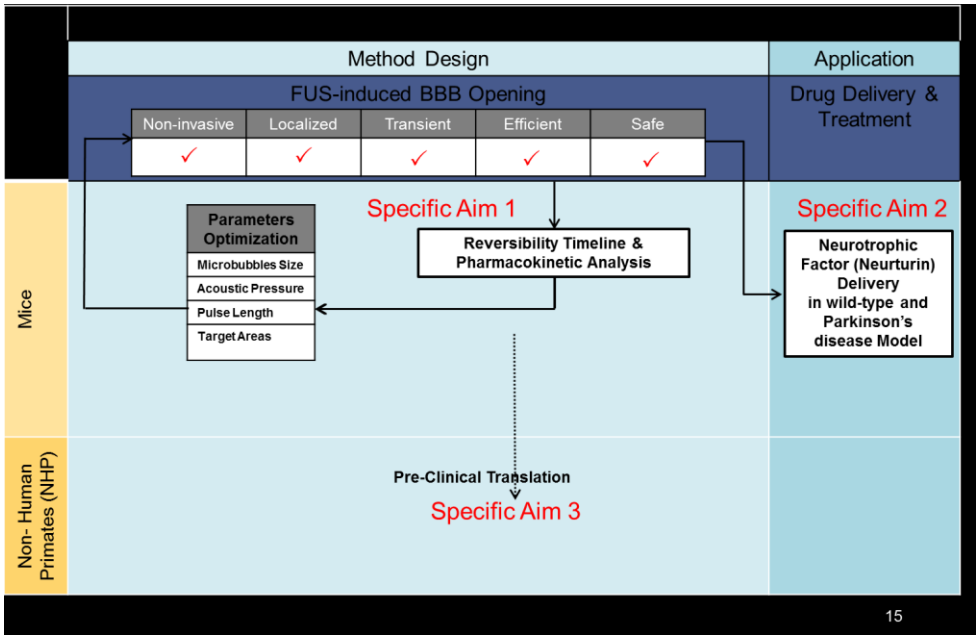

Figure 22. Completion of the specific aim 1 and relation to specific aims 2 and 3.

Regarding the research contribution, Babak Baseri, M.D. (Biomedical Engineering, Columbia University) and James Choi, PhD (Columbia University) mentored the experimental technique, Yao-Sheng Tung, PhD (Biomedical Engineering, Columbia University) assisted with the experimental procudures, Fotios Vlachos PhD (Biomedical Engineering, Columbia University) mentored and assisted with MRI scans, data acquisition, data processing and data interpretation. Jameel Feshitan, PhD (Chemical Engineering, Columbia University) and Mark Borden, PhD (Chemical Engineering, Columbia University) assisted with the microbubble manufacturing and size isolation technique.

CHAPTER FOUR:

Quantitative assessment of the delivery of the Neurturin (NTN) neurotrophic factor to specific murine brain targets and potential reversibility of Parkinson's disease phenotype

Having designed a method that can induce safe and efficient BBB opening in mice as demonstrated in Chapter 3, along with the reversibility timeline and pharmacokinetic analyses, the next specific aim and milestone was the use of the FUS method for drug delivery in an animal disease-model as shown in Figure 23. In chapter 3, the studies were targeting the hippocampus, a formation profoundly affected in Alzheimer's disease. In this chapter, the interest was switched to Parkinson's disease which is the second most important CNS disease.

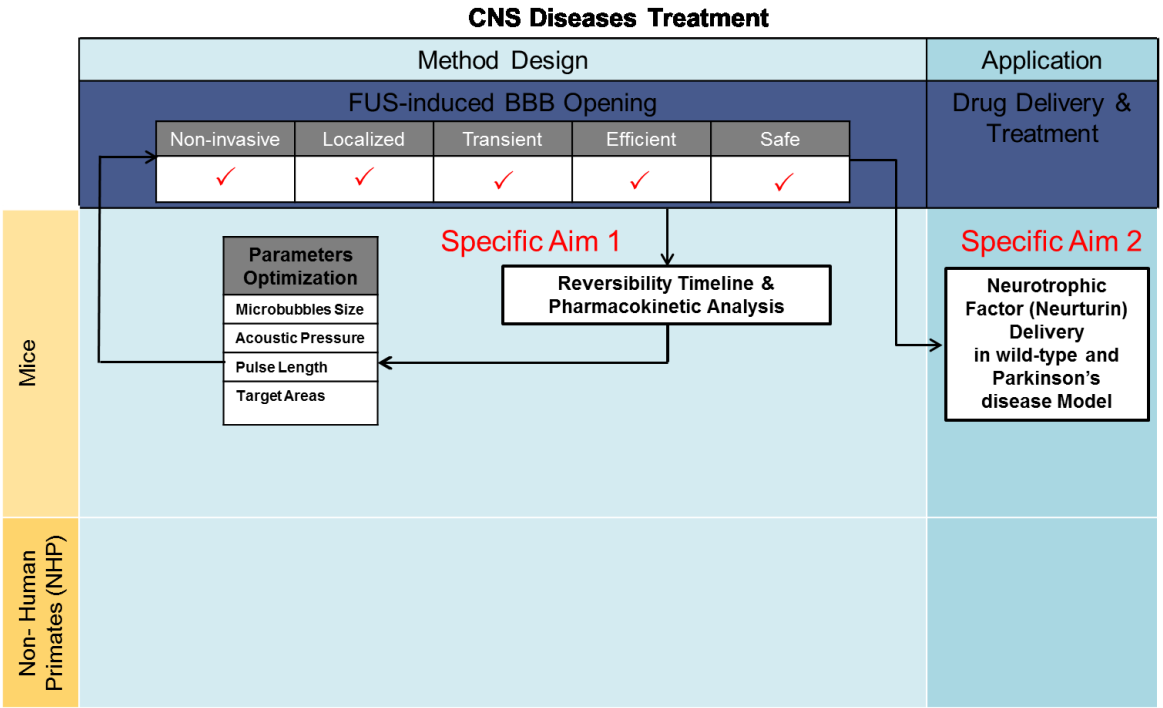

Figure 23. Relation between the first and second specific aims

This specific aim had to be divided into two studies in order to ensure success. First, the method design for optimal BBB opening had to be evaluated for the brain regions affected in PD as well as for the drug of interest which was available to our research group, i.e. Neurturin, which

is a neurotrophic factor. Therefore, the enhanced delivery of Neurturin through the FUS-induced BBB opening was first established in wild-type mice. Second, application of the technique was performed after a study design that would allow the demonstration of any potential reversibility in Parkinson's disease phenotype, i.e. neurodegeneration, following the FUS-enhanced delivery of Neurturin, in a PD model.

Section 4.1: Localized Delivery of the Neurturin (NTN) Neurotrophic Factor through Focused Ultrasound-Mediated Blood-Brain Barrier Opening in wild-type mice

4.1.1. Abstract

The blood-brain barrier (BBB) constitutes a major obstacle in brain drug delivery. Focused Ultrasound (FUS) in conjunction with microbubbles has been shown to open the BBB non-invasively, locally and transiently to allow large molecules diffusion. Neurturin (NTN), a member of the GDNF family, has been demonstrated to have neuroprotective and regenerative effects on dopaminergic neurons in vivo using invasive drug delivery methods. The brain's ascending nigrostriatal pathway is severely damaged in Parkinson's disease (PD), and therefore the Substantia Nigra (SN) and striatal Caudoputamen (CP) were selected as the target areas. The objective of the study was to investigate whether safe and efficient NTN delivery can be achieved through FUS-induced BBB opening via intravenous administration, and trigger the neuroregeneration cascade in the nigrostriatal pathway. Following the optimization of FUS parameters and target locations in the murine brain, NTN bioavailability and downstream signaling were detected and characterized through immunostaining. FUS significantly enhanced the delivery of NTN compared to the direct injection technique, while triggering of the signaling cascade was detected downstream to the neuronal nuclei. These findings thus indicate the potential of the FUS method to mediate transport of proteins through the blood-brain barrier in a PD animal model.

4.1.2. Introduction

To date, there are no central nervous system (CNS) disease-modifying treatments, except for treatments limited to the symptomatic relief of such diseases, such as Alzheimer's and Parkinson's. Neurotrophic factors, i.e., such as members of the glial cell-derived neurotrophic family glial-derived neurotrophic factor (GDNF), neurturin (NTN) and brain-derived neurotrophic factor (BDNF), are proteins with therapeutic potential in the treatment of CNS neurodegenerative

diseases through neuroprotection and neuroregeneration. The blood-brain barrier (BBB) is the rate-limiting factor for the treatment of the central nervous system (CNS) diseases as it hinders drugs and other agents from reaching their end-targets at the brain parenchyma [3], [122]. Meanwhile, FUS in conjunction with systemically administered microbubbles has been shown to be the sole non-invasive method to open the BBB locally and safely [7], [8], [124], [125], and to allow the penetration of molecules including pharmacologically-relevant agents and drugs such as anti-cancer therapeutic drugs, therapeutic antibodies, neurotrophic factors, adeno-associated virus and neural stem cells. [61], [62], [74]–[76], [79], [81], [85], [86], [126].

Parkinson's disease (PD) is a neurodegenerative disorder where severe damage is observed in the dopaminergic neuronal cell bodies in the Substantia Nigra (SN) which are projecting their terminals in the Caudate-Putamen (CP) [127]. Previous studies have shown that GDNF has a strong therapeutic potential in rodents [128], non-human primates [129]–[132] and PD patients in a phase I clinical trial [133]–[135] with restoration of dopaminergic (DA) neurons and functional improvements; however, there have been conflicting findings in phase II clinical trials [136], [137] and studies were halted due to safety concerns, including but not limited to the presence of neutralizing antibodies to GDNF in some patients. As an alternative to GDNF, NTN has been demonstrated to have enormous neuroprotective and neuroregenerative effects on DA neurons and trophic effects on the parkinsonian brain through intrastriatal injections in rodent PD models [12], [13], convection-enhanced delivery (CED) in a non-human primate PD model [14] as well as intracranial lentiviral (AAV2) injection [138]. AAV2-neurturin gene therapy in PD patients showed that both SN and CP have to be targeted as terminal fields to ensure maximal benefits [139], and therefore, in the more recent clinical trial [140], two infusions through one needle tract for the SN and three infusions through three needle tracts in the CP, passing through a single burr hole per hemisphere, were performed.

The aim of this study was the efficient *in vivo* delivery of systemically administered NTN via the safely, locally and reversibly opened BBB through FUS to the brain parenchyma, followed by downstream bioactivity to the neurons in wild type mice. In the first part of the study, FUS acoustic parameters and targeting sonication locations for efficient and safe BBB opening at the SN and CP were investigated and optimized, using molecules of similar size to NTN (MW: 23. 6 kDa), i.e. fluorescently tagged dextrans. MRI was used for the quantification of the BBB-opening volume (V_{BBB}), permeability mapping, i.e. transfer rate of gadolinium from blood-plasma to the extravascular, extracellular space (K_{trans}), as well as the opening's reversibility timeline. In the second part, NTN was administered after FUS treatment, and brains were harvested for the assessment and quantification of the diffusion as well as bioactivity through downstream signaling, the outcome was also compared to NTN direct injection findings.

Objective	Number of animals	Son.Loc. CP/SN	Agent or Drug administered	Survival time	Method
Acoustic parameters and Sonication Locations optimization	n=5 n=5 & n=10	1/1 (PL: 5000) 1/1 & 2/1 (PL: 10000)	Gd-DTPA-BMA (6 mmol/g) & Fluorescent Dextrans (60 μg/g)	1h or 1week	MRI & Fluorescence Microscopy
NTN delivery & bioactivity assessment after FUS	n=6 n=6	1/1 2/1	NTN (20 μg/g) or Saline (iv 2μl/g)	1 h	MRI & Immunostaining
NTN delivery assessment after D.I.	n=2	-/- (No FUS)	NTN (0.02 μg/g ~0.5 μg per mouse per target area)	1 h	Immunostaining

PL: Pulse Length (cycles)

Son. loc. CP/SN: Number of Sonication locations at Caudate-Putamen and Substantia Nigra; 1/1 : one sonication location at CP and one sonication location at SN, 2/1: two sonication locations at CP and one sonication location at SN, -/-: no FUS

D.I.: Direct Injection

Table 7 Study Design

4.1.3. Materials and Methods

All animal experimental procedures were approved by the Columbia University Institutional Animal Care and Use Committee (IACUC) and Columbia University's Research and Compliance Administration System (RASCAL). All efforts were made to minimize animal suffering and to reduce the number of subjects used. As shown in Table 7**,** depending on each specific objective of this study, different methods and techniques were used in a total of 34 (n=34) wild-type adult male mice (strain: C57BL/6, Harlan Sprague Dawley, Indianapolis, IN, USA) weighing 20 to 25 g, with a minimum of two animals in one group and four in the other groups. Animals were individually housed under standard conditions (12 hours light/dark cycles, 22^{o}C), were fed a standard rodent chow (3kcal/g; Harlan Laboratories, Indianapolis, IN, USA) and bidistilled water, and had *ad libitum* access to their diets and drinking water.

FUS

A single-element, spherical-segment FUS transducer (center frequency: 1.5 MHz, focal depth: 60mm, radius: 30mm; axial full-width half-maximum intensity: 7.5 mm, lateral full-width half-maximum intensity: 1 mm, Imasonic, France), driven by a function generator (Agilent, Palo Alto,

CA, USA) through a 50-dB power amplifier (E&I, Rochester, NY, USA) as shown in Figure 24 **(a)-(c)** was used to target the SN or the CP, as shown in Figure 24**(d)**. A needle hydrophone (HGL-0400, Onda Corp., Sunnyvale, CA) was used for the transducer calibration, which measured the acoustic beam profile in a tank filled with degassed water. A central void of the therapeutic transducer held a pulse-echo ultrasound transducer (center frequency: 10 MHz, focal depth: 60mm, radius 11.2 mm; Olympus NDT, Waltham, MA) used for alignment, with their two foci aligned. The imaging transducer was driven by a pulser-receiver (Olympus, Waltham, MA, USA) connected to a digitizer (Gage Applied Technologies, Inc., Lachine, QC, Canada). A cone filled with degassed and distilled water was mounted onto the transducer assembly. The transducers were attached to a computer-controlled 3D positioning system (Velmex Inc., Lachine, QC, Canada). A bolus of 1 µl/ g of body mass polydisperse manufactured in-house [106] microbubbles diluted in saline ($8x10^{8}$#/ mL, mean diameter: 1.4 µm) was intravenously injected immediately preceding the sonication at each target, i.e. SN or CP. A 20-min time interval was allowed between SN and CP targeting, to allow the microbubble concentration to be cleared from the circulation [141]. Each animal was sonicated for 60 s, with a pulse repetition frequency (PRF) of 10 Hz, with one or two sonication locations at each target in order to safely open the entire area of interest with acoustic parameters that do not cause damage, at peak negative acoustic pressure (PNP) of 0.45 MPa [9], [10] after accounting for 18% and 33% murine skull attenuation for the SN and CP respectively.

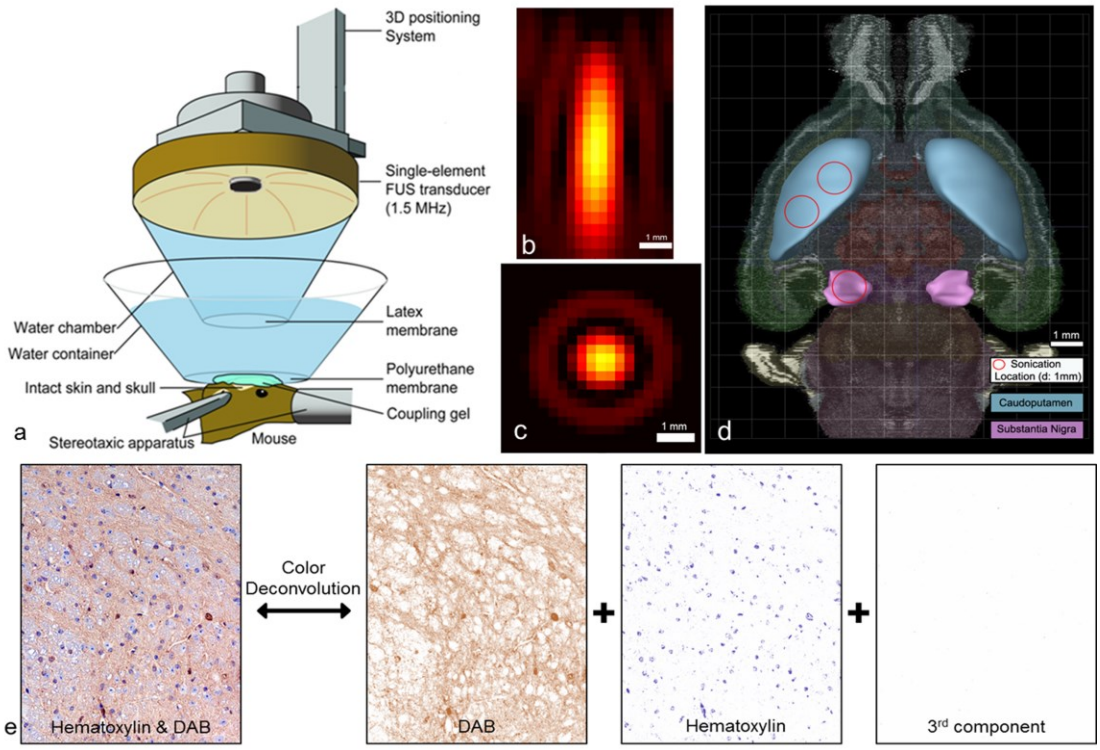

Figure 24 Methods (a) Experimental Setup, (b) Lateral focal beam profile, (c) Axial focal beam profile, (d) Axial brain section overlaid with the sonication locations targeted at the formations of interest, i.e. Caudoputamen (CP) and Substantia Nigra (SN), adapted from Allen Brain Atlas, (e) An example of color deconvolution which was used to calculate the contribution of each stain to the RGB image. All samples were stained with DAB and Hematoxylin, and using this robust method the DAB color could be extracted and used for qualitative and quantitative measurements.

Acoustic parameters and Sonication Locations optimization

The PL tested varied between 5500 cycles (3.3 ms) and 10000 cycles (6.6 ms) in order to investigate which parameter would induce more efficient drug delivery to the areas of interest. It has been previously shown that the PL plays an important role in the BBB opening characteristics, such as the permeability and the volume of opening [10], as well as the closing timeline.

In order to target the SN, the transducer which was placed perpendicular to the brain surface, was aligned with the posterior fontanelle, i.e. the sagittal suture's junction with the lambdoid suture, with a method described elsewhere [125] and was then moved anteriorly 1.5 mm on the sagittal suture, and laterally 1.7 mm onto the left hemisphere, as shown in Figure 24**(d)**.

The CP is located in the striatum, which is a large area relative to the FUS focal size; it is therefore challenging to induce BBB opening in the entire CP using a single sonication. For example, it has been shown that the acoustic parameters used to increase the volume of opening with a single sonication can also increase the probability of damage [10],[9]. For this reason, the effect of having two non-overlapping sonication locations at that target was studied, each one at a relative low PL, aiming at inducing sufficient BBB opening while staying within the safe acoustic parameters range. When FUS was applied only at one sonication location, the transducer focus was moved 4.5 mm anteriorly from the posterior fontanelle, and 2.5 mm laterally to the sagittal suture. When FUS was applied at two ipsilateral non-overlapping sonication locations, the transducer focus was moved 4 mm anteriorly and 3 mm laterally for the first location, and was immediately moved after the first sonication 1 mm anteriorly and 1 mm laterally towards the sagittal suture for the second sonication location as shown in Figure 24**(d)**. There was no additional microbubble administration between the two sonications locations.

Fluorescence Microscopy

In the first objective, animals were injected with a bolus of fluorescein-tagged dextrans (Invitrogen, CA, USA) at a dosage of 6 µg/g of body mass, diluted in 100 µl of saline though the tail vein, immediately after sonication. Animals were transcardially perfused 1 h following FUS, with 30 mL PBS and 60 mL 4% paraformaldehyde. Heads were soaked in paraformaldehyde for 24h. Skulls were removed, and the brains were fixed again in 4% paraformaldehyde for 24 h, and transferred to 10% (30 min), 20% (60 min), and 30% (24 h) sucrose solutions for cryoprotection. Brain samples were then embedded in an optimal cutting temperature medium and were frozen using dry ice and isopentane. Frozen blocks were sectioned horizontally at 60 µm thickness for fluorescent imaging. Fluorescence images were acquired using a fluorescence microscope (BX61; Olympus, Melville, NY, USA) with a filter set at excitation and emission wavelengths of 490 and 525 nm, respectively.

MRI

All mice were imaged using a 9.4 T vertical bore microimaging MRI system (DRX400, Bruker, Biospin, Billerica, MA, USA). Each mouse was scanned 20-30 min after sonication, using a 30-mm-diameter 1H resonator. Isoflurane gas (1-2%) was used to keep the mouse anesthetized at 50-70 breaths/min during the entire MRI procedure. On the day of sonication, Dynamic Contrast-Enhanced MR imaging (DCE-MRI) was performed using a 2D FLASH T1- weighted sequence (40 acquisitions, 192×128 matrix size, in-plane resolution: 130×130 μm^2, slice thickness: 600 µm, TR/TE=230/2.9 ms). During the 3rd acquisition of the dynamic sequence, a 0.30-mL non-diluted

bolus of Gd-DTPA-BMA (Omniscan, 287 mg/ mL) was injected intraperitoneally (IP) and was used as a tracer to depict the area of opening, as shown in Figure 2(a).After completion of DCE-MRI, a post-contrast enhancement, T1-weighted 2D FLASH high-resolution acquisition (TR/TE: 230/3.3 ms, resolution 100 μm x 100 μm, slice thickness: 400 μm) was acquired. The scanning time of each DCE and T1-weighted MRI image was 40 min and 4 min respectively. Depending on the objective, T1-weighted MR imaging was repeated on a daily basis starting from the day of sonication (1 h) and lasting up to 1 week after sonication.

Permeability mapping, volume quantification and timeline

The general kinetic model (GKM) [142] was used to measure the BBB permeability following the the general expression of

$$\frac{dC_t}{dt} = K_{trans}C_p - K_{ep}C_t \quad (1)$$

where C_t is the tracer concentration in the extravascular extracellular space (EES) at time t, C_p is the tracer concentration in the blood plasma and K_{trans} and K_{ep} are the transfer rate constants from the intravascular system to the EES and backwards respectively. The consecutive images from the DCE-MRI were entered in a custom algorithm implemented on Matlab (MathWorks, Inc. Natick, MA, USA), with a method described elsewhere [55], and K_{trans} maps were generated. The maps when then overlaid onto the MR images to provide information on the BBB opening permeability characteristics as shown in Figure 3(a).

The volume of opening (V_{BBB}) and reversibility timeline were quantified by processing the high resolution T1-weighted images with a custom algorithm in Matlab (MathWorks, Inc. Natick, MA, USA) as described elsewhere [9]. A 3D reconstruction of the opening in CP and SN is shown in Figure 2(a). Thresholded voxels within the VOI with signal intensity (S.I.) of 2.5 standard deviations or above the S.I. of a reference region in the non-sonicated area, counted towards the opening volume while the volume of contrast-enhanced vasculature was excluded. The longitudinal measurements, i.e. the closing timeline, are shown in Figure 3(b).

NTN administration

Human Neurturin neurotrophic factor (NTN, Invitrogen, CA, USA) was injected via a tail vein bolus injection at dosage of 20 μg/ g diluted in saline immediately after sonication and mice were survived for 1 h to allow sufficient time for circulation and bioactivity effects (see Table 7).

In order to investigate the advantage of using FUS for NTN delivery to the brain, over the conventional method of direct injection, experiments with direct injection of 5 μg/g in the CP and 5

μg/g in the SN, diluted in saline (9.8 mg/ mL) with a total volume of 0.02 μl/ g, were performed on two (n=2) mice (see Table 1). Using a stereotaxic frame, one hole for SN and one hole for CP were opened with the use of a surgical drill on the skull surface. To reach the SN, the hole through which the needle was inserted into the brain was 3.7 mm posterior to the bregma and 1.85 mm lateral, and it was injected 5 mm deep from the skull surface. To reach the CP, the hole was opened 1 mm posterior to the bregma and 2.2 mm lateral, and the needle was injected at a depth of 3 mm. The needle syringe was withdrawn 5 min after injection at each location, to avoid potential back flow of NTN via the needle path outside the brain.

Tissue Fixation and Staining

Animals were sacrificed and transcardially perfused with 30 mL PBS and 60 mL 4% paraformaldehyde. All heads were soaked in paraformaldehyde for 24h. Skulls were removed, and the brains were fixed again in 4% paraformaldehyde for 6 days, followed by conventional post-fixation procedures. Paraffin-embedded specimens were sectioned horizontally at a thickness of 6-10 μm covering the SN and CP formations.

For the detection of bioactivity and the downstream signaling cascade of NTN, four primary antibodies were selected: an antibody against human NTN (anti-NTN Ab8061, Abcam, MA,USA), an antibody against phosphorylated Ret (p-Ret rabbit, Tyr 1062, Santa Cruz Biotechnology, USA) which is a receptor tyrosine kinase on the neuronal cell surface with NTN specificity, an antibody against phosphorylated ERK1/2 (Phospho-p44/42 MAPK (Erk1/2), Cell Signaling Technology, MA, USA),which is a cytoplasmic protein kinase which promotes neuronal growth and differentiation, and finally an antibody against phosphorylated CREB (p-CREB-1 Antibody (Ser 133), Santa Cruz Biotechnology, CA, USA) which is a transcription factor in the neuronal nucleus.

A standard protocol for deparaffinization and hydration was then followed. Sections were put in citrate buffer (1L, pH 6) in a pressure cooker and microwaved for 20 min, then let to cool down for 30 min at room temperature for antigen retrieval. Slides were then washed in dH_2O one time and in PBS three times for 5 min each, incubated in 30% hydrogen peroxide in PBS for 10 min, and washed again in dH_2O and PBS. 10%, 10%, 10% and 5% normal goat serum was used for blocking for 20 min for human NTN, Ret, ERK1/2 and CREB respectively. The blocking serum was then removed and the primary antibody to each section was added; anti-NTN (1:100) p-Ret(1:100 rabbit), p-ERK1/2 (1:200 rabbit) and phospho-CREB (1:200 goat). The slides were then washed in PBS three times for 5 min each. ABC reagent (A 1:50, B 1:50 in PBS 30min prior mixed) were added for 30min at room temperature. Slides were again washed in PBS three times

for 5 mins each. DAB solution was added to each section (DAKO North America, CA, USA), and as soon as the sections developed (brown stain) the slides were immersed in dH_2O, and counterstained with Hematoxylin (dark blue/purple stain), were dehydrated and mounted with coverslips.

Imaging and Staining Quantification

Bright-field images were acquired using a light microscope (BX61; Olympus, Melville, NY, USA) and were white corrected. The mean DAB intensity was computed using an algorithm implemented in Matlab (MathWorks, Inc. Natick, MA, USA) using the color deconvolution method [143] for sections that had developed with DAB and were counterstained with Hematoxylin, as shown in Figure 24**(e)**. DAB intensity was used for immunostaining detection of NTN diffusion through the BBB and bioavailability to different brain regions, and the areas of bioavailability thereafter as shown in Figure 27, as well as for the downstream molecules phosphorylation as shown in **Figure 28, Figure 29** and **Figure 30.**

4.1.4. Results

Optimization of Acoustic Parameters and Targeting Sonication Locations for efficient drug delivery

The PL for efficient drug delivery was determined upon the comparison of the diffusion of dextrans (40 kDa) and Gd-DTPA-BMA, which is a small tracer (574 Da), that was administered via intra-peritoneal injection in the same animal each time. Even though the MRI contrast agent when used as an opening tracer showed diffusion in relatively large areas at both PL's in both the SN and CP as shown in Figure 25**(a)**, dextrans diffused in smaller areas as shown in Figure 25**(b)-(d)** and did not sufficiently diffuse in those areas for the shorter PL as shown in Figure 25**(e)**. For these reasons, the PL of 10,000 cycles was selected for more efficient drug delivery.

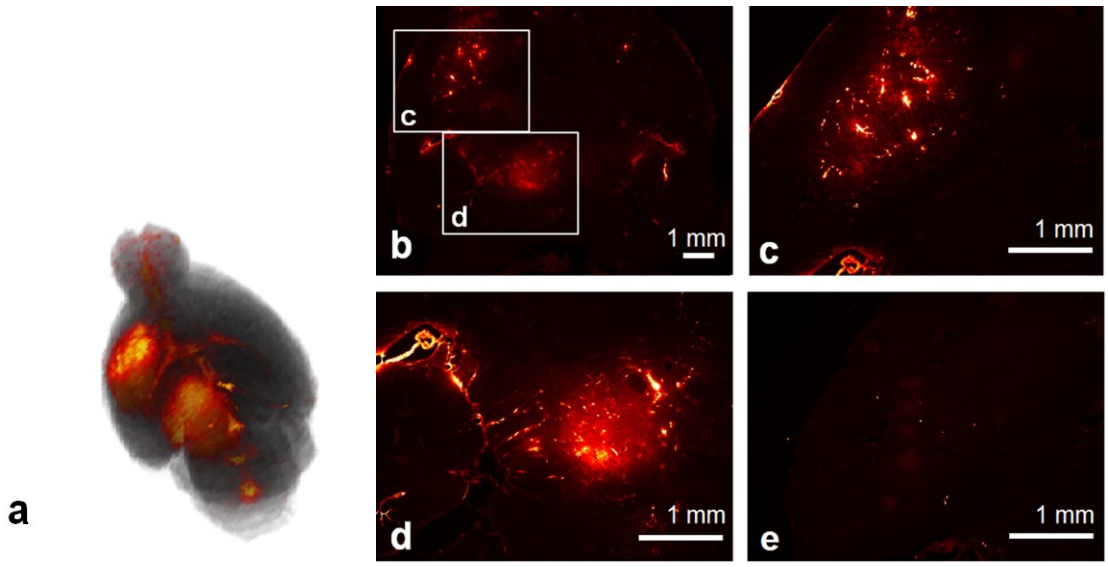

Figure 25 (a) 3D reconstructed T1-w MRI showing gadolinium diffusion, (b)- (d) Horizontal fluorescence microscope images showing fluorescent 40 kDa dextran diffusion in the same brain. The area where the larger molecule diffused was smaller compared to gadolinium. A 10,000 cycles PL was necessary for the diffusion of the 40 kDa dextran. (e) With a 5,000 cycle gadolinium could diffuse to the brain parenchyma, but the 40 kDa dextrans could not.

The design of a reversible BBB opening is critical for planning BBB opening for drug delivery. The results of the BBB opening characteristics (permeability, opening volume and timeline) before and after optimizing the sonication locations at each target are shown in **Figure 26**. In **Figure 26 (a)**, the permeability K_{trans} maps are shown. The two sonication locations at the CP increased the affected area at the two distinct foci without dramatic increases in permeability, which are also often correlated with damage [10], while covering the entire region of interest. One sonication location at the SN was sufficient to be covered entirely.

In **Figure 26 (b),** it is shown that when two sonication locations are targeted, which are non-overlapping, the overall opening volume is doubled, while the closing timeline is similar to that of 1 sonication location. The volume of opening after FUS could cover the entire CP with an average volume of opening 39.4 ± 4.1 mm^3 when two non-overlapping sonication locations were targeted. A single sonication location target could provide coverage of the entire SN with an opening volume of 18.6 ± 4.7 mm^3, while the BBB-openings were monitored longitudinally and their closing, i.e. reversibility timeline was found to 4-5 days for both the CP and SN.

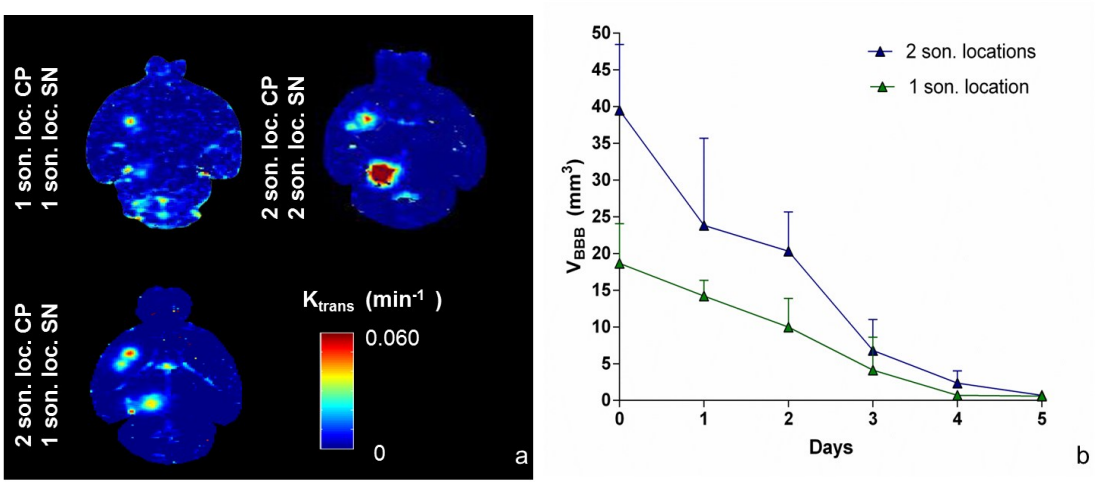

Figure 26 (a) Horizontal permeability maps showing the difference between 1 and 2 non-overlapping sonication locations (son.loc.) at each region of interest, i.e. Caudoputamen (CP) and Substantia Nigra (SN); the optimal was 2 son. loc. at the CP and 1 son. loc. at the SN. (b) Quantification and reversibility of the opening volume (VBBB); using 2 non-overlapping sonication locations VBBB was doubled without increase of the reversibility time.

NTN: Bioavailability

The immunostaining of human NTN after FUS BBB-opening is shown in Figure 27**.** In Figure 27**A** an example of one sonication location (son. loc.) at SN is shown, in Figure 27**B** an example of one son. loc. at the CP is shown, and in Figure 27**C** an example of two son. loc. at the CP is shown. In Figure 27**A(a)**, Figure 27**B(a)** and Figure 27**C(a)** the RGB low magnification (1.25x) images are shown, where the boundaries of the region of interest are outlined with a red dotted line, while the respective (b) and (c) are magnified at the targeted and contralateral regions. In order to better illustrate the bioavailability and diffusion of NTN, only the DAB channel, i.e. NTN, was extracted and is shown in (d)-(e) via color deconvolution, as was previously described and shown in Figure 24**e**. These findings indicate that the intravenously administered NTN diffused through the opened BBB into the brain parenchyma on the FUS-targeted side and, under high magnification, was detected in the extracellular space. NTN was not found to diffuse in the brain tissue in the non-targeted contralateral area following NTN circulation in the bloodstream, indicating highly localized delivery to the FUS targeted areas only. NTN bioavailability was increased two-fold in the CP when two sonication locations were used, suggesting that two sonication locations are preferred over a single location for the whole CP formation coverage.

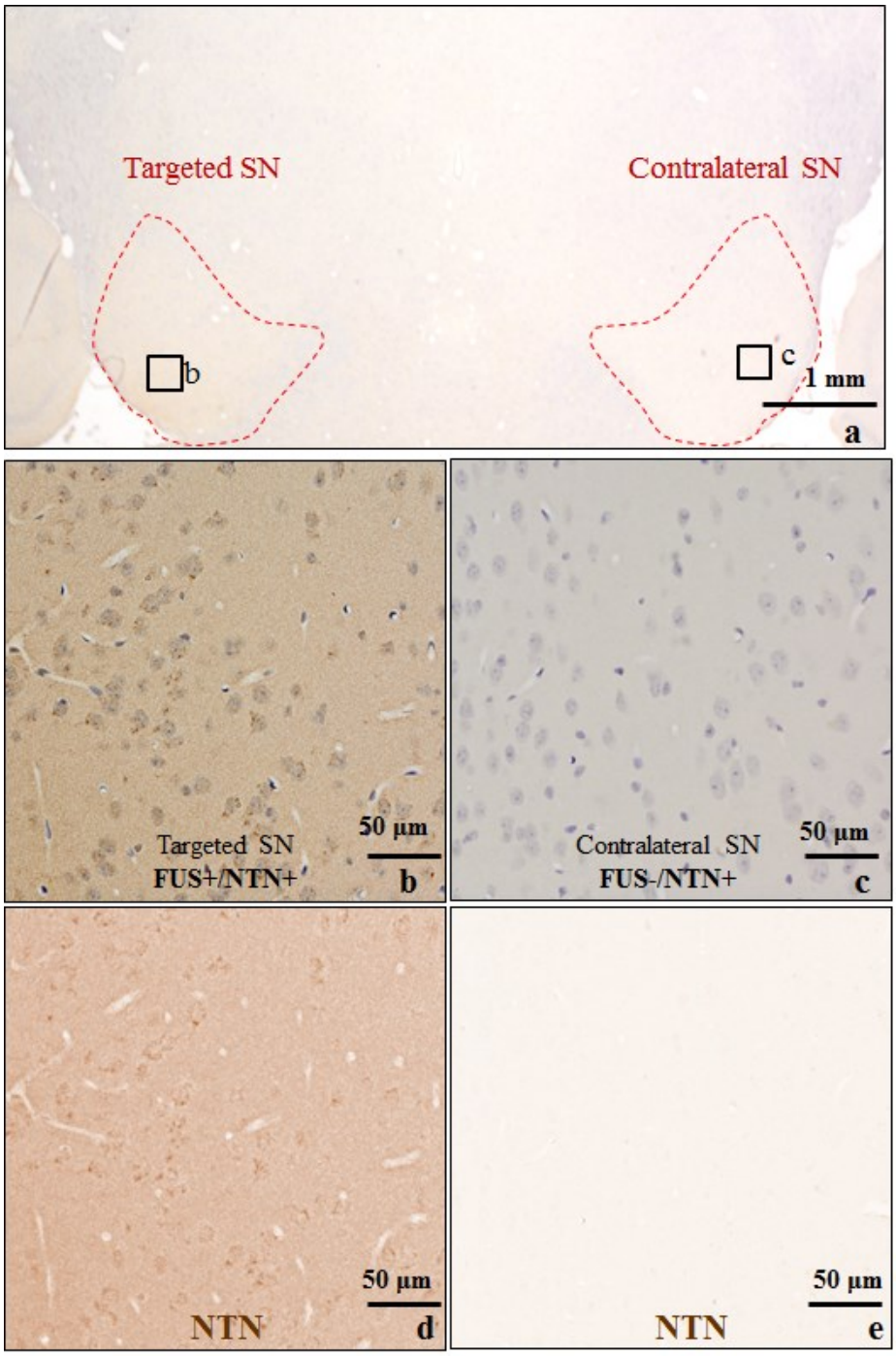
Targeted SN
Contralateral SN
b
c
1 mm
a
Targeted SN
FUS+/NTN+
50 μm
b
Contralateral SN
FUS-/NTN+
50 μm
c
50 μm
NTN
d
50 μm
NTN
e

A

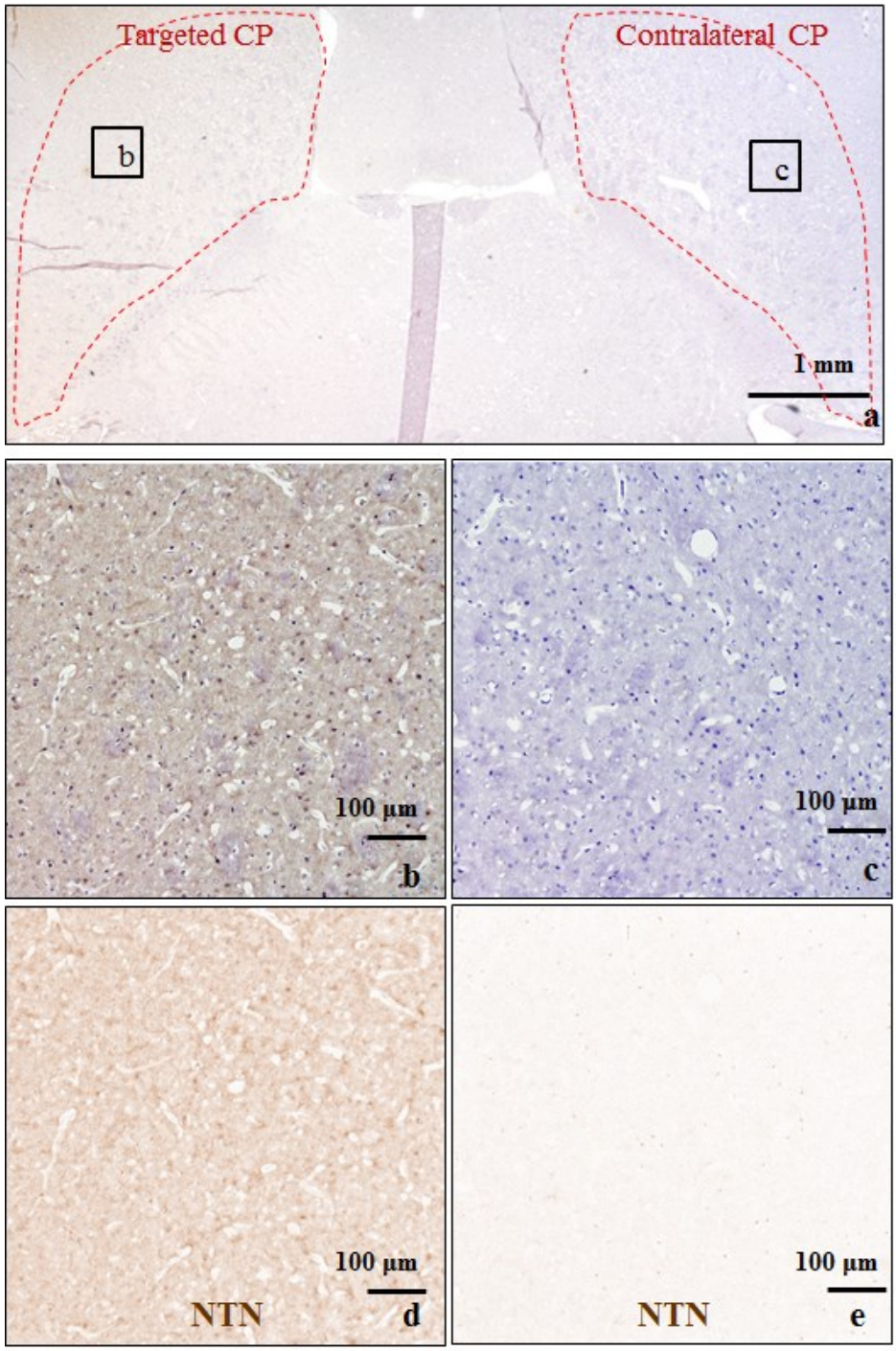
Targeted CP
Contralateral CP
b
c
1 mm
a
100 μm
b
100 μm
c
100 μm
NTN
d
100 μm
NTN
e

B

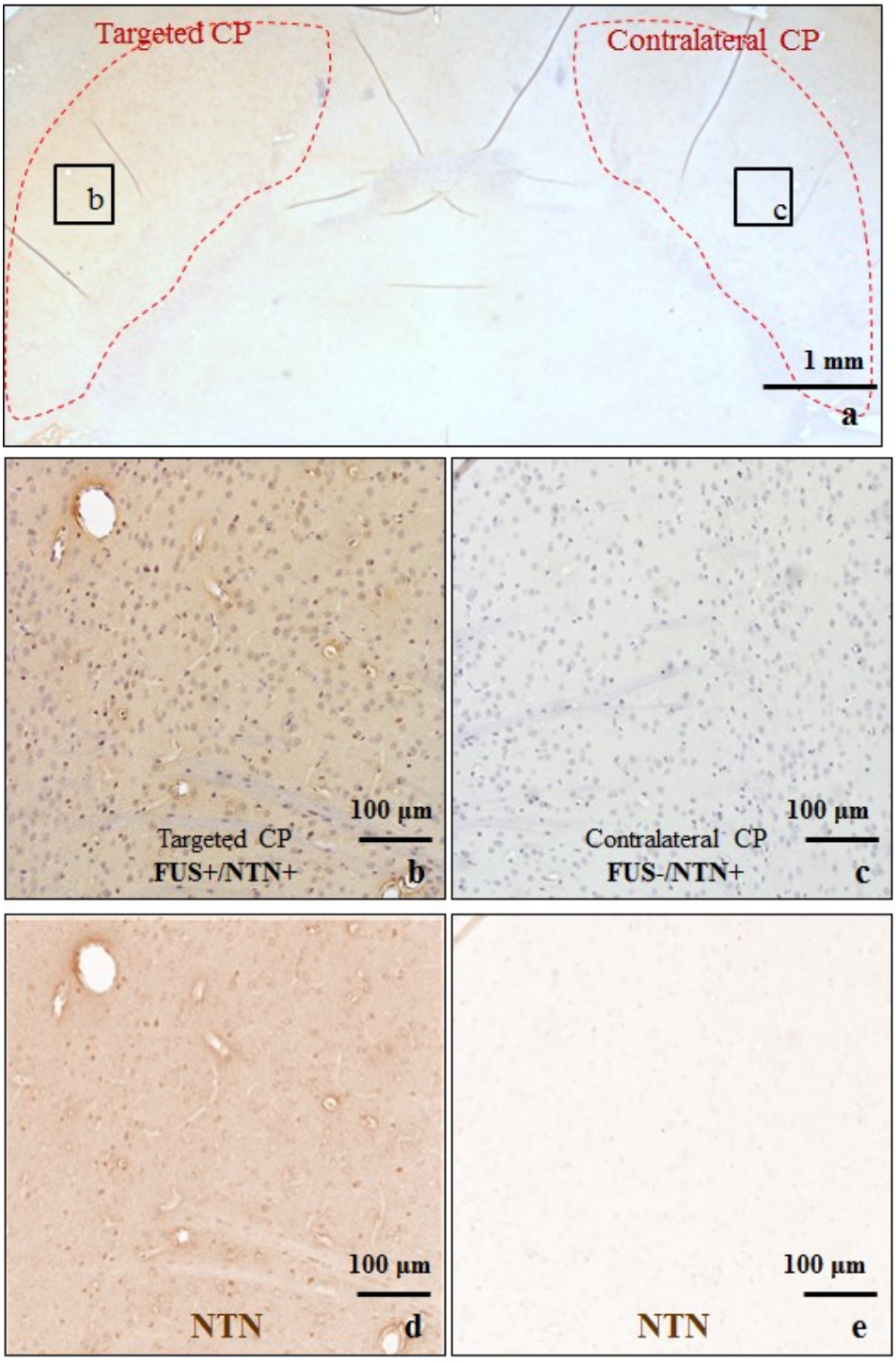
Targeted CP
Contralateral CP
b
c
1 mm
a
100 µm
Targeted CP
FUS+/NTN+
b
100 µm
Contralateral CP
FUS-/NTN+
c
100 µm
NTN
d
100 µm
NTN
e

C

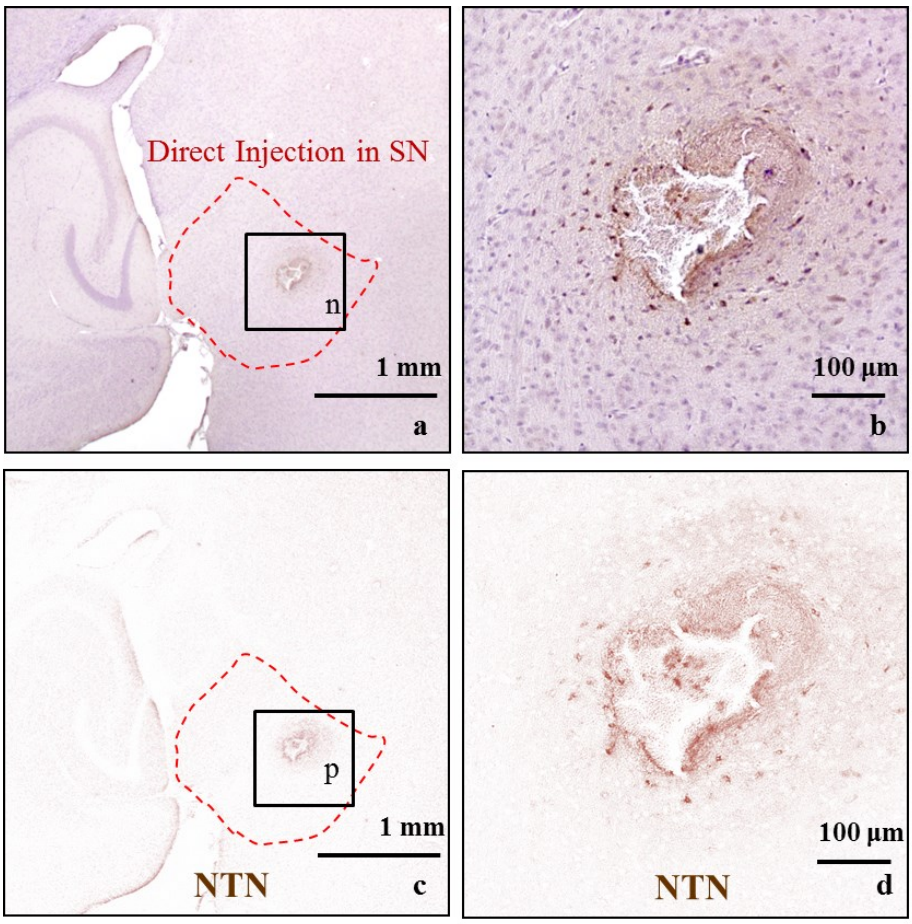

D

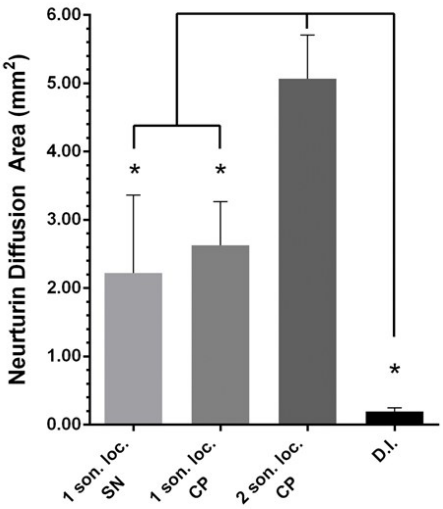

E

Figure 27 Horizontal section at the levels of SN or CP, which are outlined with red-dotted lines, immunostained for NTN (DAB development- brown colour) and counterstained with Hematoxylin:A: (a)

sonicated SN (1 son.loc.) and contralateral SN, (b)-(c) higher magnification at sonicated and contralateral SN respectively, (d)-(e) extraction of the DAB color only corresponding to NTN for (b)-(c) respectively. B: (a) sonicated CP (1 son.loc.CP) and contralateral CP, (b)-(c) higher magnification at sonicated and contralateral SN respectively, (d)-(e) extraction of the DAB color only corresponding to NTN for (b)-(c) respectively. C: (a) sonicated CP (2 son.loc.CP) and contralateral CP, (b)-(c) higher magnification at sonicated and contralateral SN respectively, (d)-(e) extraction of the DAB color only corresponding to NTN for (b)-(c) respectively. D: (a) direct injection to the SN, (b) higher magnification at the D.I. site, (c)-(d) extraction of the DAB color only corresponding to NTN for (a)and (b) respectively. NTN was successfully delivered to the targeted CP and/or SN, while the contralateral areas did not show evidence of NTN just due to the iv circulation. E: Area quantification of the NTN bioavailability, asterisks denote significance ($p<0.05$)

Immunostaining for NTN after D.I. in the SN is shown in Figure 27**D**, as indicated by a red dotted line in (a). The injection needle was inserted perpendicular to the plane of the figure. Under higher magnification, the area of NTN diffusion around the injection point is shown in (b). The DAB color for NTN was extracted from (a) and (b) and is shown in (c) and (d) where the diffusion area is better illustrated.

The area of bioavailability in horizontal sections corresponding to the center of the FUS beam at each target was directly calculated from the extracted DAB channel, i.e., NTN immunostaining following the color deconvolution (Figure 27**E)**. NTN bioavailability in the CP was found to be 5.07 mm^2 ± 0.64 mm^2 with two sonication locations used, compared to 2.63 ± 0.64 mm^2 with one sonication location was targeted**.** For the SN, the NTN bioavailability area was measured to be 2.25 ± 1.14 mm^2. The protein bioavailability after FUS was also compared to that with direct injection of NTN to the CP and SN formations independently, with the latter found to be limited to an average area of 0.20 ± 0.05 mm^2 around the injection site. The use of FUS significantly increased the bioavailability of NTN compared to D.I. in all cases studied. Using two sonication locations was found also to increase significantly the bioavailability by a two-fold increase compared to one sonication location, and by a 25-fold increase compared to D.I.

NTN: Bioactivity and downstream signaling

The signaling cascade of NTN starting from the neuronal membrane where the Ret receptor is found, to the axons where the cytoplasmic Erk1/2 can be found, and further downstream to the nucleus where the CREB transcription factor is located, was also activated within 1 h after IV administration as with immunostaining (Figure 28**-**Figure 30**)**. No immunostaining was detected in the contralateral sides, except for some areas in the close vicinity of some blood vessels, potentially due to perivascular transport as reported during cerebral infusion or CED delivery of neurotrophic factors [128]. In addition, no immunostaining was observed due to FUS only (results

not shown here).

In Figure 28**(a)** an RGB horizontal brain section including both the targeted SN and CP and their contralateral sides is shown, where DAB staining is for phosphorylated Ret (p-Ret). The p-Ret only color is shown in Figure 28**(b)**. Under higher magnification as shown in Figure 28 **(c)-(d)** and **(g)-(h)** and in the corresponding p-Ret only images are shown in Figure 28**(e)-(f)** and **(i)-(j)**, p-Ret expression was increased in the targeted areas compared to the contralateral side, and the immunostaining was detected in the neuronal bodies as well as in the dendrites and axon terminals, where the receptor is supposed to be located. There was increased p-Ret staining in the CP compared to the SN.

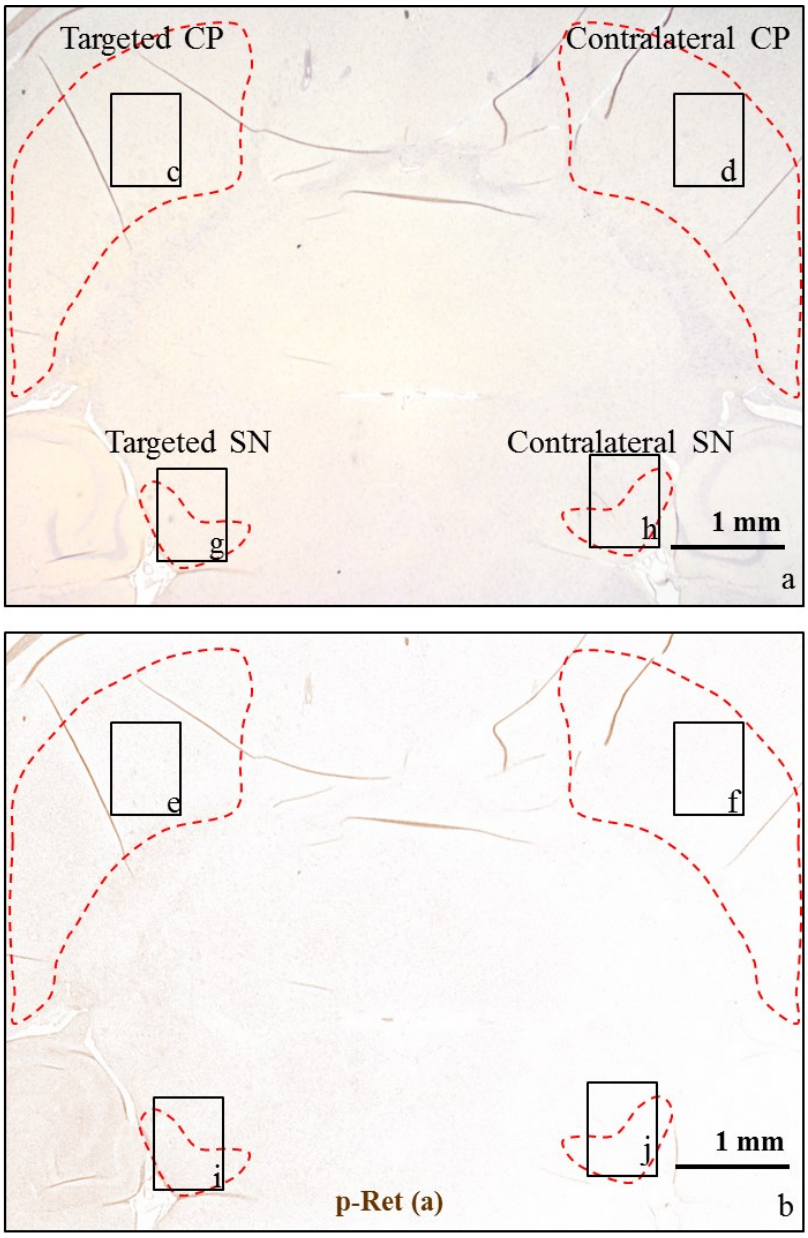

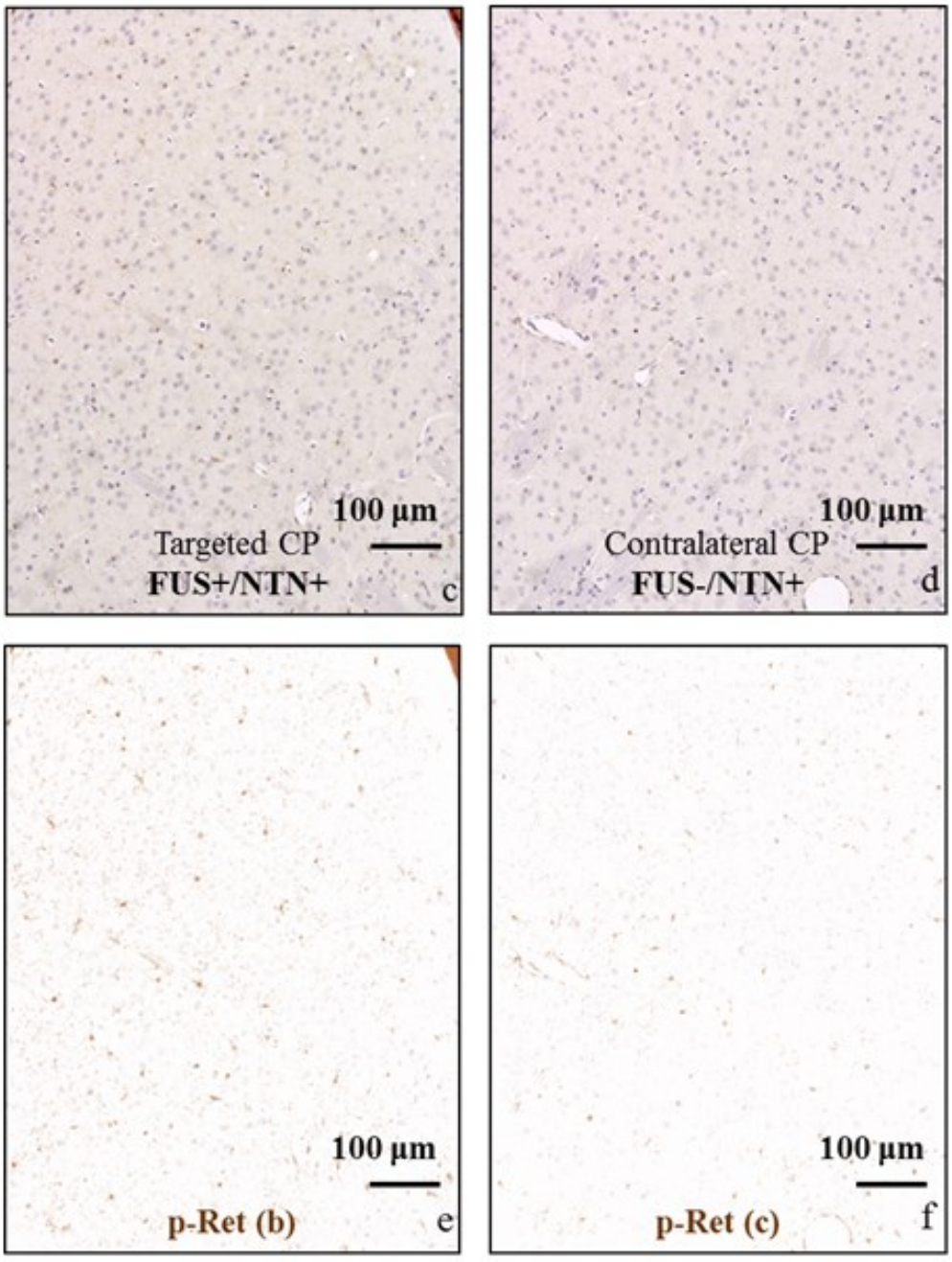
100 µm
Targeted CP
FUS+/NTN+
c
100 µm
Contralateral CP
FUS-/NTN+
d
100 µm
p-Ret (b)
e
100 µm
p-Ret (c)
f

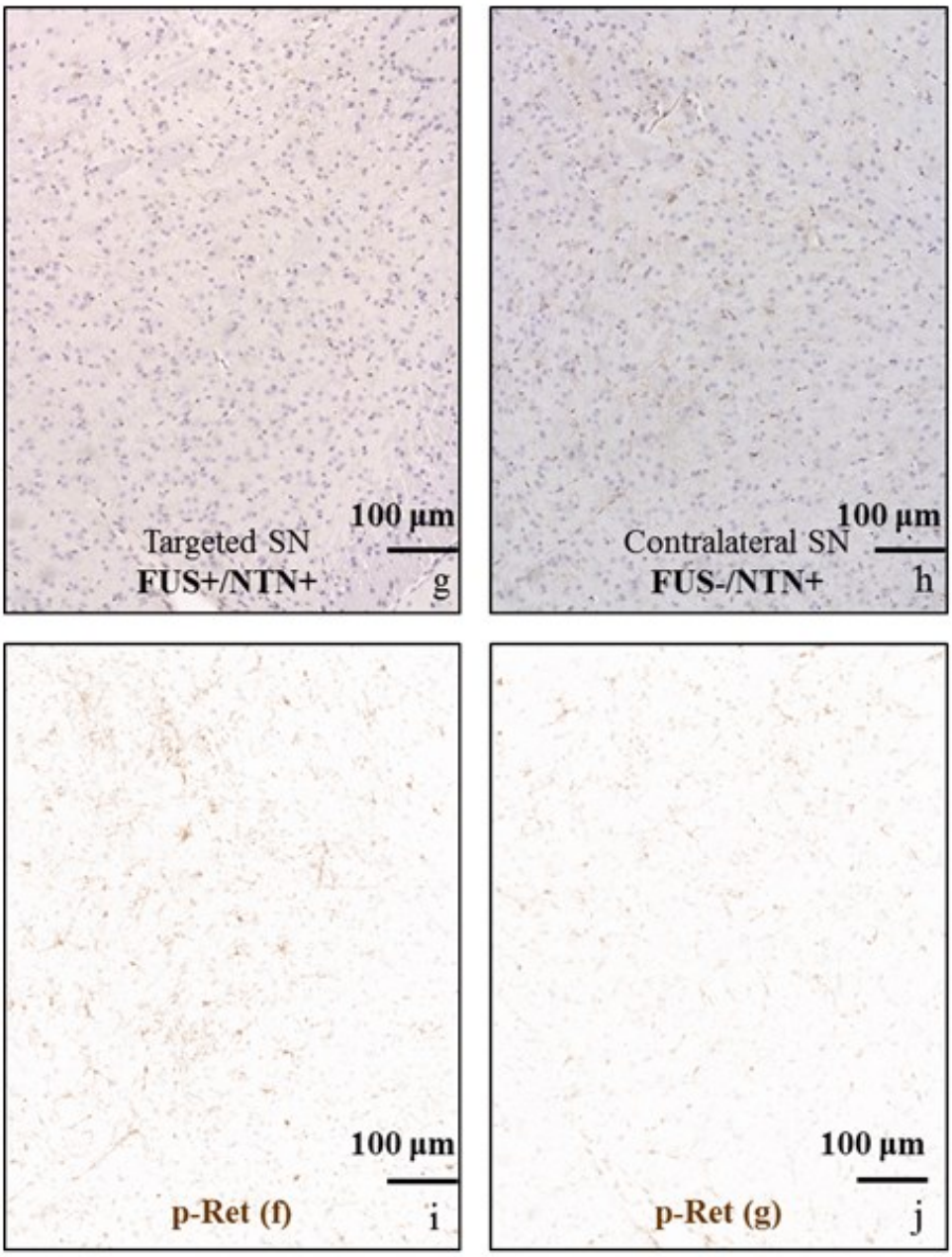

Figure 28(a)Horizontal brain section, where the left CP and SN only were targeted with FUS, immonostained for p-Ret and counterstained with Hematoxylin, (b) is image (a) after the extraction of the DAB color only corresponding to p-Ret. (c),(d),(g),(h) is higher magnification at the targeted and contralateral CP and SN. (e),(f) and (i),(j) are the corresponding images after the the extraction of the DAB color only corresponding to p-Ret. At the targeted with FUS side shown in (e) and (i) there is increased p-Ret compared to the contralateral side shown in (f) and (j) respectively. Both sides were exposed to NTN through the systemic circulation for 1 h following the iv administration. Immunostaining is detected in the neuronal bodies as well as in the dendrites and axon terminals, providing information on the location of the Ret receptor in the DA neurons.

In Figure 29**(a),** an RGB horizontal brain section including both the targeted SN and CP and their contralateral sides is shown, where DAB staining is for the phosphorylated kinase Erk1/2 (p-Erk1/2). The p-Erk1/2 only (brown color) is shown in **Figure 29(b)**. Under higher magnification as shown in **Figure 29 (c)-(d)** and **(g)-(h)** and in the corresponding p-Erk1/2 only images are shown in **Figure 29(e)-(f)** and **(i)-(j)**, p-Erk1/2 expression was increased in the targeted areas compared to the contralateral side, while immunostaining was mainly detected along the neuronal axon fiber bundles. It should be noted that p-Erk1/2 was detected in terminals projecting from the SN to the CP, in areas that exceeded the FUS focal spot size.

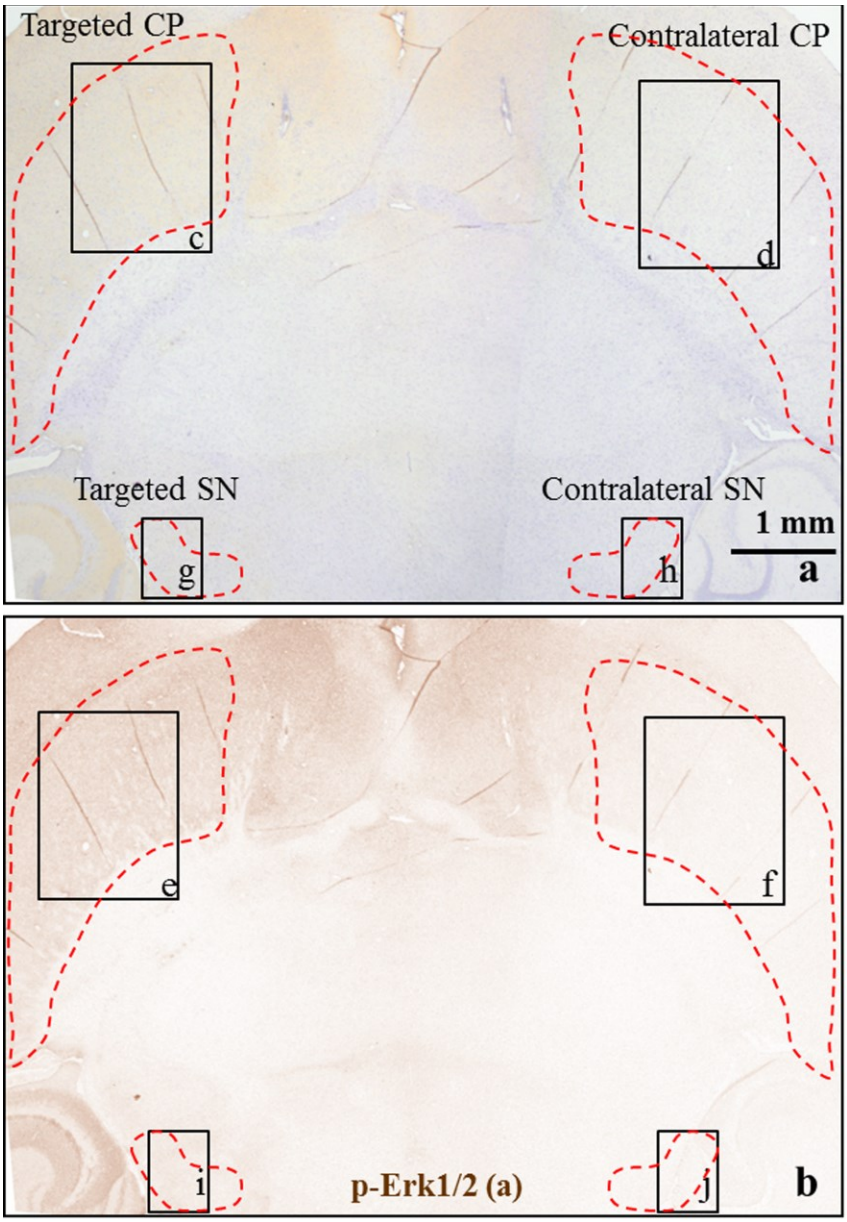

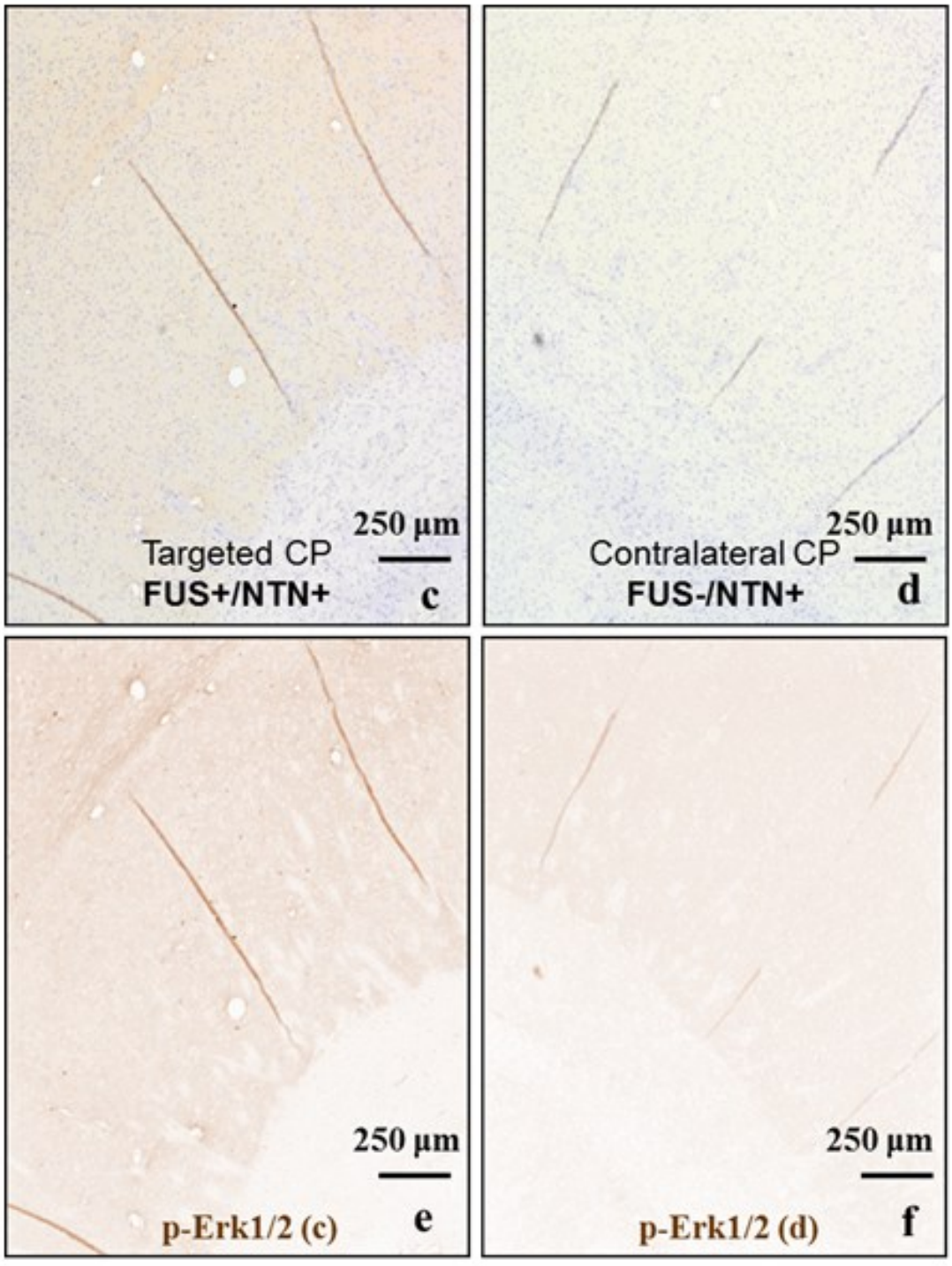
Targeted CP
FUS+/NTN+
250 µm
c
Contralateral CP
FUS-/NTN+
250 µm
d
250 µm
p-Erk1/2 (c)
e
250 µm
p-Erk1/2 (d)
f

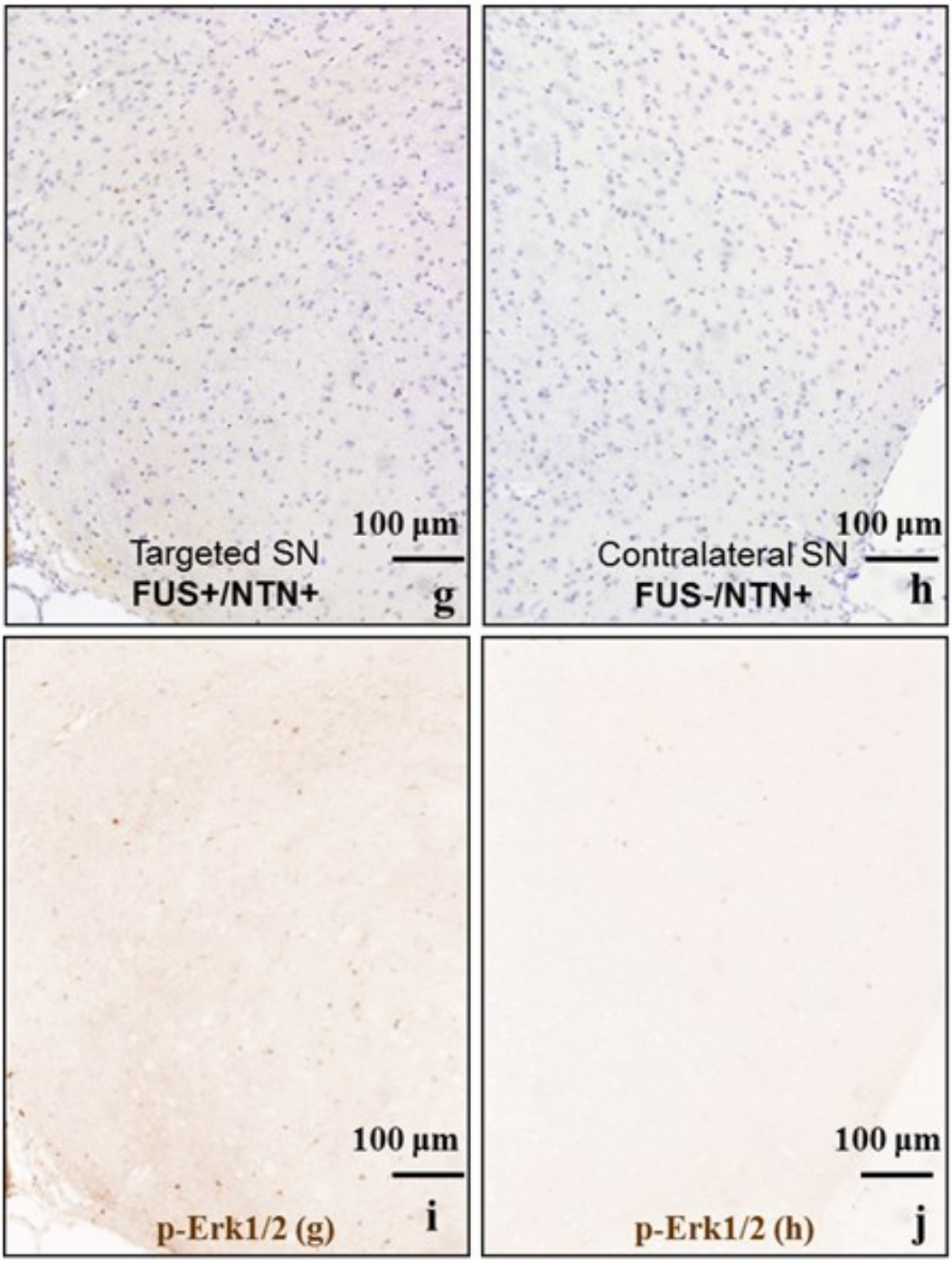

Figure 29 (a) Horizontal brain section, where the left CP and SN only were targeted with FUS, immonostained for p-Erk1/2 and counterstained with Hematoxylin, (b) is image (a) after the extraction of the DAB color only corresponding to p-Ret. (c),(d),(g),(h) is higher magnification at the targeted and contralateral CP and SN. (e),(f) and (i),(j) are the corresponding images after the the extraction of the DAB color only corresponding to p-Ret. At the targeted with FUS side shown in (e) and (i) there is increased p-Ret compared to the contralateral side shown in (f) and (j) respectively. Both sides were exposed to NTN through the systemic circulation for 1 h following the iv administration. Immunostaining for the phosphorylated cytoplasmic kinase Erk1/2 is detected in the neuronal axons mainly.

The effects of FUS with microbubbles-only in the downstream signaling cascade were also investigated. In Figure 30, an example for phosphorylated CREB (p-CREB) is shown where CP and SN were targeted with FUS while the contralateral side remained intact and NTN was administered. In Figure 30**(a),** a horizontal brain section is shown, stained for p-CREB and counterstained with Hematoxylin, while Figure 30**(b)** shows the corresponding p-CREB binary image after color deconvolution for DAB. In Figure 30**(a)** and Figure 30**(c)**, p-CREB immunostaining was increased in the targeted regions compared to their contralateral side (Figure 30 **(b)** and Figure 30 **(d)**). The effect is more evident in the SN where is denser in neuronal nuclei. Finally, FUS was detected to induce BBB opening but it was not detected to trigger the signaling cascade for p-CREB and no differences were detected between the FUS-targeted and the contralateral non-targeted sides (results not shown here).

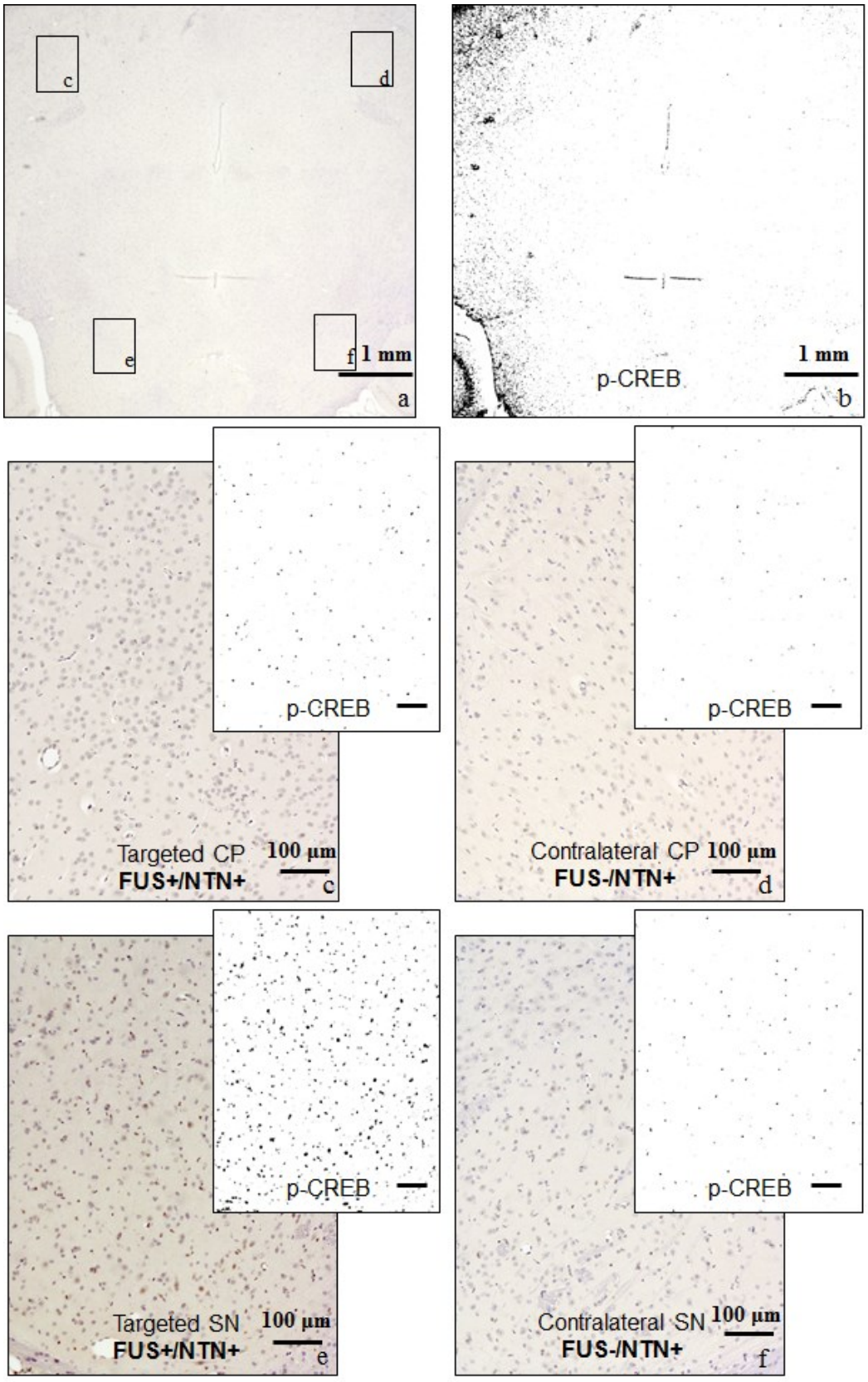
c
d
e
f
1 mm
a
p-CREB
1 mm
b
p-CREB
Targeted CP
FUS+/NTN+
100 µm
c
p-CREB
Contralateral CP
FUS-/NTN+
100 µm
d
p-CREB
Targeted SN
FUS+/NTN+
100 µm
e
p-CREB
Contralateral SN
FUS-/NTN+
100 µm
f

Figure 30 Horizontal brain sections following sonication at the CP and SN, and NTN iv administration. (a) Horizontal brain section, where the left CP and SN only were targeted with FUS, immonostained for p-Erk1/2 and counterstained with Hematoxylin, (b) is the binary image of (a) after the extraction of the DAB color only corresponding to p-Ret. (c),(d),(e) and (f) is higher magnification at the targeted and contralateral CP and SN respectively, with the corresponding binary image after the extraction of the DAB color only. At the targeted with FUS side shown in (A.c) and (A.e) there is increased p-CREB compared to the contralateral side shown in (A.d) and (A.f). Both sides were exposed to NTN through the systemic circulation for 1 h following the iv administration. Immunostaining for the phosphorylated CREB is detected in the neuronal nuclei only, where the transcription factor is located.

4.1.5. Discussion

The objective of the study was to investigate whether safe and efficient NTN delivery could be achieved through FUS-induced BBB opening via intravenous administration. It was shown that the NTN was efficiently delivered through the safely and reversibly FUS-opened BBB in the Caudoputamen and Substantia Nigra following intravenous systemic administration, while bioeffects via downstream signaling to neuronal nuclei were also detected within 1 h. Intrastriatal injections of NTN in rodent models of PD have demonstrated neuroprotective and neuroregenerative effects on DA nigrostiatal function [12], [13], and most recently, intraputamenal infusion in the globus pallidus of MPTP-lesioned rhesus monkeys showed behavioral improvement and elevated locomotor activity levels [14]. Nevertheless, in this study, it was shown that FUS in conjunction with microbubbles can induce high levels of NTN bioavailability through the safely-opened BBB volume, and increased bioactivity, indicating the strong therapeutic potential for Parkinson's and other neurodegenerative diseases of this non-invasive drug delivery methodology.

Enhanced bioavailability of NTN using FUS

Aside from the safety concerns associated with intracranial delivery methods, NTN tissue distribution enhancement in order to achieve trophic effects in the Parkinsonian brain using the aforementioned techniques remains a challenge. A critical advantage of using FUS for drug delivery, as shown in this study, is that it could induce BBB opening throughout the SN and CP with relatively large volumes (~20 mm^3), while non-overlapping sonication locations could be used to induce a two-fold increase in the opening volume (~40mm^3) (Figure 26). The tissue distribution of the trophic factors is a critical variable to achieve optimal effects on DA function, since it has been previously shown that the volume distribution of GDNF, for example, significantly correlated with the motor function improvements [131]. To this end, other studies [131], [144] implemented multiport catheters implanted into the putamen to achieve greater tissue bioavailability, i.e. trophic factor distribution in larger tissue volumes. In order to better

investigate the advantages of FUS over the conventional methods, in this study, the areas of delivery of NTN after FUS was compared to direct injection and was found to be significantly higher and able to cover the entire formation of CP or SN, whereas diffusion of NTN after DI was restricted around the injection site (Figure 27). It was shown in this study that FUS in conjunction with microbubbles is the only non-invasive technique that can be used for the treatment of large areas, thus achieving efficient trophic factor tissue bioavailability.

Here, the single application of both the FUS and the DI methods were compared. However, the DI injection method was not optimized for the purpose of this study. For example, the use of multiple injection sites instead of one, could lead to better diffusion results. Therefore, the comparison reported in this study should be used qualitatively. A different study investigating the differences of the DI procedure would be necessary to reach conclusions on the exact difference between this technique and FUS.

Bioeffects of NTN on neurons

In this study, it was shown for the first time that NTN could diffuse in the extracellular space following iv administration and trigger a downstream signaling cascade in neurons of the nigrostiatal pathway following FUS. First, successful phosphorylation of its receptor Ret was confirmed, and was found to be more pronounced in the CP (Figure 28) than in the SN, which could possibly be due to the receptor's abundance in the axon terminals rather than the dendrites. Then, successful phosphorylation of the cytoplasmic kinase Erk1/2 was detected, along the neuronal axons revealing the neuronal structure (Figure 29). Neurons of the thalamus did not show up-regulation of p-Erk1/2, suggesting that mainly the dopaminergic neurons of the nigrostiatal pathway were affected by NTN in the extracellular space. It is important to note that the phosphorylation of Erk1/2 was detected in areas outside the FUS-targeted region, following the anatomical form of the neurons of the SN projecting their terminals in the CP. This may be due to the fact that the cytoplasmic kinase moved along the neuronal fibers of the neurons that responded to the NTN delivery in the CP and the SN, during the 1 h survival post FUS. Finally, the phosphorylation of the CREB transcription nucleic factor was confirmed (Figure 30), and was more pronounced in the SN than in the CP, possibly due to the abundance of neuronal nuclei in the former area.

The contralateral areas were always found to have very low, if any, immunostaining intensity confirming that the iv administration of the NTN alone was not capable of having any effects to the brain tissue. Moreover, FUS alone, with the acoustic parameters used in the study,

was not found to have any bioeffects on neurons, and did not cause upregulation of p-Ret, p-Erk1/2 or p-CREB.

Reversibility of BBB-opening and potential of repetitive FUS for long-term treatment

Regarding the reversibility of BBB opening, it was shown here that a maximum of 5 days is required for the BBB to be reinstated, in agreement with previous studies [10], [145], even for agents with small molecular size. It has also been shown that longitudinal sonications can be safely used to repeatedly induce reversible BBB opening in rodents [9], [10] and non-human primates [56]. In the intracranial delivery of NTN studies [12]–[14], administration of the trophic factor varied from a one-time single dose to recurring daily doses for 3 months in order to achieve neuroprotection or neuroregeneration in models of PD disease. In other words, the required pharmacological treatment dosage rate remains to be established. In the case of a long-term treatment, which may vary from subject to subject depending on the condition, the findings of FUS studies thus far have shown that the BBB could be repeatedly opened for drug delivery in a sterile environment at desired time intervals.

Collateral BBB opening on adjacent areas

One challenge of using FUS for drug delivery in the murine brain is that due the focal beam size, shape and propagation pathway, it may not affect only a distinct region of interest in the brain, but also induce BBB opening in adjacent structures. For example, SN is a relative small area located more ventrally in the brain, and since the focal length of the FUS acoustic beam was 7 mm, the entire coronal thickness of the murine brain was covered, including the dorsal adjacent regions to the SN such as some posterior regions of the thalamus and the hypothalamus, some small area of the dentate gyrus of the dorsal hippocampus and the cerebral cortex. Moreover, in studies such as this one where CP was targeted, one major challenge was to avoid FUS propagation through the ventricles. Leakage into the ventricles can lead to transportation of the drug to neighboring or more distant structures via the cerebrospinal fluid (CSF), while delivery of NTN beyond the desired target regions and outside the motor pathway could lead to potentially dangerous adverse effects, and should be taken into consideration. Contrary to the FUS transducer used in this study for the murine brains, in a clinical setting, the focal size using FUS transducers designed for acoustic propagation through the human skull, would be small relative to the brain and it could therefore be easier to further localize the effect of FUS onto the desired regions of interest only.

Other limitations

Limitations in this study included the limited number of mice used mainly due to the high cost of NTN acquisition. Due to this limitation, all animals were sacrificed after the same survival time (1 h) post sonication and injection, in order to have a statistically significant number of repetitions of the experiment. Therefore, other effects could not be studied, such as extended circulation time in the brain and different dosages. Possibly, extended animal survival could have more intense immunostaining of NTN, or increased diffusion of NTN inside the brain.

5. Conclusion

In this study, it was found that the BBB could be safely and reversibly disrupted in the Caudate Putamen and Substantia Nigra allowing the penetration of neurotrophic factors and subsequently triggering downstream effects. A pulse length of 10,000 cycles was found to be necessary for efficient protein delivery at 0.45 MPa. In addition, two sonication locations in close proximity were used in order to safely increase the BBB opening volume while covering the entire region of interest.

Neurturin delivery was shown feasible in both the Caudate Putamen and Substantia Nigra. Downstream signaling activation from its receptor to the nucleus was confirmed, and detected within 1 h after IV administration. Neurturin delivery using FUS was shown to be more effective compared to administration to the brain through a direct injection showing enhanced delivery of the protein in the targeted areas.

Section 4.2: Dopaminergic neuron regeneration after Neurturin delivery through the FUS-induced BBB opening in a Parkinsonian model

4.2.1. Introduction

Neurotrophic factors are proteins with enormous therapeutic potential in the treatment of neurodegenerative diseases such as Parkinson's disease (PD). They have been shown to impede the degeneration in the dopaminergic (DA) neurons of the substantia nigra because of their neuroprotective properties, while they also enhance the function of residual DA neurons, repair and restore the function to injured DA neurons. Following the discovery of the glial-derived neurotrophic factor (GDNF), numerous neurotrophic treatments have been studied for PD in vitro and in vivo. GDNF has been shown to promote postnatal development, survival from cell death, neurite outgrowth and synaptic efficacy on DA neurons.

Based on promising results following chronic intra-parenchymal GDNF in nonhuman primate (NHP) models of PD, some studies were also conducted in PD patients; however, the clinical translation has encountered numerous difficulties. Discrepancies between two phase I clinical trials, where functional improvement was reported in 15 advanced PD patients receiving intraputamenal infusion of GDNF, and one phase II clinical trial, where the 25% amelioration in motor scores was not achieved in the 17 out of the 34 PD patients who received intraputamenal infusion of GDNF caused the termination of these trials. Differences in the infusion protocol and the variability of GDNF distribution into the brain parenchyma could be possible reasons for the discrepancy. Also, human trials delivering recombinant human GDNF adenoassociated virus were halted due to safety issues, which for example included the presence of neutralizing antibodies to GDNF is some patients.

Neurturin (NTN) is the second member of the GDNF family, it is structurally homologous to GDNF, and has also been shown to have neuroprotective and neuroregenerative effects in DA neurons in vitro, and in vivo on the parkinsonian brain through intrastriatal injections in rodent PD models [12], [13], and convection-enhanced delivery (CED) in a non-human primate PD model [14]. While gene delivery allows long-term expression of NTN and there is no need for additional treatment sessions, the techniques for determining and controlling dosing and timing remain challenging. Delivery of exogenous NTN has been shown to be effective for PD treatment[14]; however, it was noted that the tissue distribution of NTN in the brain should be further enhanced in order to maximize the trophic effects in the PD brain.

Regarding the PD animal models, the MPTP regimen is a toxin which causes parkinsonism in humans, but among the various toxic models for PD, the MPTP model has

become the most commonly used toxin for several reasons. Most importantly, it is the only known dopaminergic neurotoxin capable of causing a similar phenotypes in both humans and monkeys [146] indistinguishable from PD and also because MPTP produces a reliable and reproducible lesion of the nigrostiatal dopaminergic pathway after its systemic administration [147]. In mice, although MPTP can be given by a number of different routes, the most common and reliable reproducible lesion is caused by its systemic s.c. or i.p. administration.

In the first part of this chapter, it was showed that the neurotrophic factor Neurturin (NTN) was successfully delivered to the Substantia Nigra and Caudate-Putamen of wild type mice, through the FUS-induced BBB opening. It was shown that the technique provided sufficient delivery of NTN in the entire formation of the regions of interest, while activation of a downstream pathway signaling was also detected, from the receptor to the nuclei. It was therefore demonstrated that NTN can reach its intended targets, i.e. CP and SN, following IV administration and FUS-induced BBB opening in the murine brain. There regions were selected because DA neurons have their nuclei in the SN and they innervate the CP with their terminals. It was also shown, that the tissue distribution of NTN through the FUS was significantly enhanced compared to direct injection, suggesting the strong potential of the technique for reversibility of PD phenotype.

The aim of this study is to investigate the regenerative effects of NTN on the MPTP mouse model of PD following FUS-induced BBB opening and iv administration of the trophic factor. To visualize the effect of the MPTP and the NTN treatment, brain samples were stained with anti-TH antibody, a marker of DA neurons.

4.2.2. Methods

Study Design and MPTP lesions

All procedures used in this study involving animals were approved by the Columbia University Institutional Animal Care and Use Committee. A total of thirty-two (n=32) wild-type mice, (strain C57BL/6, age: 12 weeks, mass: 25g, sex: male, Harlan, Indianapolis, IN, USA) was used for the purposes of this study, separated into four groups. Animals were individually housed under standard conditions (12 hours light/dark cycles, 22oC), were fed a standard rodent chow (3kcal/g; Harlan Laboratories, Indianapolis, IN, USA) and bidistilled water, and had *ad libitum* access to their diets and drinking water.

The animals were divided in the four groups, as shown in Table 8. Group A was the control group, where animals received intraperitoneal injections of saline for 5 days, whereas the animals in groups B,C and D received a *sub-acute* intoxication MPTP regimen[148] which involves one injection of 30 mg kg^{-1} free base MPTP daily for five consecutive days. This regimen

causes apoptosis and depletes striatal DA neurons by 40-50% in young adult C57/BL mice, and the dopaminergic lesion stabilizes by 21 d after MPTP administration [149].

A. Control (MPTP-/FUS-/NTN-)	n=7	Saline	-	-
B. Sham (MPTP+/FUS-/NTN-)	n=7	MPTP+	-	Saline
C. FUS only (MPTP+/FUS+/NTN-)	n=8	MPTP+	FUS	Saline
D. FUS and NTN (MPTP+/FUS+/NTN+)	n=8	MPTP+	FUS	NTN

Table 8. Neuroregeneration Study Design

From the groups that received the MPTP regimen, group B was used as a sham control, while both C and D groups received FUS. The animals in the sham group B and in the FUS group C received also intravenous saline injection, i.e. vehicle only, while the animals in group D also received 20 μg/g diluted in 50 μL of Neurturin (NTN, Invitrogen, CA, USA) via a tail vein bolus injection.

As shown in the scheme in **Figure 31**, all groups were initially healthy as in (a). Groups B,C and D later received MPTP toxin causing DA neurons apoptosis as in (b). However, hypothesizing that NTN could induce neuroregeneration at the FUS-treated side following BBB-opening in that area, within 4 weeks after iv administration, neurons are expected to be regenerated as in (c).

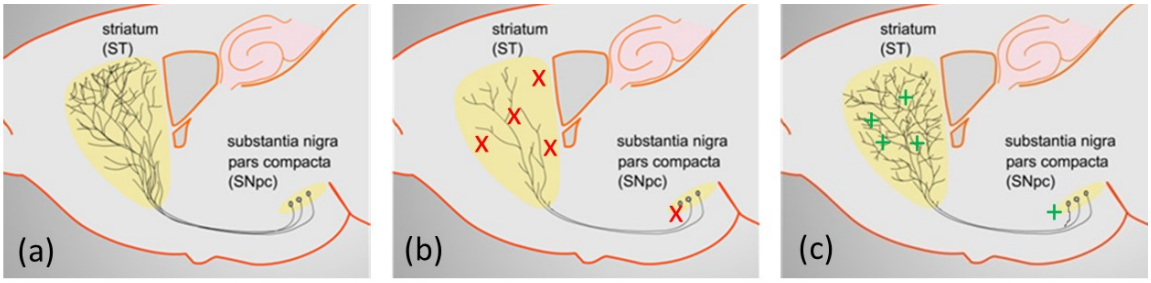

Figure 31 Scheme representing DA neurons of the SN projecting their terminals (a) before the MPTP lesions, (b) after the MPTP lesions, and (c) in a scenario of neuroregeneration after MPTP lesions

Focused Ultrasound

A single-element, spherical-segment FUS transducer (center frequency: 1.5 MHz, focal depth: 60mm, radius: 30mm; axial full-width half-maximum intensity: 7.5 mm, lateral full-width half-maximum intensity: 1 mm, Imasonic, France), driven by a function generator (Agilent, Palo Alto, CA, USA) through a 50-dB power amplifier (E&I, Rochester, NY, USA) was used to target the SN or the CP. A needle hydrophone (HGL-0400, Onda Corp., Sunnyvale, CA) was used for the transducer calibration, which measured the acoustic beam profile in a tank filled with degassed water. A central void of the therapeutic transducer held a pulse-echo ultrasound

transducer (center frequency: 10 MHz, focal depth: 60mm, radius 11.2 mm; Olympus NDT, Waltham, MA) used for alignment, with their two foci aligned. The imaging transducer was driven by a pulser-receiver (Olympus, Waltham, MA, USA) connected to a digitizer (Gage Applied Technologies, Inc., Lachine, QC, Canada). A cone filled with degassed and distilled water was mounted onto the transducer assembly. The transducers were attached to a computer-controlled 3D positioning system (Velmex Inc., Lachine, QC, Canada). A bolus of 1 μl/ g of body mass polydisperse manufactured in-house [106] microbubbles diluted in saline ($8x10^8$#/ mL, mean diameter: 1.4 μm) was intravenously injected immediately preceding the sonication at each target, i.e. SN or CP. A 20-min time interval was allowed between SN and CP targeting, to allow the microbubble concentration to be cleared from the circulation [141]. Each animal was sonicated for 60 s, with a pulse repetition frequency (PRF) of 10 Hz, with one sonication location at SN and two sonication locations at CP in order to safely open the entire area of interest with acoustic parameters that do not cause damage, at peak negative acoustic pressure (PNP) of 0.45 MPa [9], [10] after accounting for 18% and 33% murine skull attenuation for the SN and CP respectively.

MRI

Groups C and D were imaged using a 9.4 T vertical bore microimaging MRI system (DRX400, Bruker, Biospin, Billerica, MA, USA). Each mouse was scanned 20-30 min after sonication, using a 30-mm-diameter 1H resonator. Isoflurane gas (1-2%) was used to keep the mouse anesthetized at 50-70 breaths/min during the entire MRI procedure. A T1-weighted 2D FLASH high-resolution acquisition (TR/TE: 230/3.3 ms, resolution 100 μm x 100 μm, slice thickness: 400 μm, duration: 240 s) was acquired. MRI was done in order to confirm the accuracy of targeting in these two groups.

Immunohistochemistry

Animals were survived for 28 days after treatment in order to allow for any neuroregeneration to occur. Animals were then sacrificed and transcardially perfused with 30 mL PBS and 60 mL 4% paraformaldehyde. All heads were soaked in paraformaldehyde for 24h. Skulls were removed, and the brains were fixed again in 4% paraformaldehyde for 2 days, and then chilled in ice-cold saline. The central striatum was sliced into 30 μm thick sections on a cryostat and collected serially in anti-freezing solution. Every 6^{th} section of the posterior striatum and the SN, and every 6^{th} section of the anterior striatum and the CP were processed for TH-immunohistochemistry, carried-out in free-floating sections. Sections were washed 3 x 5 min in 0.1 M Tris Buffered Saline (TBS), were then incubated 5 x 10 min in 10% methanol/3% H_2O_2) 0.1M TBS to block the endogenous peroxidase activity. The sections were washed again 3 x 5 min in TBS, followed by incubation for 60 min in 5% normal goat serum (NGS, Vector, USA), to

be then incubated for 49 h at 4^{o}C in ani-TH antibody (Calbiochem, USA, 1:2000 for SN; 1:1000 for CP) in 0.1 M TBS containing 2% NGS. The sections were washed again 3 x 5 min in 0.1 TBS, followed by incubation for 60 min in the secondary antibody, anti-rabbit (Goat, 1:400 in 0.1 M TBS), washed again in 0.1 M TBS 2 x 5 min, incubated in ABC solution for 60 min, washed in 0.1 M TBS for 2 x 5 min, and then the antibody binding was visualized using diaminobenzidine (DAB substrate kit, Vector Labs. Neurons in the SN were also stained with Nissl stain. Sections were mounted on gelatin-coated slides and cover slipped with mounting medium.

Stereological unbiased methods were performed in order to estimate the total number of TH-IR neurons in the SN in a standard manner established elsewhere [150], [151]. In the CP, in order to visualize the TH-immunoreactivity and the difference between the ipsilateral and the contralateral to the FUS sides, the images were converted to grayscale. Then, the average and the standard deviation of the intensity in the cortex was measured and used as reference intensity. Afterwards, the pixels that met the criterion of exceeding the threshold of the reference intensity by 2.5 times its standard deviation were used to create a mask. The mask was overlaid on the original image to better illustrate the difference of TH-IR in the CP.

Statistical analysis

Statistical analyses were performed using Prism 6 (Graphpad Software, San Diego, CA< USA). Two-way mixed factorial ANOVA was performed to detect possible effects of FUS and NTN. Statistical significance was determined at an alpha level of 0.05. Following the ANOVA, the data from the two sides (FUS+ and FUS-) from all groups were submitted to post-hoc paired *t*-test within each group, were the FUS- side served as the control in each animal, in order to detect any difference in the number of TH+ cells in the FUS+ treated sided. A value of $p<0.05$ was considered to be significant.

4.2.3. Results

Immunohistochemistry revealed some DA regeneration in the ipsilateral to the FUS side in group D where NTN was administered iv. Some representative results are shown in **Figure 32.** As shown in this figure, the two sides (i) and (ii) of the SN in the control group A, the sham group B and the FUS only group C, are very similar in terms of TH-IR neurons. Only in group D, which received FUS for BBB opening in one side (D(ii)), there were more DA neurons observed compared to the contralateral (D(i)). Since the MPTP lesions and the DA neurons apoptosis preceded NTN delivery, neuroregeneration is being observed in this group.

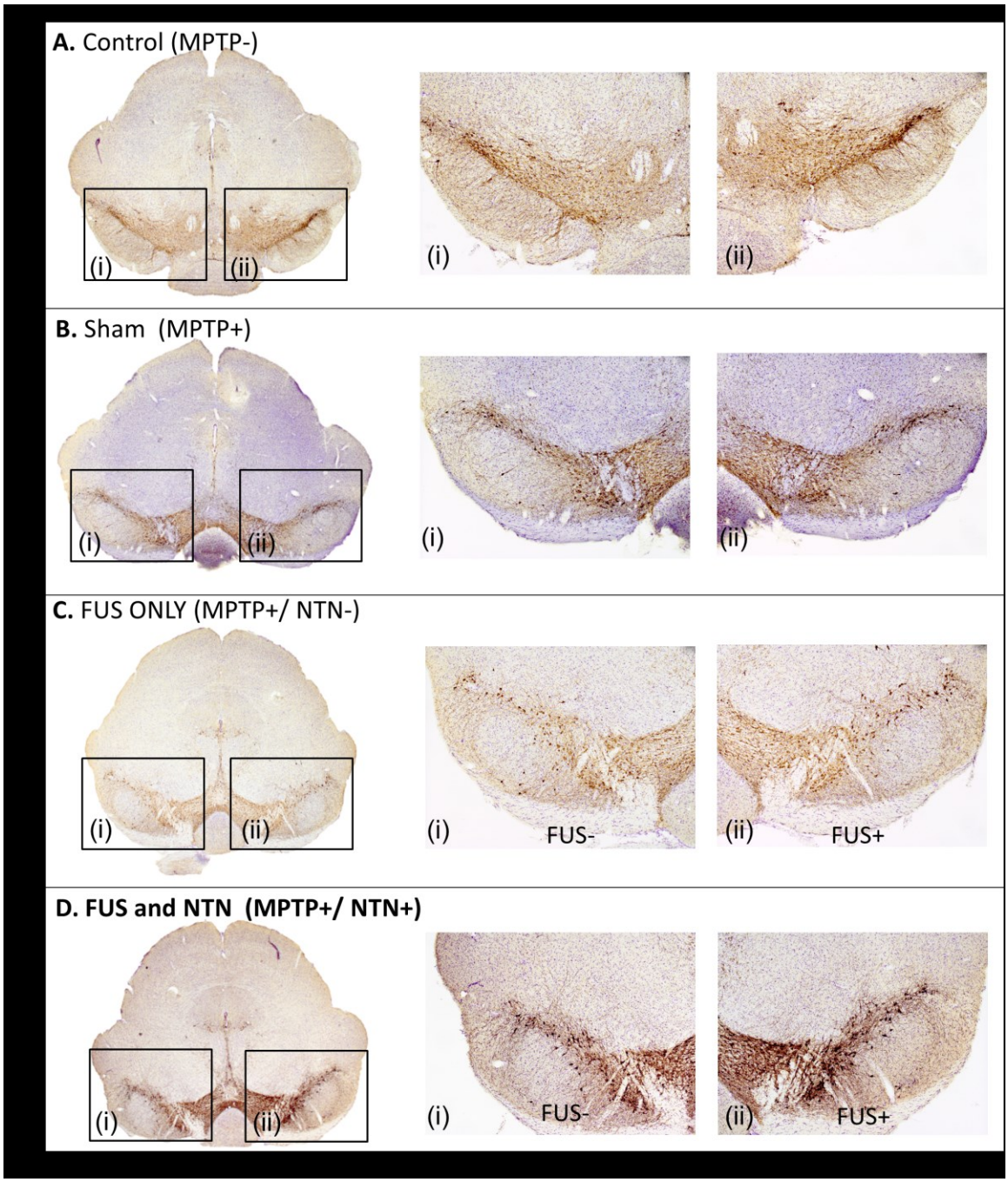

Figure 32 TH immunohistochemistry images of the substantia nigra (SN) level of all groups (A,B,C,D). High-power (4x) magnification of the SN is shown in (i) and (ii) for each group. Groups C and D received FUS on one side, and group D also received iv NTN. As shown here in D(ii) compared to D(i) there are more TH-IR, ie DA neurons on the sonicated side.

The difference in the number of TH-IR cells between the ipsilateral to the FUS side (FUS+) and to the contra-lateral side (FUS-) is shown in **Figure 33**. In order to better analyze

the effect of NTN on DA neurons the difference between the ipsilateral and the contralateral side was also investigated. Two-way mixed factorial ANOVA followed by paired t-tests revealed significant difference ($p<0.05$) among the two different sides only in the group that received NTN as well as FUS (group D). The results of each subject individually from groups C and D, which both received FUS in one side of the brain, but only group D received NTN are shown in **Figure 34.** The FUS+ NTN+ group D was the only group where there was significant difference between the two sides revealing neuroregenerative effects of NTN.

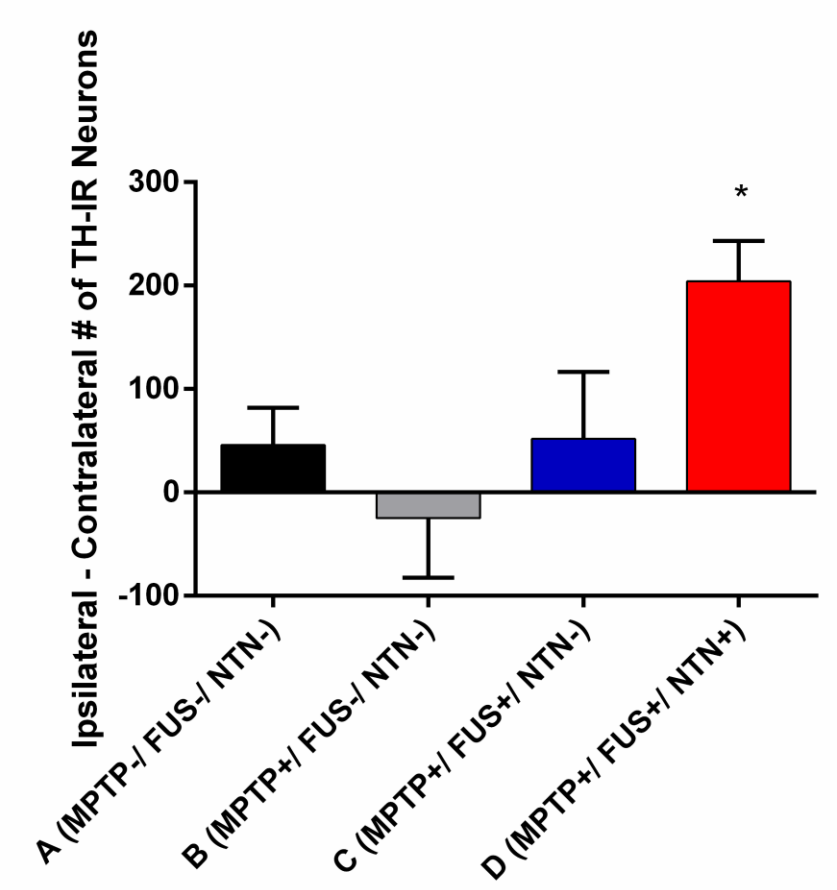

Figure 33 Difference in the number of TH-IR neurons between the ispilateral to the FUS side and the contralateral side

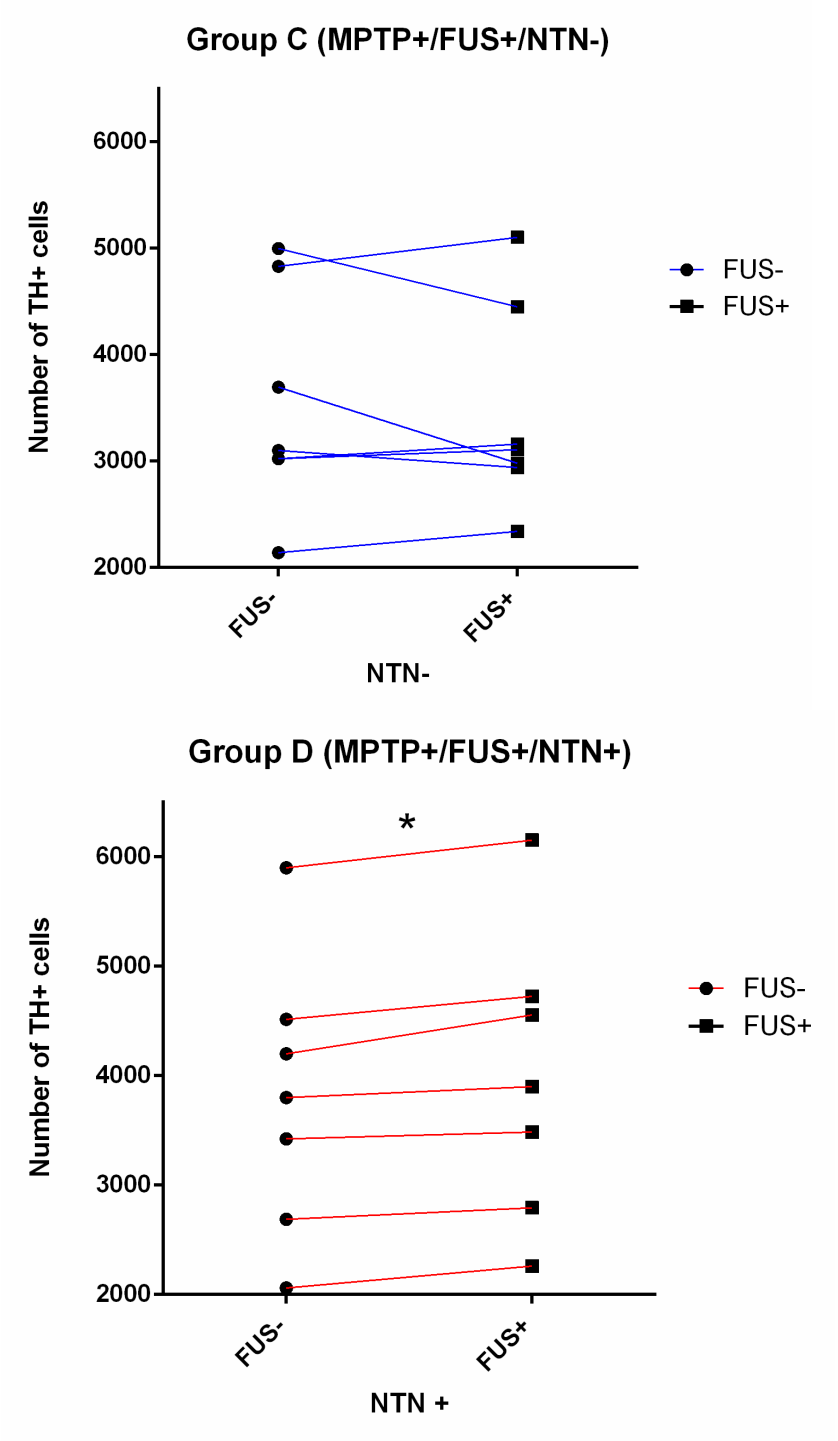

Figure 34. Number of TH-IR (TH+) neurons between the ispilateral to the FUS side (FUS+) and the contralateral side (FUS-). Paired t-tests revealed significant difference ($p<0.05$) among the two sides within each group only in Group D, which received NTN.

Regarding the CP, some differences between the two sides were detected only in group D (MPTP+/FUS+/NTN+), and visualized as explained in the methods, i.e. with thresholding. Representative examples are shown in **Figure 35.**

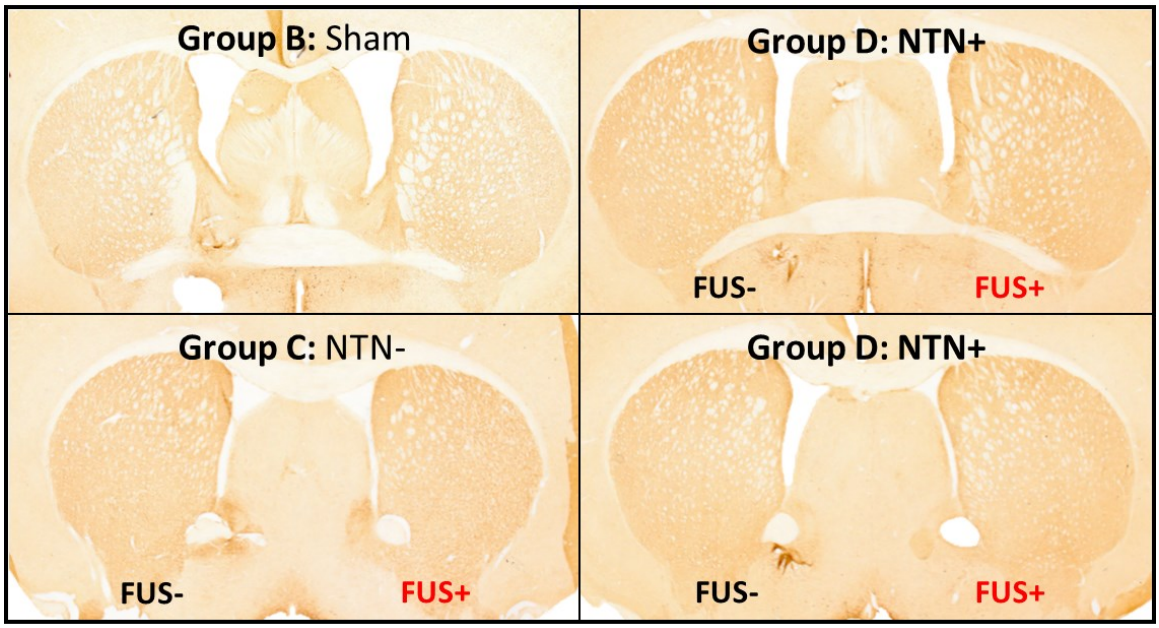

A

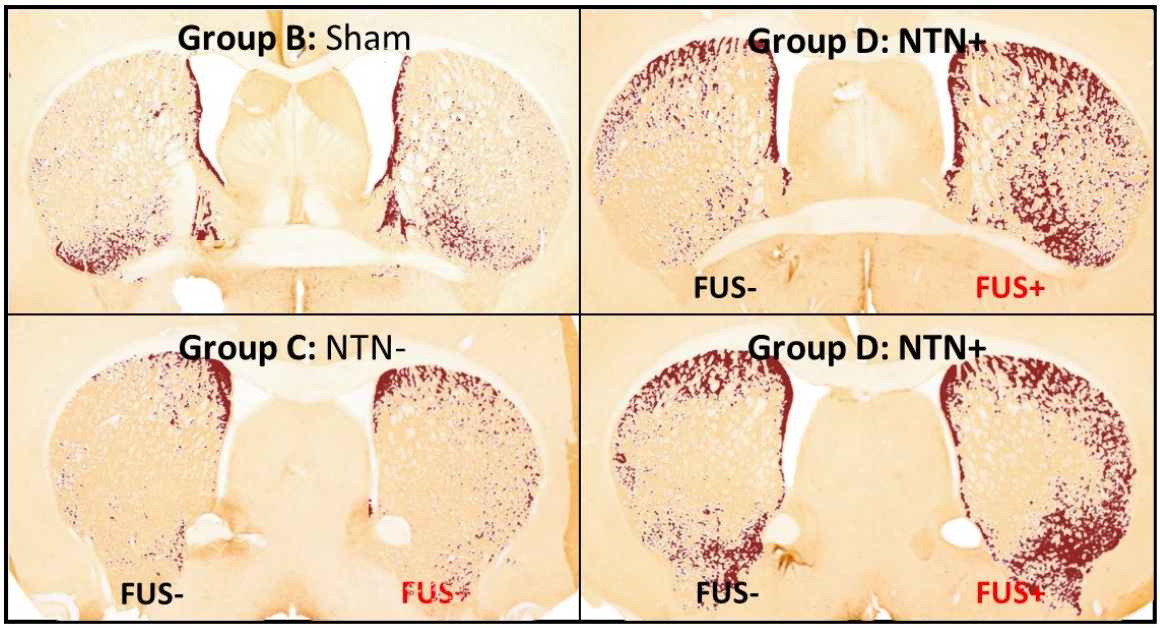

B

Figure 35 A: Representative examples of the CP from groups B and D in the posterior CP, and C and D in the anterior CP. **B:** Identical to A, overlaid with a dark red mask, which represents the

pixels that met the thresholding criterion. In group D only, there are significantly more TH-IR neurons in the ipsilateral to the FUS (FUS+) side.

4.2.4. Discussion and conclusion

In this study, the neuroregenerative effects of the Neurturin neurotrophic factor through the FUS-induced BBB opening in a Parkinsonian mouse model were shown for the first time, suggesting the potential of this technique in the reversibility of the PD phenotype. A single administration of NTN achieved subtle but consistent increase in the number of neurons on the side of FUS-induced BBB opening, four weeks post- treatment.

Due to the expenses related to acquiring NTN, a limited number of mice were used here, a sufficiently large number though for the proof of concept and statistical analysis. Even though there were variations, there was always an increased number of neurons in the ipslilateral to the FUS side, and the difference between the two sides was found to be significant only in the group where NTN was delivered following FUS.

In this study, only DA neurons were detected through their TH-immunoreacitvity, therefore the effect on other neurons was not studied. In another study, staining of other neurons could also be done in order to see whether there are any neuroprotective or neuroregenerative effects on these neurons as well.

The animal model used here is the MPTP toxin model, which is characterized by loss of DA neurons as patients with PD do. It is a well-established PD model, widely used in the PD research. The efficacy of our technique in other mouse models could be tested as well.

Finally, since NTN is a neurotrophic factor, one hypothesis is that it is capable of upregulating the TH expression by itself, therefore introduce some source of error in the variable used for neuroregeneration here, ie. TH immunoreactivity. This possibility cannot be completely excluded, however, since there was a 4 week survival following the NTN administration, it can be hypothesized that the TH-IR neurons were not only more detectable compared to the contralateral side due to this TH up-regulation, but actual new neurons.

Following these promising results, multiple NTN delivery sessions could potentially prove more beneficial for the reversibility of PD phenotype, i.e. DA neurons regeneration

Section 4.3: Contribution

Overall, in this specific aim, a method for enhanced delivery of a neurotrophic factor to a PD animal model was optimally designed and implemented, and the therapeutic potential of the method was shown. Enhanced delivery of the drug was shown, along with some reversibility of the PD's phenotype, i.e. neurodegeneration of the DA neurons, after a single administration of the drug.

As previously mentioned, there have been several studies where various molecules have been delivered to the brain using FUS-induced BBB opening, but a very limited number of studies has shown reversibility of CNS disease phenotype, and none of these were done for PD. Here, it was shown for the first time that efficient amount of the NTN neurotrophic factor could be delivered through the FUS-induced BBB opening, while through a single treatment, a consistent increase in the number of dopaminergic neurons in the treated side could was observed.

For the first part of the study, the efficient delivery of NTN though FUS was investigated and shown. In order to cover the entire region of interest in the CP maintaining low and safe acoustic parameters, two sonication locations were used and increased the diffusion in the CP two-fold. Also, the FUS was compared to the direct injection technique and was found to be significantly more efficient. Also, bioactivity of NTN and downstream signaling cascade from the receptor on the neuronal surface to the nucleus, were detected within 1 h after iv administration of NTN in the side where FUS was applied. The results of the part of this study were recently published [152], and were used for the second part which was performed on the MPTP PD-model.

For the first time here an actual neurotrophic factor with demonstrated therapeutic potential on PD was delivered through the FUS-induced BBB opening in MPTP mice, i.e., a mouse parkinsonian model and some neuroregenerative effects were shown. A single administration increased significantly the number of DA neurons in the side of the FUS compared to the contralateral side.

Given the technique can be translated to a pre-clinical and eventually a clinical setting, these results here show the potential of the FUS-induced BBB opening technique in the CNS treatment with use of neurotrophic factors in PD patients eventually.

Regarding the research contribution, Oluyemi Olumolade (B.A. Biomedical Engineering, Columbia University) assisted with the selection of anti-bodies for this study, and animal surgery. Anushree Srivastava (B.A. Biomedical Engineering, Columbia University) assisted with animal surgery. Shutao Wang (Ph.D., Biomedical Engineering, Columbia University) performed the the direct injections, assisted with experiments, assisted and supervised the TH staining procedure and shared the staining protocol, discussed the study design and assisted with data

interpretation. Camilo Acosta (B.A. Biomedical Engineering, Columbia University) performed the trans-cardial perfusions, all tissue preparation (from tissue fixation to sectioning), assisted with immune-staining and performed the stereological counting of TH neurons. The author also wished to thank Vernice Jackson, PhD (Associate Research Scientist) and Javier Blesa De Los Mozos, PhD, for preparing the MPTP mouse model, sharing staining protocols, providing us with the microscope necessary for the stereology TH neuron counting and all their invaluable scientific input. And finally Serge Przedborski, MD, PhD, for his contribution in the study design, data interpretation and his general feedback, input and suggestions for the study, as well as providing us with resources (animal facilities, etc) from his laboratory, without which this study could have never progressed.

CHAPTER FIVE:
Pharmacodynamic analysis of FUS-induced BBB opening in non-human primates

As demonstrated in Chapter 3, a pharmacokinetic analysis was necessary in order to further investigate the efficacy and safety profile of the FUS-induced BBB opening in mice, and define a window with optimized acoustic parameters to achieve drug delivery with the potential therapeutic effect on CNS treatment, as shown in Chapter 4. In order to proceed to the next step which can be no other than a preclinical translation, a pharmacokinetic analysis has to be performed in non-human primates, along with some parameters optimization. This is the third milestone and specific aim of this thesis, as shown in Figure 36. Our group has shown BBB opening feasibility in NHP, and has created a prototype for the FUS application[56], [153]. Discrepancies in the results among different subjects[154], as well as the need to investigate the effect of FUS and microcubbles in the NHP brain, made the pharmacokinetic analysis conducted here necessary.

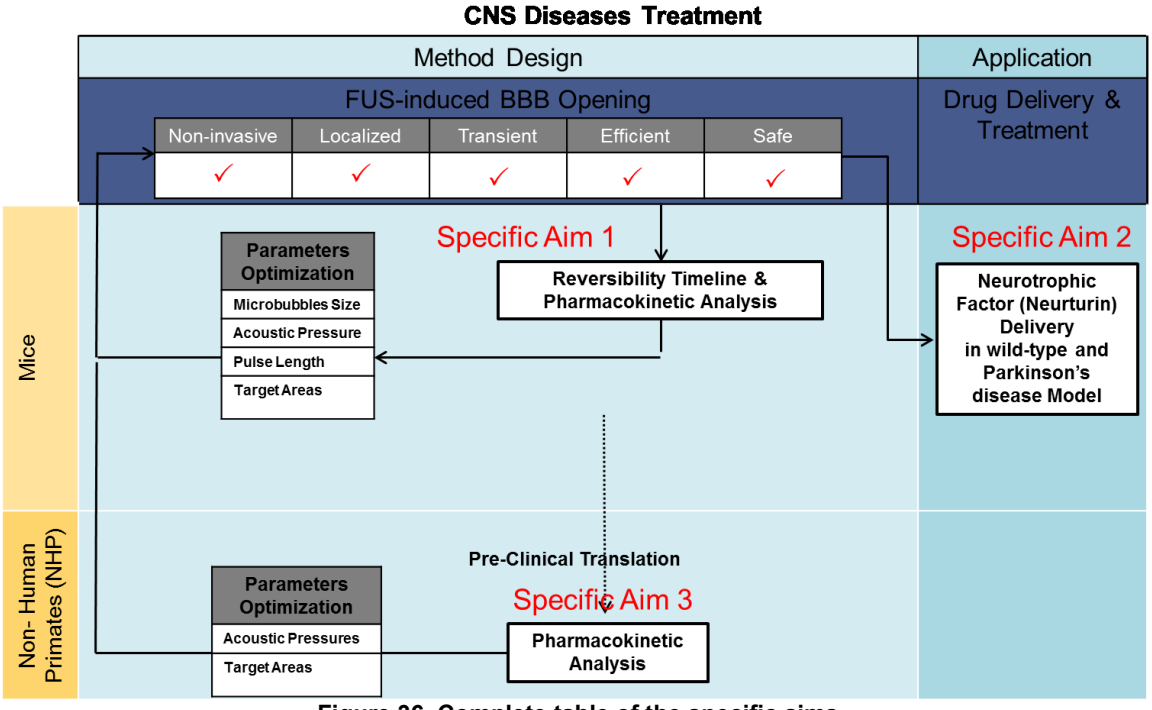

Figure 36. Complete table of the specific aims

Section 5.1: Permeability mapping, gadolinium concentration mapping and drug delivery efficiency estimation in vivo

5.1.1. Introduction

Focused Ultrasound (FUS) in conjunction with systemic administration of microbubbles has previously been shown to open the Blood-Brain Barrier (BBB) locally, non-invasively and reversibly on MRI in non-human primates [48], [56], [153]. In rodents, physiological properties of the BBB opening, such as permeability, volume, contrast agent concentration mapping and reversibility timeline, have been studied [9], [10], [55], [145]; these studies provided invaluable bases for optimal design for drug delivery to the brain using FUS, and in vivo tools for the quantification of the efficacy of this technique. However, in NHP, such an analysis has never been conducted, which is very critical given the urgent need for pre-clinical and clinical translation. The purpose of this study is the investigation of properties of BBB opening in non-human primates (NHP), more specifically the permeability and the drug delivery dose, in vivo for the first time, in order to assess the efficiency of the FUS-induced BBB opening as a technique with therapeutic potential for neurodegenerative diseases such as Parkinson's disease.

The quantification of a drug across the BBB is rather challenging, and current techniques face limitations such as increased radiation when measured with PET-CT, or sacrifice of the animal in order to perform *post mortem* protein quantification (ELISA). Magnetic Resonance Imaging, on the other hand, offers an *in vivo* tool for quantification of the MRI contrast agent (CA), which is used as model drug. It is mandatory to model the interaction of the CA with the surrounding water molecules and protons in order to quantify the CA concentration using MRI, since the MRI CA in principle decrease the relaxation times T_1 and T_2 of the aforementioned water molecules. Here, a standard Relaxometry technique for T_1 mapping [155] was implemented acquiring gradient-echo images with variable flip angles (VFA) with short TR. In this study, VFA-based T_1 mapping was validated on a phantom and provided T_1 value estimation with high accuracy and high spatial and temporal resolution. The gadolinium MRI-contrast agent was used as a model drug that diffused in the brain parenchyma. The comparison of the T_1 times before and after gadolinium injection provided CA concentration maps, which were used for quantitative pharmacodynamic analysis. Moreover, since grey matter and white matter have distinctive T_1 times, T_1 mapping can be used as a robust method for BBB opening detection with grey and white matter segmentation.

Permeability mapping in rodents after FUS-induced BBB opening using MRI has provided further insight into the study of BBB opening, following the generalized Tofts and Kermode kinetic model [142]. It has been shown that permeability increases with acoustic pressure in rodents and

that DCE-MRI can be used as an in vivo evaluation tool for the efficacy of the procedure. In NHP studies though, only T1-weighted imaging has been used for the BBB opening analysis, which provided very limited information on the physiologic changes in the brain, the relation to the underlying structures, while detection of opening is arbitrary based upon subjective criteria which induce discrepancies among different studies and experiments. For these reasons, in this study, a DCE-MRI sequence and an offline processing algorithm were designed to quantify permeability and further analyze the physiologic changes in the brain following FUS-induced BBB disruption.

Pre- and post-contrast high resolution relaxometry imaging and DCE-MRI were used for the pharmacokinetic analysis in this study for the first time in NHP *in vivo*. Diffusion of gadolinium into the brain parenchyma, which otherwise does not cross the BBB, was used as a tracer to depict the BBB-opened areas. Quantitative analysis of T_1 relaxometry mapping and permeability was performed to detect and quantify the volume of opening, separately in the grey and white matter, the CA concentration, and the drug delivery efficiency in two NHP. The acoustic pressure dependence was also investigated. Finally, T2-weighted and Susceptibility Weighted Imaging (SWI) were performed in order to detect edema or hemorrhage. The aim of this study was to provide the *in vivo* quantitative tools for safe and optimal drug delivery using FUS in a pre-clinical setting.

5.1.2. **Methods**

Animal Preparation

All procedures were approved by the Institutional Animal Care and Use Committee at Columbia University and the New York Psychiatric Institute. Two male rhesus macaques (*Macaca mulatta*) weighing 10 kg were used in this study. The animal handling was described previously [56], [156]. For the entire procedure the animals were anesthetized with a mixture of oxygen and 2% isoflurane, while their vital signals were being monitored. The animals' heart rate was kept at 100 heartbeats per minute and their respiratory rate was kept at 60 breaths per minute. Prior to sonication, the scalp hair was removed with a depilatory cream in order to ensure maximal acoustic transmission with minimum attenuation. For the FUS part the animal's head was placed in a stereotactic frame for targeting of ultrasound to specific brain regions, using a manipulator and a positioning rod which indicated the focus relatively to the stereotactic coordinates, as shown in Figure 37.

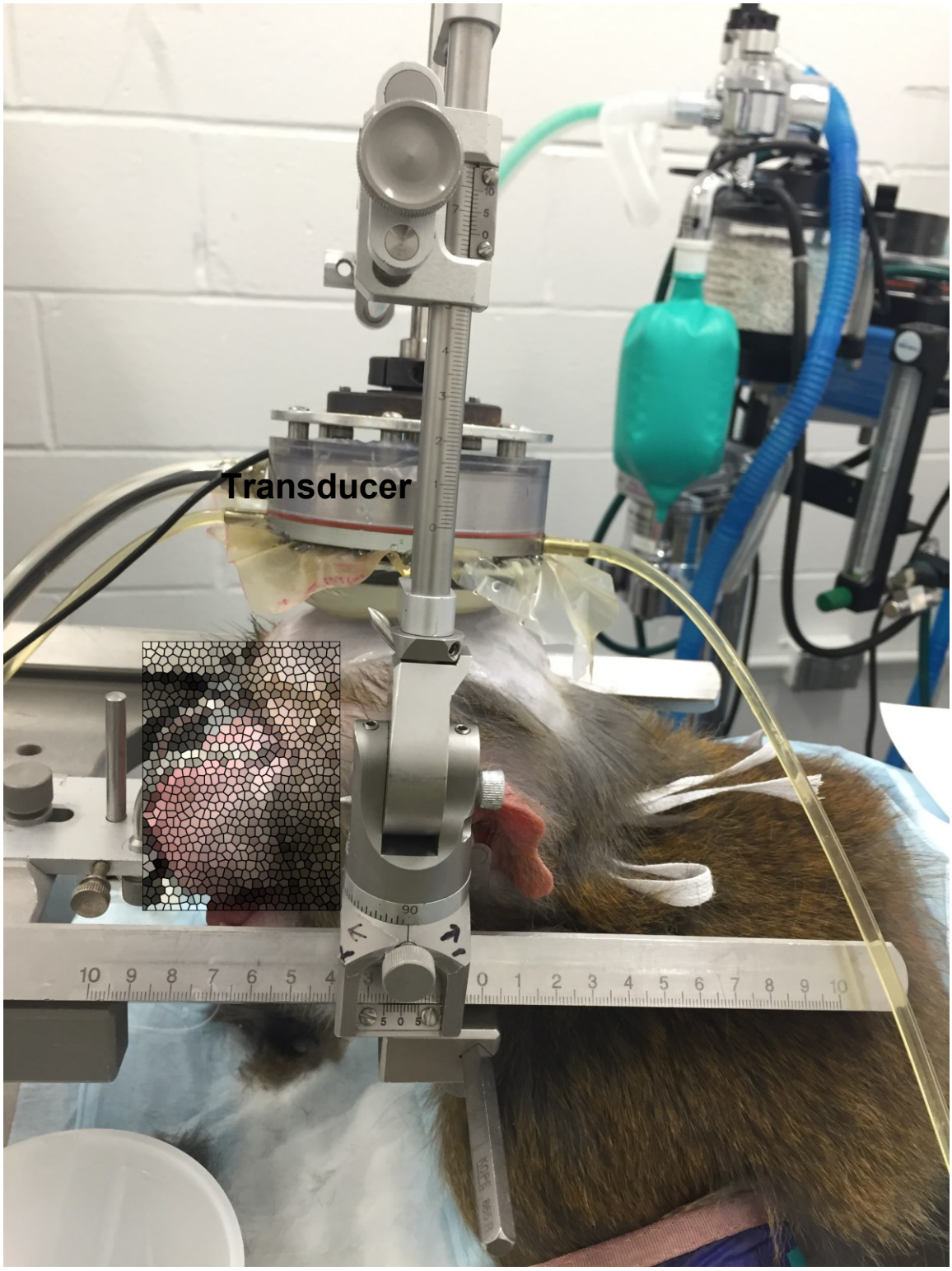

Figure 37. Sonication NHP setup

Focused Ultrasound induced BBB opening

Two regions with relevance to Parkinson's disease, the Caudate and the Putamen, were targeted transcranially with FUS in two (n=2) rhesus macaques, for a total of 32 sonications, 16 sonications each. The targets were in one hemisphere and the contralateral side remained intact. The FUS setup as described elsewhere [154] consists of a single-element FUS transducer (H-107, Sonic Concepts, Bothell, WA) driven at 500 kHz with a focal size of 5.85 mm by 34 mm (-6dB) and a focal depth 62.2 mm which overlapped with the targeted regions. The sonication was controlled through a customized algorithm in Matlab (The MathWorks Inc., Natick, MA), where the signal was generated through a function generator (model 33220A, Agilent Technologies Inc., Santa Clara, CA) amplified by 50 dB (A075, Electronic Navigation Industries, Rochester, NY). The sonication acoustic pressure varied from 200 kPa to 600 kPa while the rest of the acoustic parameters remained constant (PRF: 2Hz, sonication duration: 120 s, pulse length: 10 ms). A bolus (1.25×10^8 bubbles/kg) of manufactured in-house mono-disperse (4-5 μm in diameter), lipid-coated microbubbles was administered intravenously in the beginning of the sonication. The pressure decrease resulting from transcranial FUS transmission was compensated based on vitro calibration as previously described [156].

Magnetic Resonance Imaging

Following sonication, the macaques were being placed in the 3T MR scanner (Philips Medical Systems, Andover, MA, USA). 3D T2-weighted imaging (Turbo Spin Echo, TR/TE = 3000/80 ms; flip angle (FA): 90°; NEX= 3; spatial resolution: 1 x 1 x 2 mm^3) and 3D SWI (TR/TE = 19/27 ms; flip angle: 15°; NEX= 1; spatial resolution: 1 x 1 x 1 mm^3) sequences were acquired. The T2-w and the SWI acquisitions are performed for the detection of hyperintensity, i.e. edema, and/or hypointensity, i.e. hemorrhage respectively.

Five pre- and post-CA injection, 3D Spoiled Gradient Echo (SPGR) images (FOV:16 cm, matrix 160x160, TR/TE: 20/5ms, FA: 5^o -35^o , NEX=2, 0.89 x 0.89 x1 mm^3) were acquired and used for variable flip angle (VFA) based T1 relaxivity mapping, before and after intravenous injection of gadodiamide (Gd-DTPA-BMA, 0.2 ml/kg).

The DCE-MRI sequence was acquired between the pre- and post-CA SPGR sequences. In total, 90 sets of T1 3D Fast Field Echo (FFE) images were acquired at 15 s intervals (TR/TE: 4.2/1.7 ms; FA= 20^o, resolution: 1x1x2.5 mm^3). During the 6^{th} acquisition a bolus of 0.2 mL/kg of Gd-DTPA-BMA (Omniscan®, GE Healthcare, Princeton, NJ, USA) was injected intravenously in the saphenous leg vein.

VFA-based T_1 mapping

Based upon the Bloch equation[157], a steady-state MR signal intensity (s_k) acquired by a T1-weighted SPGR sequence with a flip angle (FA) of a_k (k=1,2,.., N_{FA}; N_{FA} is the number of FAs) and a repetition time TR is given by:

$$S_k = \frac{M_o \sin a_k (1-E)}{1-E*\cos a_k} \qquad \text{Eq. (1)}$$

where M_o is the equilibrium longitudinal magnetization, and $E= e^{(-TR/T1)}$. Pre and Post- contrast 3D SPGR images were processed off-line using an in-house algorithm developed in Matlab (The MathWorks, Inc., MA, USA). T1 and M_0 maps using the VFA method were generated by fitting the voxel-wise image intensities at Eq. [1] using polynomial curve fitting algorithm and $a_1=5^o$, $a_1=5^o$, $a_2=10^o$, $a_3=15^o$, $a_4=20^o$ $a_5=35^o$. Since grey matter (GM), white matter (WM), CSF etc. have distinctive characteristic T_1 times, T_1 mapping was used for GM and WM segmentation. The method was first validated in a phantom (Mahgphan® Quantitative Imaging Phantom) with known T_1 times as shown in Figure 38Figure 38, while the results are summarized in Table 9.

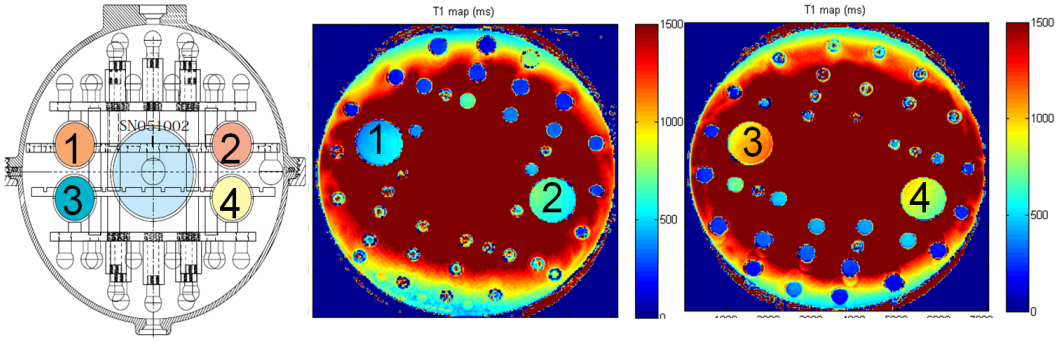

Figure 38. Phantom validation of the VFA-based T_1 mapping technique

Sphere #	Target T1 (ms)	
	Actual	Measured
1	450	460 ± 37
2	600	619 ± 48
3	900	897 ± 24
4	750	760 ± 36

Table 9. A comparison between the actual and the estimated T_1 times. A good agreement was found.

DR1 mapping and BBB opening detection in the Grey and White Matter

The relaxivity maps R1 before ($R1_{pro}$) and after ($R1_{post}$) the CA injection were also generated (R1=1/T1) offline. Since R_1 relaxation rate increases only where Gd-DTPA-BMA diffuses, $\Delta R1=R1_{post} - R1_{pre}$ maps were generated and used for the detection and quantification

of the BBB opening, using the CA as a tracer for the BBB opening. In principle, DR1 should be greater than zero in the areas where Gd-DTPA-BMA diffused through the opened BBB. In practice, a threshold of DR1>0.05 s^{-1} was set, due to the noise in the background in order for the BBB opening to be detected. Also, each voxel within the BBB opening region satisfied the positive DR1 criterion also had a known T_1 relaxation time and therefore the structure (GM or WM) in which it belonged was characterized. In that manner, the volume of opening (V_{BBB}) in the GM and WM were quantified.

Concentration mapping and delivery efficiency estimation

Magnetic resonance contrast agent concentration maps ([Gd]) were then generated from the $T_{1,0}$ time before MR-CA injection and the T_1 time after MR-CA injection using the equation [158]

$$\frac{1}{T_1} = \frac{1}{T_{1,o}} + r_{Gd} * [Gd] \leftrightarrow [Gd] = \frac{1}{r_{Gd}} \left(\frac{1}{T_1} - \frac{1}{T_{1,o}}\right) \qquad \text{Eq. (2)}$$

The Gd-DTPA-BMA concentration [Gd] was then converted to the mass amount of the CA delivered in the BBB opening area by multiplying with the voxel volume, i.e. 0.89 mm x 0.89 mm x 1 mm = 0.79 mm^3 = 0.79 μL, since 1 mM= 1mmol/L. The total amount of Gd-DTPA-BMA delivered to the brain through the BBB opening was therefore estimated. Using the GM and WM T_1-mapping based segmentation, the total amount of Gd-DTPA-BMA was also separately estimated in the GM and WM as shown in **Figure 39**.

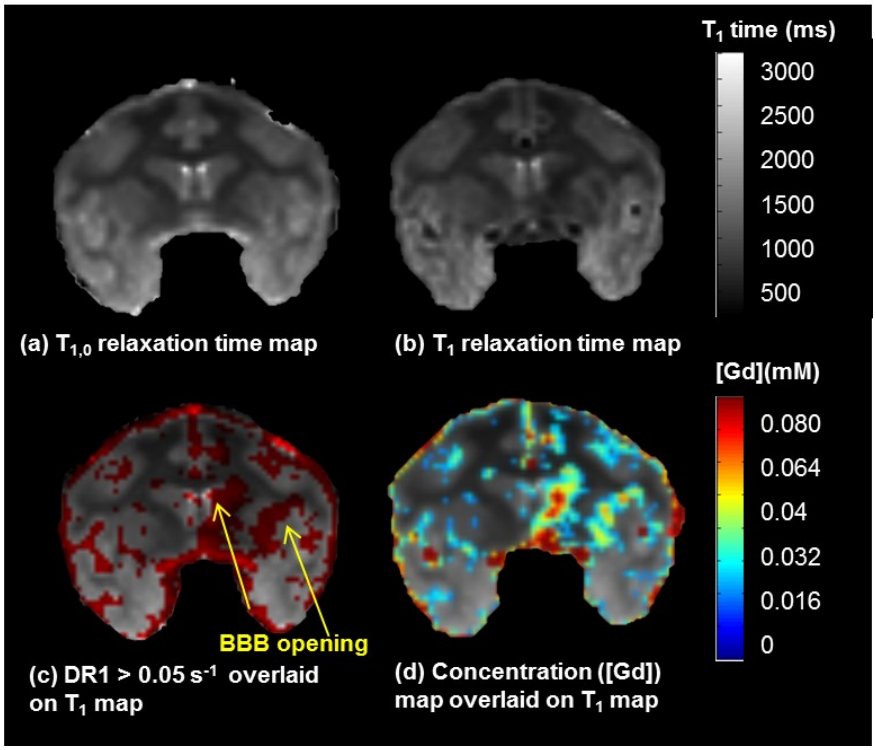

Figure 39. $T_{1,0}$ relaxation times map before contrast agent injection and (b) T_1 relaxation times map after contrast agent injection. (c) The voxels that are satisfied the DR1 > 0.05 s^{-1} threshold criterion are red and are depicting only the brain areas where gadolinium diffused; apart from the BBB-opening area gadolinium also appears in the vasculature. DR1 is overlaid on $T_{1,0}$ map in order to visualize the V_{BBB} in the gray matter (GM) and white matter (WM). In (d) gadolinium concentration map ([Gd]) is shown, overlaid again on the $T_{1,0}$ map in order to visualize the [Gd] in the GM and WM. Most of the V_{BBB} was detected in the GM, along with higher [Gd] in these areas.

The amount of CA injected in the bloodstream was also known, so the ratio of the amount of CA that was delivered to the BBB opening over the amount of CA that was injected in the bloodstream was measured and reported for delivery efficiency estimation.

Permeability mapping

The General Kinetic Model (GKM), and in particular the extended modified Tofts model[142], [159] was used to quantify the permeability in the NHP brain following the first order differential equation:

$$\frac{dC_t(t)}{dt} = K_{trans}C_P(t) - K_{ep}C_t(t) \qquad \text{Eq. (3)}$$

where K_{trans} and K_{ep} are the transfer rates from the blood plasma to the extravascular extracellular space (EES) and vice versa, $C_p(t)$ and $C_t(t)$ are the concentrations of Gd-DTPA-BMA in the blood plasma and EES respectively. The plasma concentration $C_P(t)$ is a fraction of the concentration in the blood $C_B(t)$ defined as $C_P(t)=(1-H_{ct})\ C_b(t)$, where H_{ct} is the animals hematocrit. The $C_P(t)$ also

provides the Arterial Input Function (AIF) which, following a bolus injection in the bloodstream, follows a bi-exponential decay of the form:

$$C_P(t) = A_1 e^{-m_1 t} + A_2 e^{-m_2 t} \qquad \text{Eq. (4)}$$

where A_1,A_2 and m_1,m_2 are the amplitude and decay rates respectively. The AIF was fitted individually for each experiment in a custom algorithm in Matlab (MathWorks, Inc. Natick, MA, USA) in order to provide accurate and robust estimations for each case. Eq(4) is substituted in eq.(3) which then can be expressed in the equivalent form:

$$C_t(t) = \left(\frac{K_{trans}A_1}{m_1 - K_{ep}} + \frac{K_{trans}A_2}{m_2 - K_{ep}}\right) e^{-K_{ep}t} - \frac{K_{trans}A_1}{m_1 - K_{ep}} e^{-m_1 t} - \frac{K_{trans}A_2}{m_2 - K_{ep}} e^{-m_2 t} \text{ Eq. (5)}$$

The measured signal for the DCE-MRI T1-weighted images is converted to concentration using the Solomon-Bloembergen equation [160]:

$$[Gd(t)] = \frac{S_{post}(t) - S_{pre}}{S_{pre} \times T_{1,0} \times r_1} \quad \text{Eq.(6)}$$

where the $T_{1,0}$ which is the longitudinal relaxation time of the voxel as measured using the VFA-bases T1 mapping technique mentioned earlier. The K_{trans} and K_{ep} values at each voxel were conventionally estimated from the measured [Gd(t)] by a non-linear least squares (NLS) fitting

$$\Phi(K_{trans}, K_{ep}) = \sum_{t=1}^{NR} (C_t(t) - Gd(t))^2$$

where NR is the the number of repetitions, i.e. 90, implementing a trust region reflective algorithm developed in Matlab (MathWorks, Inc. Natick, MA, USA). K_{trans} and K_{ep} maps were generated for the whole brain, to better visualize the opening in the FUS-targeted regions. The average K_{trans} was also calculated in the entire V_{BBB}, as well as separately in the GM and WM.

Statistical Analysis

One-way analysis of variance (ANOVA) was performed for each NHP to compare the differences among different pressures for V_{BBB}, total Gd-DTPA-BMA amount delivered and K_{trans}. When the null hypothesis was rejected based on the ANOVA, a post-hoc statistical analysis was performed using Tukey's multiple comparisons test. This test was selected because it assumes independence of the observations being tested, as well as equal variation across observations. It is essentially a Student's t-test, except that it corrects for family-wise error-rate.

5.1.3. Results

An example of the BBB-opening in the Caudate and the Putamen of the left hemisphere of NHP 1, sonicated at 300 kPa is shown in **Figure 40**. The opening is not easily detected in the post-Gd T1-w image. No edema or hemorrhage is detected in the T2-w and SWI respectively. V_{BBB} is detected using the DR1 mapping and is shown in red overlaid on T_1 map, revealing that it was mostly induced in the GM. The concentration map reveals the diffusion pattern, where higher

[Gd] was detected in the GM mostly. Finally, the 3D permeability map reveals an increase in the sonicated areas only.

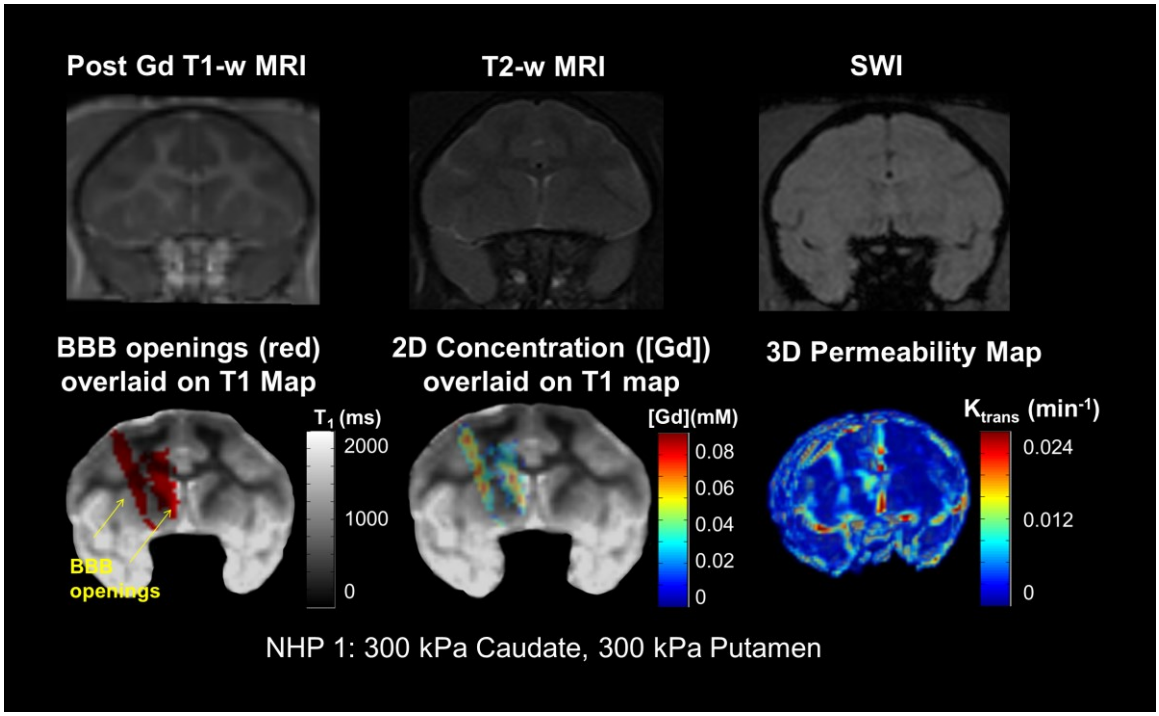

Figure 40. Example of the BBB-opening in the Caudate and the Putamen of the left hemisphere of NHP 1, sonicated at 300 kPa.

An example of the BBB opening in the Caudate of the right hemisphere of NHP 2, sonicated at 450 kPa is shown in **Figure 41**. The opening is not easily seen in the post-Gd T1-w image. No edema or hemorrhage is detected in the T2-w and SWI, respectively. V_{BBB} is detected using the DR1 mapping and is shown in red overlaid on T_1 map, revealing that it was mostly induced in the GM, interrupted by the WM. The concentration map reveals the diffusion pattern, where lower [Gd] was detected than in **Figure 40** and NHP 1. Finally, the 3D permeability map reveals an increase in the sonicated area only, discontinued in the WM.

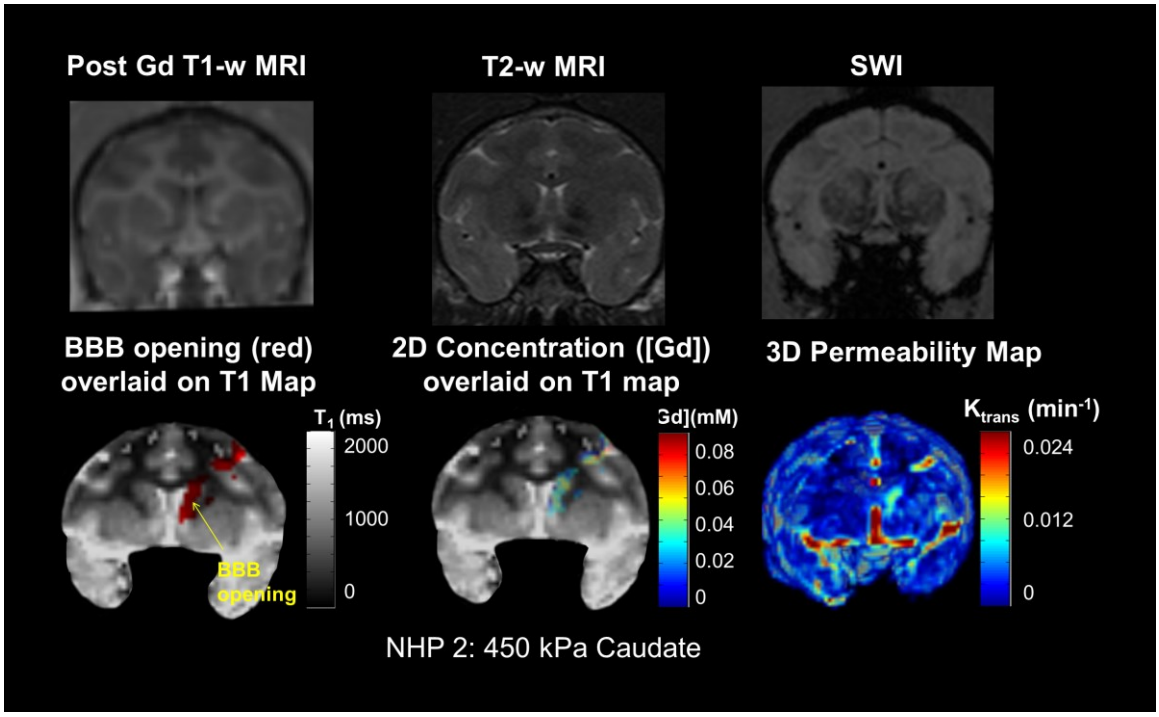

Figure 41. Example of the BBB-opening in the Caudate of the right hemisphere of NHP 2, sonicated at 450 kPa.

Quantifative measurements of the volume of opening (V_{BBB}) in NHP 1 and NHP 2, along with the GM and WM segmentation are shown in **Figure 42 (a)** and **(b)**. V_{BBB} in NHP 2 as shown, was lower than the V_{BBB} in NHP 1 for the pressures tested. For NHP 1, ANOVA revealed statistically significant differences among the groups, and in particular significant difference ($p<0.01$) was detected between the lowest pressure (200 kPa) and the medium pressure (300 kPa), and even more significant difference ($p<0.001$) was detected between the lowest and the highest pressure (600 kPa). The V_{BBB} was increased in the GM, compared to the WM. For NHP 2, ANOVA did not reveal any statistically significant differences among the three acoustic pressures used; however, there was an increase with pressure.

The total amount of gadoloinium (Gd-DTPA-BMA) detected in the GM and the WM is shown in **Figure 42(c)** for NHP 1 and **Figure 42 (d)** for NHP 2. For NHP 1, a statistically significant difference of $p<0.001$ and $p<0.0001$ was detected between the lowest pressure and the medium and highest pressures respectively. There was also significant difference ($p<0.05$) between the medium and the highest pressure amplitude. For NHP 2, the only significance ($p<0.05$) in the total amount of gadolinium delivered to the BBB opening was between the lowest and the highest pressure.

Boxplots of the average K_{trans} measured in both the GM and WM for all pressures used for NHP 1 and NHP 2 are shown in **Figure 42 (e)** and **(f)** respectively. The far left side shows the background permeability of the brain in GM and WM. On average, the permeability in the GM was

higher than the permeability in the WM by 1.29 ± 0.23 $*10^{-4}$/s, while they both increased with acoustic pressure. Again, the average K_{trans} was greater in NHP 1 than in NHP 2.

The total amount of Gd-DTPA-BMA for all PNP and both NHPs are shown together in **Figure 42 (g).** The amount delivered at the lowest PNP for NHP 1, i.e. 200 kPa, was not significantly different from the amount delivered at the lowest PNP for NHP 2, i.e. at 300 kPa. However, at 300 kPa there was significantly more amount delivered in NHP 1 than in NHP 2, for both the caudate and the putamen. The amount delivered in NHP 1 increased rapidly with PNP, but for NHP 2 the slope was less steep. The average increase in permeability for all PNPs in both NHPs is shown in **Figure 42 (h).** It increased with pressure but no significant differences were detected.

Finally, the average V_{BBB} calculated using the DR1 method was on average 73 mm^3 higher than the V_{BBB} detected with permeability mapping.

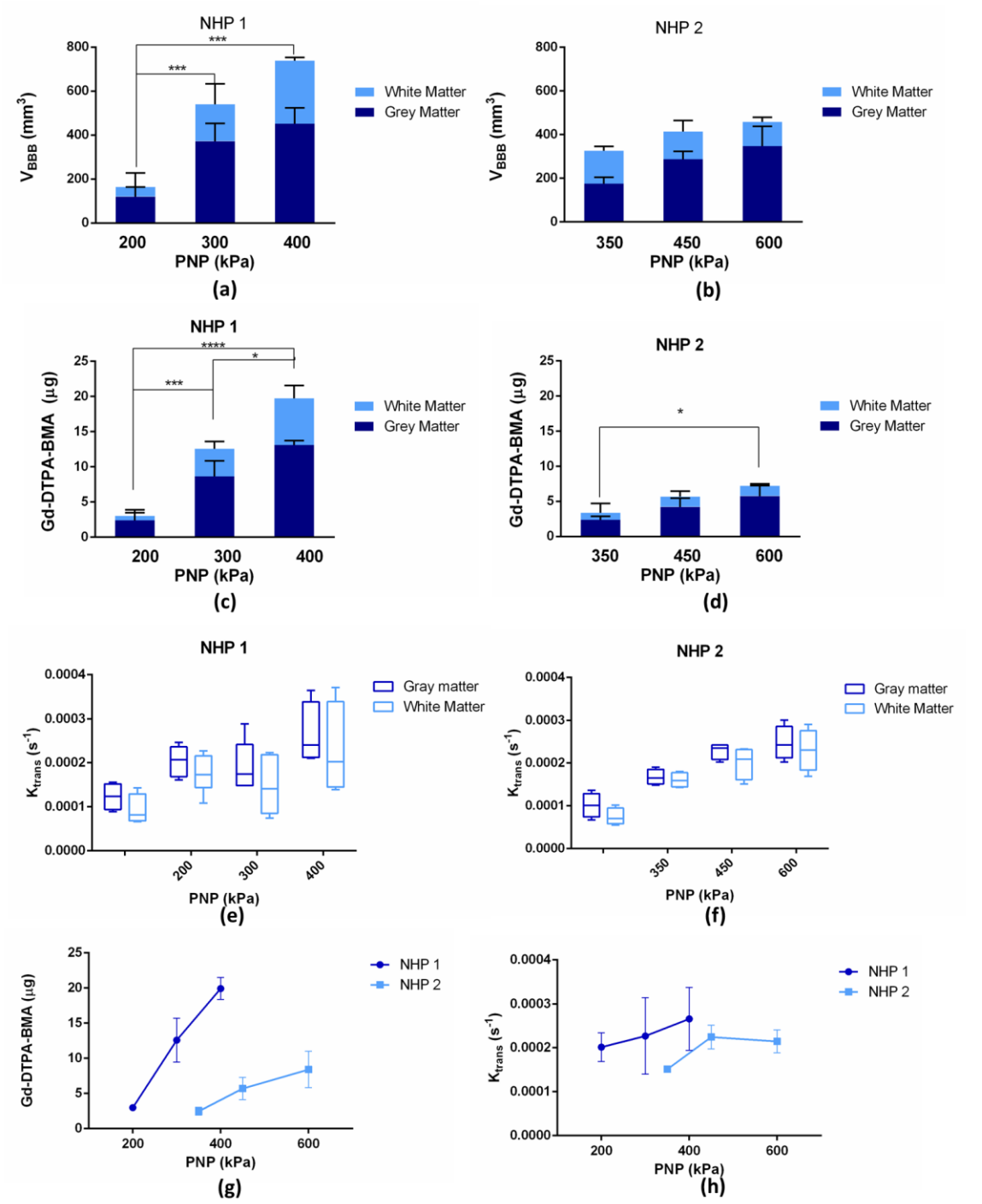

Figure 42. Volume of opening (V_{BBB}) in NHP 1 in the GM and WM. Two asterisks (**) denote $p<0.01$, three asterisks (***) denote $p<0.001$ and was detected between the lowest and the highest pressure (600 kPa). V_{BBB} was increased in the GM, compared to the WM. (b) V_{BBB} in NHP 2 is shown, in the GM and WM. (c) Total amount of gadoloinium (Gd-DTPA-BMA) in NHP 1, divided in the amount detected in the GM and the WM, and in NHP 2 in (d). (e) Boxplots of the average K_{trans} in NHP 1, showing the background K_{trans} of the brain in the GM and WM, and in NHP 2 in (f).

Scatter plots of Gd-DTPA-BMA versus V_{BBB} and K_{trans} are shown in **Figure 43 (a) and (b)** respectively. For the Gd-DTPA-BMA and V_{BBB} correlation, a linear regression showed a correlation of R^2=0.91 for NHP 1, compared to R^2=0.51 for NHP 2. Combining the results from both the NHPs, the R^2 was measured equal to 0.80. No correlation was detected between Gd-DTPA-BMA and K_{trans}.

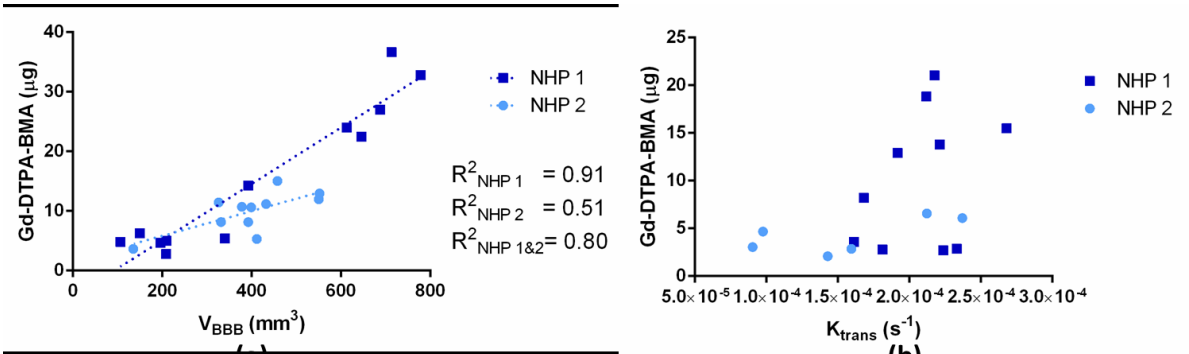

Figure 43. Correlation between Gd-DTPA-BMA and V_{BBB} and (b) K_{trans}

The amount of Gd-DTPA-BMA delivered for all PNPs and NHPs is summarized in **Table 10,** along with the delivery efficiency estimation. Efficiency was increased with pressure, however, it was different for the two NHPs.

NHP 1			NHP 2		
PNP	**Amount delivered (µg)**	**Delivery efficiency (%)**	**PNP**	**Amount delivered (µg)**	**Delivery efficiency (%)**
200	2.99 ± 0.42	0.0007 ± 0.0001	**300**	2.47 ± 0.55	0.0005 ± 0.0001
300	9.18 ± 5.84	0.0022 ± 0.0012	**450**	5.71 ± 1.58	0.0012 ± 0.0003
400	19.93 ± 1.56	0.0043 ± 0.0003	**600**	7.22 ± 1.27	0.0016 ± 0.0003

Table 10. Drug delivery efficiency

5.1.4. Discussion

In this study, pharmacodynamic analysis was performed for the first time in order to characterize the physiologic characteristic changes as well as the delivery efficiency in two non-human primates following the FUS-induced BBB opening in vivo. The acoustic pressure was also varied in order to investigate the effects of this parameter and design an optimal and efficient drug delivery treatment plan. The volume of opening, the amount of model drug delivered and the permeability increased with the acoustic pressure. However, the increase was more profound in

one NHP compared to the other, suggesting the effect of individual differences in the outcome of the treatment.

A major innovation in this study is the introduction of quantitative MR relaxometry techniques, i.e. DR1 mapping, for the detection and characterization of BBB opening. Previously, pre- and post- contrast T1-weighted imaging has been used for detection of BBB opening in NHP, with arbitrary opening detection thresholds, which may induce further variability and discrepancy in results among different studies and experiments. The methods and analysis implemented here provide a robust protocol for detection of BBB opening, user-independent, along with quantitative information with high spatial resolution. The MR sequences and offline algorithms for data processing were also validated in phantoms (**Figure 38)**, in order to safely report accurate quantitative measurements. Segmentation of grey and white matter (**Figure 39)**, based upon their distinctive T_1 relaxation times and quantification of the opening volume in each of them individually was done in this study for the first time, revealing further insights to the effect of the FUS-application to the highly inhomogeneous brain.

MR-contrast agent concentration mapping and permeability mapping have been previously used for brain studies in rodents [10], [107], [145]; however, it is used here for the first time in NHP, and additionally, delivery efficiency was estimated following a three-dimensional analysis. Firstly, the analysis provided in this study offers very critical insights for the clinical application of the FUS-induced BBB opening, since the ultimate goal is drug delivery in therapeutically-relevant doses. Moreover, it constitutes an *in vivo* tool for studying drug delivery efficiency, indirectly and non-invasively, without the need to sacrifice or expose the subject to radiation; this is a major advantage compared to other techniques that are used for the same purpose such as protein quantification in excised brains *post-portem*, or PET-CT in conjunction with the injection of radiolabelled molecules. Gadolinium Gd-DTPA-BMA is used in this study as a model drug and it has relatively low molecular weight (574 Da), thus, the delivery efficiency and permeability may be different using different drugs with higher molecular weight, different half-life, apparent diffusion coefficient etc. Nevertheless, the trend and the patterns shown in the mapping can still be used for qualitative as well as statistical analysis afor optimization of the acoustic parameters in order to achiever efficient and safe drug delivery.

One interesting finding is the difference in the effect of acoustic pressure between the two NHPs, which belong to the same species, have the same age and weight. Consistently, NHP 1 had larger volumes of opening, higher amount of Gd-DTPA-BMA delivered, and slightly higher average permeability than NHP 2 (**Figure 42**). For these reasons, different pressures were selected for the two NHPs, based on their acoustic pressure opening threshold which was studied before selecting the parameters shown in this study. For NHP 1, the lowest pressure used was 200 kPa, compared to 350 kPa which was the lowest pressure used for NHP 2. Also the highest pressure was 400 kPa for NHP 1, and was shown to cover the entire area of interest, for NHP 2 it

was 600 kPa and it never reached the same amount of opening volume. The results of the statistical analysis confirmed that there are significant differences among the two NHP's, and therefore, the results from the two NHPs were studied independently, and further statistical analyses were performed among experiments from the same NHP in all cases.

For NHP 1, significant difference was detected between the lowest acoustic pressure and the each of the higher pressures in the opening volume (**Figure 42**). Significant difference was detected among all different pressures in the amount of Gd-DTPA-BMA delivered. These findings indicate that the volume of opening might have reached a plateau at the higher pressures, whereas the amount of Gd-DTPA-BMA delivered kept increasing with pressure. The average K_{trans} did not significantly vary with acoustic pressure; however, it is significantly increased compared to the sham group. It could thus be hypothesized, as previously reported [10], that the average K_{trans} might be underestimating the effect of permeability change in the brain and might not be a very sensitive indicator, but it can still be used to reveal the trend.

For NHP 2, no significant differences were detected in the volume of opening among the groups with different acoustic pressures used (**Figure 42)**. Significance between the the lowest and the highest acoustic pressure was detected in the amount of Gd-DTPA-BMA though. NHP 2, as previously mentioned, also consistently had lower opening volumes etc than NHP 1. Inherently, the permeability of the sham experiments in NHP 2 was slightly lower than in NHP 1, which could be one possible explanation as to why NHP 2 was more "resistant" to BBB opening. Furthermore, the shape of the skulls of these two NHP's is not identical, a variation which simulates the differences among different individuals that should be expected in a clinical setting. The incidence angle, along with aberration effects could be another reason why higher acoustic pressures were required in NHP 2; factors which were not analyzed within this study, but are currently being analyzed by the group and will be reported independently.

Despite the offset between the two NHP's and the different outcomes with the acoustic pressure, there were also some findings that were observed in both NHPs. Firstly, BBB opening was mainly contained within the grey matter, and in many cases it was shown to be discontinued in the white matter. At the same time, white matter was measured to be less permeable than grey matter, which could be a possible explanation for this phenomenon. White matter is known to be less vascular than grey matter [161], therefore it could be hypothesized that less microbubbles were able to circulate in the white matter area to interact with the FUS acoustic wave and induce BBB opening, and also, less amount of Gd-DTPA-BMA was able to reach the white matter and diffuse through the disrupted BBB.

An interesting finding comparing the V_{BBB} as quantified through the DR1 method and the the permeability increase was that on average it was found to be 73 mm^3 higher using the former technique. This could be attributed to the fact that K_{trans} takes into consideration only the first 20 min post contrast agent injection, whereas the $R1_{post}$ is acquired after the end of the DCE-MRI

and lasts for another 20 min, a time frame during which Gd-DTPA-BMA may be able to further diffuse into the tissue. This finding supports that permeability and diffusion should not be confused and they are affectively different.

Moreover, both NHP's had a good correlation when a linear regression was fit between the amount of Gd-DTPA-BMA delivered and the volume of opening V_{BBB}. NHP 1 had better linear correlation coefficient than NHP 2, although, when combined R^2 remained pretty high and equal to 0.80 (**Figure 43**). No correlation was found between the amount of Gd-DTPA-BMA and the average increase in permeability. These findings imply that the amount of drug delivered linearly increased with the volume of opening, while the average permeability change was not an accurate predictor for the amount of drug that could be delivered.

Finally, the delivery efficiency, which was the ratio of the amount of Gd-DTPA-BMA that was delivered in the entire BBB opening volume over the amount that was injected in the bloodstream, showed that the percentage was very low for both NHP's, however, it is within the clinical relevant dose (**Table** 10). For example, in a recent study[14], a total of 30 μg of exogenous Neurturin (NTN) was infused in the putamen of MPTP-lesioned rhesus monkeys in multiple sessions over 3 months and some motor and dopaminergic function restoration was observed. In this study, we were able to deliver up to 20 μg with the use of FUS and cover the entire putamen, and the experiments were performed biweekly in each monkey. Also, in that study, enhanced tissue distribution remained a challenge, whereas with our technique the model drug was detected in the entire putamen using a single FUS sonication, suggesting the high potential of the technique for the treatment of neurodegenerative diseases.

5.1.5. Conclusions

In this study, permeability and drug delivery dose were measured in vivo in NHP for the first time, in order to assess the efficiency of the FUS-induced BBB opening as a technique with therapeutic potential for neurodegenerative diseases such as Parkinson's disease. Relaxometry techniques, i.e. T_1 and DR1 mapping were used for the robust quantitative detection of the BBB opening and the grey and white matter segmentation. Differences between the two NHPs used were detected and attributed to physiologic differences among individuals as observed after characterizing their brain permeability. Overall, the volume of opening was greater in the grey matter than the white matter, and was sometimes found to be discontinued in the white matter, which was also shown to be less permeable. The contrast agent's oblique diffusion patterns revealed important information of the FUS-induced BBB opening following the patterns of the underlying brain structures. FUS-induced drug delivery increased with the acoustic pressure used, suggesting the importance of the technique for clinical applications. The dose of Gd

delivered to the brain parenchyma remained within the 1-25 μg range with the acoustic parameters used in this study; which is a clinically relevant dose for brain applications.

Section 5.2: Contribution

Our group, among others[48],[49], has already completed a significant amount of work towards the pre-clinical translation, conducting feasibility studies which confirmed that FUS-induced BBB opening in NHP can be achieved [156], and it is non-invasive, localized and transient [56]. Moreover, a study has been conducted investigating the acoustic emissions during the application and the impact on the brain based on T_1-weighted MRI [154]. Overall, in this specific aim, an in vivo tool for the characterization of the FUS-induced BBB opening in a larger animal model was designed and used for the first time. This study used an indirect method to measure the amount of the model drug delivered to the brain, for the first time, while the permeability changes and the volume of opening were also measured and correlated to the underlying structures, such as the gray and white matter. This step was critical and necessary to ensure the efficiency and safety of the technique in a pre-clinical setting in order to eventually be applied in humans.

Regarding the research contribution, Professor Vincent P. Ferrera, Ph.D. (Associate Professor, Neuroscience, Psychiatry, Columbia University) provided the animal subjects in the study and his scientific input throughout the experiments. Carlos Sierra Sánchez, Ph.D. (Postdoctoral Research Scientist, Department of Biomedical Engineering, Columbia University) manufactured the microbubbles necessary for the experiments, Matthew Downs (PhD student, Department of Biomedical Engineering, Columbia University) assisted with the animal preparation, Shih-Ying Wu (PhD student, Department of Biomedical Engineering, Columbia University) and Amanda Buch (Intern, Department of Biomedical Engineering, Columbia University) conducted the FUS part of the experiment, and assisted with the animal preparation and anesthesia. Stefanos Papadopoulos (MSC student, Department of Biomedical Engineering, Columbia University) assisted with data processing. Maria Eleni Karakatsani (PhD student, Department of Biomedical Engineering, Columbia University) assisted throughout the entire experiment for all steps (microbubble preparation and measurement, animal preparation, animal anesthesia, monitoring animal welfare, FUS application, MRI scans, drug administration) and assisted with data processing. Most importantly, the author would like to thank Dr. Sachin Jambawalikar (Assistant Professor of Radiology – Physics, Columbia University) for assisting with the design of MRI scan sequences, data handling, data analysis, mathematical processing, and his overall input in the quantification methods from data acquisition to data analysis.

CONCLUSION:

Overall contribution

This thesis entails the analysis of the focused-ultrasound induced blood-brain barrier opening *in vivo* for drug delivery for neurodegenerative diseases. In summary, the method was designed and validated to ensure a non-invasive, localized, transient, and most importantly efficient and safe FUS-induced BBB opening in mice using pharmacokinetic analysis. This was then used for a drug delivery and potential treatment application in a Parkinson's disease mouse model, investigating the effects on the reversibility of the disease phenotype of the method using a neurotrophic factor as a therapeutic agent. Finally, pharmacokinetic analysis was performed also in NHP in order to achieve a safe and efficient pre-clinical translation, as shown in Figure 44

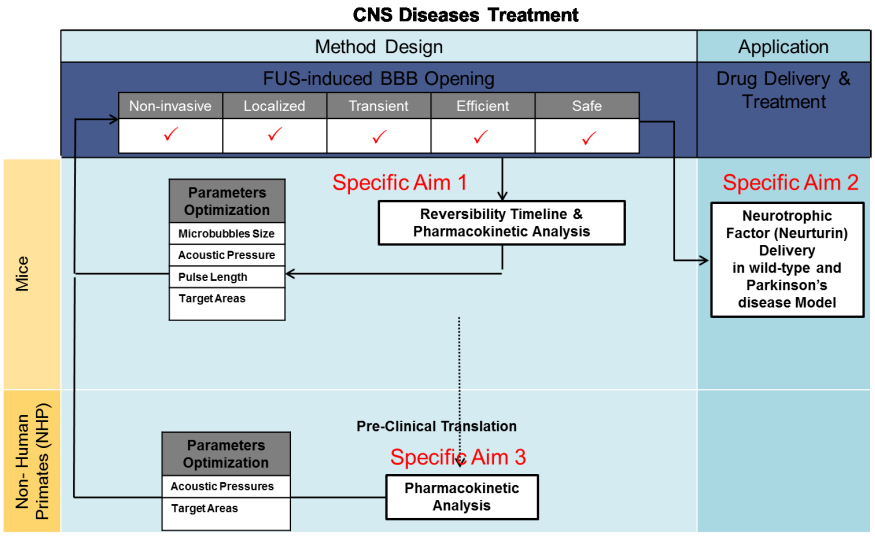

Figure 44. Specific aims of the thesis

First, the reversibility timeline and pharmacodynamic analysis were studied in wild type mice to optimize the FUS parameters for safe and efficient drug delivery. The volume of opening was found to increase with both peak negative FUS pressure and microbubble diameter. The duration required for closing was found to be proportional to the volume of opening on the day of opening, and ranged from 24 h to 5 days. Overall, larger bubbles (4-5 μm and 6-8 μm in diameter) did not show any significant differences. Also, the extent of BBB opening decreased radially towards the focal region until the BBB integrity was fully restored. Permeability and

volume of opening were both found to increase with the acoustic pressure and pulse length, while a trade-off relationship was also found. Linear regression between K_{trans} and V_{BBB} showed a good correlation fit. Also, the time required for closing linearly increased with V_{BBB}. The volume decay rate was measured to be 11.4 ± 4.0 mm^3 per day suggesting that the closing timeline could be predicted from the initial volume of opening.

For the second part of this thesis, Neurturin (NTN), a member of the GDNF family which has been demonstrated to have neuroprotective and regenerative effects on dopaminergic neurons in vivo using invasive drug delivery methods, was successfully delivered to the Substantia Nigra (SN) and striatal Caudoputamen (CP) of wild-type and parkinsonism MPTP mouse model. Following the optimization of FUS parameters and target locations in the murine brain, it was found that the FUS significantly enhanced the delivery of NTN compared to the direct injection technique, while triggering of the signaling cascade was detected downstream to the neuronal nuclei. In the MPTP model, it was found that a single administration of NTN through the FUS-induced BBB opening, achieved some increase in the number of neurons at the sonicated side after four weeks of survival post treatment. These findings thus indicate the potential of the FUS method to mediate transport of proteins through the blood-brain barrier in a PD animal model, and the potential of this technique in the reversibility of the PD phenotype.

For the third and final part of this thesis, the permeability and drug delivery dose were measured in vivo in NHP for the first time, in order to assess the efficiency of the FUS-induced BBB opening as a technique with therapeutic potential for neurodegenerative diseases such as Parkinson's disease. Relaxometry techniques, i.e. T_1 and DR1 mapping were used for the robust quantitative detection of the BBB opening and the grey and white matter segmentation. Differences between NHPs used were detected and attributed to the physiologic differences among individuals as observed after characterizing their brain permeability. Overall, the volume of opening was greater in the grey matter than in the white matter, and was sometimes found to be discontinued in the white matter, which was also shown to be less permeable. The contrast agent's oblique diffusion patterns revealed important information of the FUS-induced BBB opening following the patterns of the underlying brain structures. FUS-induced drug delivery

increased with the acoustic pressure used, suggesting the importance of the technique for clinical applications. The dose of the model drug delivered to the brain parenchyma remained within the 1-25 μg range with the acoustic parameters used; which is a clinically relevant dose for brain applications.

Future work

The promising results of this thesis strongly indicate the potential of this method in the treatment of CNS diseases, eventually in a clinical setting.

In particular, regarding the reversibility of the PD phenotype, the outcome of repeated sessions and delivery of NTN as well as other neurotrophic factors and drugs should be investigated in the future and validated in small and larger animals. Other CNS diseases, such as Alzheimer's disease and Glioblastoma, as well as other disease animal models, such as the 6-OHDA for PD, Amyloid-β transgenic mice and Tau transgenic mice models for AD, should also be studied as part of the future work following this thesis. Regarding the drugs delivered, any compounds that have shown potential in vitro on vivo using invasive or localized techniques to circumvent the BBB, could be tested with the FUS method, since it was shown that it efficiently enhanced the delivery of the drug to the brain parenchyma in this thesis.

The pharmacodynamic analysis in NHP should be continued in more subjects in order to better interpret the results and discrepancies among individuals. The methods proposed and investigated here for BBB opening characterization could be directly applied in humans. Therapeutic effects could be further tested in an MPTP NHP model as well, as a pre-clinical evaluation .

REFERENCES

[1] W. M. Pardridge, “Drug Targeting to the Brain,” *Pharm. Res.*, vol. 24, no. 9, pp. 1733–1744, Jun. 2007.

[2] N. J. Abbott and I. A. Romero, “Transporting therapeutics across the blood-brain barrier,” *Mol. Med. Today*, vol. 2, no. 3, pp. 106–113, Mar. 1996.

[3] W. M. Pardridge, “The blood-brain barrier: bottleneck in brain drug development,” *NeuroRx J. Am. Soc. Exp. Neurother.*, vol. 2, no. 1, pp. 3–14, Jan. 2005.

[4] N. J. Abbott, L. Rönnbäck, and E. Hansson, “Astrocyte-endothelial interactions at the blood-brain barrier,” *Nat. Rev. Neurosci.*, vol. 7, no. 1, pp. 41–53, Jan. 2006.

[5] J. J. Choi, M. Pernot, S. A. Small, and E. E. Konofagou, “Noninvasive, transcranial and localized opening of the blood-brain barrier using focused ultrasound in mice,” *Ultrasound Med. Biol.*, vol. 33, no. 1, pp. 95–104, Jan. 2007.

[6] K. Hynynen, N. McDannold, N. Vykhodtseva, and F. A. Jolesz, “Noninvasive MR imaging-guided focal opening of the blood-brain barrier in rabbits,” *Radiology*, vol. 220, no. 3, pp. 640–646, Sep. 2001.

[7] F.-Y. Yang, W.-M. Fu, R.-S. Yang, H.-C. Liou, K.-H. Kang, and W.-L. Lin, “Quantitative evaluation of focused ultrasound with a contrast agent on blood-brain barrier disruption,” *Ultrasound Med. Biol.*, vol. 33, no. 9, pp. 1421–1427, Sep. 2007.

[8] H.-L. Liu, Y.-Y. Wai, W.-S. Chen, J.-C. Chen, P.-H. Hsu, X.-Y. Wu, W.-C. Huang, T.-C. Yen, and J.-J. Wang, “Hemorrhage detection during focused-ultrasound induced blood-brain-barrier opening by using susceptibility-weighted magnetic resonance imaging,” *Ultrasound Med. Biol.*, vol. 34, no. 4, pp. 598–606, Apr. 2008.

[9] G. Samiotaki, F. Vlachos, Y.-S. Tung, and E. E. Konofagou, “A quantitative pressure and microbubble-size dependence study of focused ultrasound-induced blood-brain barrier opening reversibility in vivo using MRI,” *Magn. Reson. Med. Off. J. Soc. Magn. Reson. Med. Soc. Magn. Reson. Med.*, Aug. 2011.

[10] G. Samiotaki and E. E. Konofagou, “Dependence of the reversibility of focused- ultrasound-induced blood-brain barrier opening on pressure and pulse length in vivo,” *IEEE Trans. Ultrason. Ferroelectr. Freq. Control*, vol. 60, no. 11, pp. 2257–2265, Nov. 2013.

[11] T. Sun, G. Samiotaki, and E. E. Konofagou, “Prediction of the reversibility of the ultrasound-induced blood-brain barrier opening using passive cavitation detection with magnetic resonance imaging validation,” *J. Acoust. Soc. Am.*, vol. 134, no. 5, p. 4183, Nov. 2013.

[12] C. Rosenblad, D. Kirik, B. Devaux, B. Moffat, H. S. Phillips, and A. Björklund, “Protection and regeneration of nigral dopaminergic neurons by neurturin or GDNF in a partial lesion model of Parkinson’s disease after administration into the striatum or the lateral ventricle,” *Eur. J. Neurosci.*, vol. 11, no. 5, pp. 1554–1566, May 1999.

[13] Y. Oiwa, R. Yoshimura, K. Nakai, and T. Itakura, “Dopaminergic neuroprotection and regeneration by neurturin assessed by using behavioral, biochemical and histochemical measurements in a model of progressive Parkinson’s disease,” *Brain Res.*, vol. 947, no. 2, pp. 271–283, Aug. 2002.

[14] R. Grondin, Z. Zhang, Y. Ai, F. Ding, A. A. Walton, S. P. Surgener, G. A. Gerhardt, and D. M. Gash, “Intraputamenal infusion of exogenous neurturin protein restores motor and dopaminergic function in the globus pallidus of MPTP-lesioned rhesus monkeys,” *Cell Transplant.*, vol. 17, no. 4, pp. 373–381, 2008.

[15] N. J. Abbott, “Blood-brain barrier structure and function and the challenges for CNS drug delivery,” *J. Inherit. Metab. Dis.*, vol. 36, no. 3, pp. 437–449, May 2013.

[16] W. A. Banks, “Brain meets body: the blood-brain barrier as an endocrine interface,” *Endocrinology*, vol. 153, no. 9, pp. 4111–4119, Sep. 2012.

[17] W. A. Banks, “Blood-brain barrier as a regulatory interface,” *Forum Nutr.*, vol. 63, pp. 102–110, 2010.

[18] P. Grieb, R. E. Forster, D. Strome, C. W. Goodwin, and P. C. Pape, “O2 exchange between blood and brain tissues studied with 18O2 indicator-dilution technique,” *J. Appl. Physiol. Bethesda Md 1985*, vol. 58, no. 6, pp. 1929–1941, Jun. 1985.

[19] W. M. Pardridge, “Drug and Gene Delivery to the Brain: The Vascular Route,” *Neuron*, vol. 36, no. 4, pp. 555–558, Nov. 2002.
[20] J. Stockwell, N. Abdi, X. Lu, O. Maheshwari, and C. Taghibiglou, “Novel central nervous system drug delivery systems,” *Chem. Biol. Drug Des.*, vol. 83, no. 5, pp. 507–520, May 2014.
[21] S. Przedborski, M. Vila, and V. Jackson-Lewis, “Series Introduction: Neurodegeneration: What is it and where are we?,” *J. Clin. Invest.*, vol. 111, no. 1, pp. 3–10, Jan. 2003.
[22] A. V. Kabanov and E. V. Batrakova, “New technologies for drug delivery across the blood brain barrier,” *Curr. Pharm. Des.*, vol. 10, no. 12, pp. 1355–1363, 2004.
[23] W. M. Pardridge, “Drug transport across the blood-brain barrier,” *J. Cereb. Blood Flow Metab. Off. J. Int. Soc. Cereb. Blood Flow Metab.*, vol. 32, no. 11, pp. 1959–1972, Nov. 2012.
[24] S. Craft, L. D. Baker, T. J. Montine, S. Minoshima, G. S. Watson, A. Claxton, M. Arbuckle, M. Callaghan, E. Tsai, S. R. Plymate, P. S. Green, J. Leverenz, D. Cross, and B. Gerton, “Intranasal insulin therapy for Alzheimer disease and amnestic mild cognitive impairment: a pilot clinical trial,” *Arch. Neurol.*, vol. 69, no. 1, pp. 29–38, Jan. 2012.
[25] B. Pavan, A. Dalpiaz, N. Ciliberti, C. Biondi, S. Manfredini, and S. Vertuani, “Progress in drug delivery to the central nervous system by the prodrug approach,” *Mol. Basel Switz.*, vol. 13, no. 5, pp. 1035–1065, 2008.
[26] B. S. Anand, S. Dey, and A. K. Mitra, “Current prodrug strategies via membrane transporters/receptors,” *Expert Opin. Biol. Ther.*, vol. 2, no. 6, pp. 607–620, Aug. 2002.
[27] M. Gynther, K. Laine, J. Ropponen, J. Leppänen, A. Mannila, T. Nevalainen, J. Savolainen, T. Järvinen, and J. Rautio, “Large neutral amino acid transporter enables brain drug delivery via prodrugs,” *J. Med. Chem.*, vol. 51, no. 4, pp. 932–936, Feb. 2008.
[28] M. Gynther, J. Ropponen, K. Laine, J. Leppänen, P. Haapakoski, L. Peura, T. Järvinen, and J. Rautio, “Glucose promoiety enables glucose transporter mediated brain uptake of ketoprofen and indomethacin prodrugs in rats,” *J. Med. Chem.*, vol. 52, no. 10, pp. 3348–3353, May 2009.
[29] C. D. Chapman, W. H. Frey, S. Craft, L. Danielyan, M. Hallschmid, H. B. Schiöth, and C. Benedict, “Intranasal treatment of central nervous system dysfunction in humans,” *Pharm. Res.*, vol. 30, no. 10, pp. 2475–2484, Oct. 2013.
[30] S. V. Dhuria, L. R. Hanson, and W. H. Frey, “Intranasal drug targeting of hypocretin-1 (orexin-A) to the central nervous system,” *J. Pharm. Sci.*, vol. 98, no. 7, pp. 2501–2515, Jul. 2009.
[31] M. A. Reger, G. S. Watson, P. S. Green, C. W. Wilkinson, L. D. Baker, B. Cholerton, M. A. Fishel, S. R. Plymate, J. C. S. Breitner, W. DeGroodt, P. Mehta, and S. Craft, “Intranasal insulin improves cognition and modulates beta-amyloid in early AD,” *Neurology*, vol. 70, no. 6, pp. 440–448, Feb. 2008.
[32] J. J. Lochhead and R. G. Thorne, “Intranasal delivery of biologics to the central nervous system,” *Adv. Drug Deliv. Rev.*, vol. 64, no. 7, pp. 614–628, May 2012.
[33] H. L. Wong, X. Y. Wu, and R. Bendayan, “Nanotechnological advances for the delivery of CNS therapeutics,” *Adv. Drug Deliv. Rev.*, vol. 64, no. 7, pp. 686–700, May 2012.
[34] G. A. Silva, “Nanotechnology approaches to crossing the blood-brain barrier and drug delivery to the CNS,” *BMC Neurosci.*, vol. 9 Suppl 3, p. S4, 2008.
[35] L. Cruz, L. U. Soares, T. D. Costa, G. Mezzalira, N. P. da Silveira, S. S. Guterres, and A. R. Pohlmann, “Diffusion and mathematical modeling of release profiles from nanocarriers,” *Int. J. Pharm.*, vol. 313, no. 1–2, pp. 198–205, Apr. 2006.
[36] S. Parveen, R. Misra, and S. K. Sahoo, “Nanoparticles: a boon to drug delivery, therapeutics, diagnostics and imaging,” *Nanomedicine Nanotechnol. Biol. Med.*, vol. 8, no. 2, pp. 147–166, Feb. 2012.
[37] M. C. Morris, S. Deshayes, F. Heitz, and G. Divita, “Cell-penetrating peptides: from molecular mechanisms to therapeutics,” *Biol. Cell Auspices Eur. Cell Biol. Organ.*, vol. 100, no. 4, pp. 201–217, Apr. 2008.
[38] S. A. Nasrollahi, C. Taghibiglou, E. Azizi, and E. S. Farboud, “Cell-penetrating peptides as a novel transdermal drug delivery system,” *Chem. Biol. Drug Des.*, vol. 80, no. 5, pp. 639–646, Nov. 2012.

[39] V. Sebbage, “Cell-penetrating peptides and their therapeutic applications,” *Biosci. Horiz.*, Feb. 2009.
[40] J. Suhorutsenko, N. Oskolkov, P. Arukuusk, K. Kurrikoff, E. Eriste, D.-M. Copolovici, and U. Langel, “Cell-penetrating peptides, PepFects, show no evidence of toxicity and immunogenicity in vitro and in vivo,” *Bioconjug. Chem.*, vol. 22, no. 11, pp. 2255–2262, Nov. 2011.
[41] E. Koren and V. P. Torchilin, “Cell-penetrating peptides: breaking through to the other side,” *Trends Mol. Med.*, vol. 18, no. 7, pp. 385–393, Jul. 2012.
[42] R. H. Bobo, D. W. Laske, A. Akbasak, P. F. Morrison, R. L. Dedrick, and E. H. Oldfield, “Convection-enhanced delivery of macromolecules in the brain,” *Proc. Natl. Acad. Sci. U. S. A.*, vol. 91, no. 6, pp. 2076–2080, Mar. 1994.
[43] M. Choi, T. Ku, K. Chong, J. Yoon, and C. Choi, “Minimally invasive molecular delivery into the brain using optical modulation of vascular permeability,” *Proc. Natl. Acad. Sci. U. S. A.*, vol. 108, no. 22, pp. 9256–9261, May 2011.
[44] V. Andresen, S. Alexander, W.-M. Heupel, M. Hirschberg, R. M. Hoffman, and P. Friedl, “Infrared multiphoton microscopy: subcellular-resolved deep tissue imaging,” *Curr. Opin. Biotechnol.*, vol. 20, no. 1, pp. 54–62, Feb. 2009.
[45] U. K. Tirlapur, K. König, C. Peuckert, R. Krieg, and K. J. Halbhuber, “Femtosecond near-infrared laser pulses elicit generation of reactive oxygen species in mammalian cells leading to apoptosis-like death,” *Exp. Cell Res.*, vol. 263, no. 1, pp. 88–97, Feb. 2001.
[46] F.-Y. Yang, W.-M. Fu, R.-S. Yang, H.-C. Liou, K.-H. Kang, and W.-L. Lin, “Quantitative evaluation of focused ultrasound with a contrast agent on blood-brain barrier disruption,” *Ultrasound Med. Biol.*, vol. 33, no. 9, pp. 1421–1427, Sep. 2007.
[47] Y.-S. Tung, F. Vlachos, J. J. Choi, T. Deffieux, K. Selert, and E. E. Konofagou, “In vivo transcranial cavitation threshold detection during ultrasound-induced blood-brain barrier opening in mice,” *Phys. Med. Biol.*, vol. 55, no. 20, pp. 6141–6155, Oct. 2010.
[48] N. McDannold, C. D. Arvanitis, N. Vykhodtseva, and M. S. Livingstone, “Temporary disruption of the blood-brain barrier by use of ultrasound and microbubbles: safety and efficacy evaluation in rhesus macaques,” *Cancer Res.*, vol. 72, no. 14, pp. 3652–3663, Jul. 2012.
[49] C. D. Arvanitis, M. S. Livingstone, N. Vykhodtseva, and N. McDannold, “Controlled ultrasound-induced blood-brain barrier disruption using passive acoustic emissions monitoring,” *PloS One*, vol. 7, no. 9, p. e45783, 2012.
[50] K. Ferrara, R. Pollard, and M. Borden, “Ultrasound microbubble contrast agents: fundamentals and application to gene and drug delivery,” *Annu. Rev. Biomed. Eng.*, vol. 9, pp. 415–447, 2007.
[51] S. Qin and K. W. Ferrara, “Acoustic response of compliable microvessels containing ultrasound contrast agents,” *Phys. Med. Biol.*, vol. 51, no. 20, pp. 5065–5088, Oct. 2006.
[52] S. Qin, C. F. Caskey, and K. W. Ferrara, “Ultrasound contrast microbubbles in imaging and therapy: physical principles and engineering,” *Phys. Med. Biol.*, vol. 54, no. 6, pp. R27–57, Mar. 2009.
[53] J. J. Choi, M. Pernot, T. R. Brown, S. A. Small, and E. E. Konofagou, “Spatio-temporal analysis of molecular delivery through the blood–brain barrier using focused ultrasound,” *Phys. Med. Biol.*, vol. 52, no. 18, pp. 5509–5530, Sep. 2007.
[54] N. McDannold, N. Vykhodtseva, S. Raymond, F. A. Jolesz, and K. Hynynen, “MRI-guided targeted blood-brain barrier disruption with focused ultrasound: histological findings in rabbits,” *Ultrasound Med. Biol.*, vol. 31, no. 11, pp. 1527–1537, Nov. 2005.
[55] F. Vlachos, Y.-S. Tung, and E. E. Konofagou, “Permeability assessment of the focused ultrasound-induced blood-brain barrier opening using dynamic contrast-enhanced MRI,” *Phys. Med. Biol.*, vol. 55, no. 18, pp. 5451–5466, Sep. 2010.
[56] F. Marquet, Y.-S. Tung, T. Teichert, V. P. Ferrera, and E. E. Konofagou, “Noninvasive, transient and selective blood-brain barrier opening in non-human primates in vivo,” *PloS One*, vol. 6, no. 7, p. e22598, 2011.
[57] B. Marty, B. Larrat, M. Van Landeghem, C. Robic, P. Robert, M. Port, D. Le Bihan, M. Pernot, M. Tanter, F. Lethimonnier, and S. Mériaux, “Dynamic study of blood-brain barrier

closure after its disruption using ultrasound: a quantitative analysis," *J. Cereb. Blood Flow Metab. Off. J. Int. Soc. Cereb. Blood Flow Metab.*, vol. 32, no. 10, pp. 1948–1958, Oct. 2012.
[58] J. Park, Y. Zhang, N. Vykhodtseva, F. A. Jolesz, and N. J. McDannold, "The kinetics of blood brain barrier permeability and targeted doxorubicin delivery into brain induced by focused ultrasound," *J. Control. Release Off. J. Control. Release Soc.*, vol. 162, no. 1, pp. 134–142, Aug. 2012.
[59] F.-Y. Yang, H.-E. Wang, G.-L. Lin, M.-C. Teng, H.-H. Lin, T.-T. Wong, and R.-S. Liu, "Micro-SPECT/CT-based pharmacokinetic analysis of 99mTc-diethylenetriaminepentaacetic acid in rats with blood-brain barrier disruption induced by focused ultrasound," *J. Nucl. Med. Off. Publ. Soc. Nucl. Med.*, vol. 52, no. 3, pp. 478–484, Mar. 2011.
[60] E. E. Cho, J. Drazic, M. Ganguly, B. Stefanovic, and K. Hynynen, "Two-photon fluorescence microscopy study of cerebrovascular dynamics in ultrasound-induced blood-brain barrier opening," *J. Cereb. Blood Flow Metab. Off. J. Int. Soc. Cereb. Blood Flow Metab.*, vol. 31, no. 9, pp. 1852–1862, Sep. 2011.
[61] A. Burgess, C. A. Ayala-Grosso, M. Ganguly, J. F. Jordão, I. Aubert, and K. Hynynen, "Targeted Delivery of Neural Stem Cells to the Brain Using MRI-Guided Focused Ultrasound to Disrupt the Blood-Brain Barrier," *PLoS ONE*, vol. 6, no. 11, p. e27877, Nov. 2011.
[62] A. Alonso, E. Reinz, B. Leuchs, J. Kleinschmidt, M. Fatar, B. Geers, I. Lentacker, M. G. Hennerici, S. C. de Smedt, and S. Meairs, "Focal Delivery of AAV2/1-transgenes Into the Rat Brain by Localized Ultrasound-induced BBB Opening," *Mol. Ther. Nucleic Acids*, vol. 2, p. e73, 2013.
[63] K. Hynynen, N. McDannold, N. A. Sheikov, F. A. Jolesz, and N. Vykhodtseva, "Local and reversible blood-brain barrier disruption by noninvasive focused ultrasound at frequencies suitable for trans-skull sonications," *NeuroImage*, vol. 24, no. 1, pp. 12–20, Jan. 2005.
[64] M. Kinoshita, N. McDannold, F. A. Jolesz, and K. Hynynen, "Noninvasive localized delivery of Herceptin to the mouse brain by MRI-guided focused ultrasound-induced blood-brain barrier disruption," *Proc. Natl. Acad. Sci. U. S. A.*, vol. 103, no. 31, pp. 11719–11723, Aug. 2006.
[65] F. Wang, Y. Cheng, J. Mei, Y. Song, Y. Yang, Y. Liu, and Z. Wang, "Focused ultrasound microbubble destruction-mediated changes in blood-brain barrier permeability assessed by contrast-enhanced magnetic resonance imaging," *J. Ultrasound Med. Off. J. Am. Inst. Ultrasound Med.*, vol. 28, no. 11, pp. 1501–1509, Nov. 2009.
[66] N. Sheikov, N. McDannold, S. Sharma, and K. Hynynen, "Effect of focused ultrasound applied with an ultrasound contrast agent on the tight junctional integrity of the brain microvascular endothelium," *Ultrasound Med. Biol.*, vol. 34, no. 7, pp. 1093–1104, Jul. 2008.
[67] G. P. Howles, K. F. Bing, Y. Qi, S. J. Rosenzweig, K. R. Nightingale, and G. A. Johnson, "Contrast-enhanced in vivo magnetic resonance microscopy of the mouse brain enabled by noninvasive opening of the blood-brain barrier with ultrasound," *Magn. Reson. Med. Off. J. Soc. Magn. Reson. Med. Soc. Magn. Reson. Med.*, vol. 64, no. 4, pp. 995–1004, Oct. 2010.
[68] F. Xie, M. D. Boska, J. Lof, M. G. Uberti, J. M. Tsutsui, and T. R. Porter, "Effects of Transcranial Ultrasound and Intravenous Microbubbles on Blood Brain Barrier Permeability in a Large Animal Model," *Ultrasound Med. Biol.*, vol. 34, no. 12, pp. 2028–2034, Dec. 2008.
[69] N. Sheikov, N. McDannold, N. Vykhodtseva, F. Jolesz, and K. Hynynen, "Cellular mechanisms of the blood-brain barrier opening induced by ultrasound in presence of microbubbles," *Ultrasound Med. Biol.*, vol. 30, no. 7, pp. 979–989, Jul. 2004.
[70] N. Sheikov, N. Mcdannold, F. Jolesz, Y. Zhang, K. Tam, and K. Hynynen, "Brain arterioles show more active vesicular transport of blood-borne tracer molecules than capillaries and venules after focused ultrasound-evoked opening of the blood-brain barrier," *Ultrasound Med. Biol.*, vol. 32, no. 9, pp. 1399–1409, Sep. 2006.
[71] B. D. M. Meijering, L. J. M. Juffermans, A. van Wamel, R. H. Henning, I. S. Zuhorn, M. Emmer, A. M. G. Versteilen, W. J. Paulus, W. H. van Gilst, K. Kooiman, N. de Jong, R. J. P. Musters, L. E. Deelman, and O. Kamp, "Ultrasound and microbubble-targeted delivery of macromolecules is regulated by induction of endocytosis and pore formation," *Circ. Res.*, vol. 104, no. 5, pp. 679–687, Mar. 2009.

[72] M. A. O'Reilly and K. Hynynen, "Ultrasound enhanced drug delivery to the brain and central nervous system," *Int. J. Hyperth. Off. J. Eur. Soc. Hyperthermic Oncol. North Am. Hyperth. Group*, vol. 28, no. 4, pp. 386–396, 2012.
[73] A. Alonso, E. Reinz, J. W. Jenne, M. Fatar, H. Schmidt-Glenewinkel, M. G. Hennerici, and S. Meairs, "Reorganization of gap junctions after focused ultrasound blood-brain barrier opening in the rat brain," *J. Cereb. Blood Flow Metab. Off. J. Int. Soc. Cereb. Blood Flow Metab.*, vol. 30, no. 7, pp. 1394–1402, Jul. 2010.
[74] L. H. Treat, N. McDannold, N. Vykhodtseva, Y. Zhang, K. Tam, and K. Hynynen, "Targeted delivery of doxorubicin to the rat brain at therapeutic levels using MRI-guided focused ultrasound," *Int. J. Cancer J. Int. Cancer*, vol. 121, no. 4, pp. 901–907, Aug. 2007.
[75] H.-L. Liu, M.-Y. Hua, P.-Y. Chen, P.-C. Chu, C.-H. Pan, H.-W. Yang, C.-Y. Huang, J.-J. Wang, T.-C. Yen, and K.-C. Wei, "Blood-Brain Barrier Disruption with Focused Ultrasound Enhances Delivery of Chemotherapeutic Drugs for Glioblastoma Treatment1," *Radiology*, vol. 255, no. 2, pp. 415–425, May 2010.
[76] P.-H. Hsu, K.-C. Wei, C.-Y. Huang, C.-J. Wen, T.-C. Yen, C.-L. Liu, Y.-T. Lin, J.-C. Chen, C.-R. Shen, and H.-L. Liu, "Noninvasive and targeted gene delivery into the brain using microbubble-facilitated focused ultrasound," *PloS One*, vol. 8, no. 2, p. e57682, 2013.
[77] M. Aryal, N. Vykhodtseva, Y.-Z. Zhang, J. Park, and N. McDannold, "Multiple treatments with liposomal doxorubicin and ultrasound-induced disruption of blood-tumor and blood-brain barriers improve outcomes in a rat glioma model," *J. Control. Release Off. J. Control. Release Soc.*, vol. 169, no. 1–2, pp. 103–111, Jul. 2013.
[78] H.-Q. Zeng, L. Lü, F. Wang, Y. Luo, and S.-F. Lou, "Focused ultrasound-induced blood-brain barrier disruption enhances the delivery of cytarabine to the rat brain," *J. Chemother. Florence Italy*, vol. 24, no. 6, pp. 358–363, Dec. 2012.
[79] E.-J. Park, Y.-Z. Zhang, N. Vykhodtseva, and N. McDannold, "Ultrasound-mediated blood-brain/blood-tumor barrier disruption improves outcomes with trastuzumab in a breast cancer brain metastasis model," *J. Control. Release Off. J. Control. Release Soc.*, vol. 163, no. 3, pp. 277–284, Nov. 2012.
[80] M. Kinoshita, N. McDannold, F. A. Jolesz, and K. Hynynen, "Targeted delivery of antibodies through the blood-brain barrier by MRI-guided focused ultrasound," *Biochem. Biophys. Res. Commun.*, vol. 340, no. 4, pp. 1085–1090, Feb. 2006.
[81] S. B. Raymond, L. H. Treat, J. D. Dewey, N. J. McDannold, K. Hynynen, and B. J. Bacskai, "Ultrasound Enhanced Delivery of Molecular Imaging and Therapeutic Agents in Alzheimer's Disease Mouse Models," *PLoS ONE*, vol. 3, no. 5, p. e2175, May 2008.
[82] J. F. Jordão, E. Thévenot, K. Markham-Coultes, T. Scarcelli, Y.-Q. Weng, K. Xhima, M. O'Reilly, Y. Huang, J. McLaurin, K. Hynynen, and I. Aubert, "Amyloid-β plaque reduction, endogenous antibody delivery and glial activation by brain-targeted, transcranial focused ultrasound," *Exp. Neurol.*, vol. 248, pp. 16–29, Oct. 2013.
[83] H.-L. Liu, P.-Y. Chen, H.-W. Yang, J.-S. Wu, I.-C. Tseng, Y.-J. Ma, C.-Y. Huang, H.-C. Tsai, S.-M. Chen, Y.-J. Lu, C.-Y. Huang, M.-Y. Hua, Y.-H. Ma, T.-C. Yen, and K.-C. Wei, "In vivo MR quantification of superparamagnetic iron oxide nanoparticle leakage during low-frequency-ultrasound-induced blood-brain barrier opening in swine," *J. Magn. Reson. Imaging JMRI*, vol. 34, no. 6, pp. 1313–1324, Dec. 2011.
[84] A. B. Etame, R. J. Diaz, M. A. O'Reilly, C. A. Smith, T. G. Mainprize, K. Hynynen, and J. T. Rutka, "Enhanced delivery of gold nanoparticles with therapeutic potential into the brain using MRI-guided focused ultrasound," *Nanomedicine Nanotechnol. Biol. Med.*, vol. 8, no. 7, pp. 1133–1142, Oct. 2012.
[85] B. Baseri, J. J. Choi, T. Deffieux, G. Samiotaki, Y.-S. Tung, O. Olumolade, S. A. Small, B. Morrison, and E. E. Konofagou, "Activation of signaling pathways following localized delivery of systemically administered neurotrophic factors across the blood-brain barrier using focused ultrasound and microbubbles," *Phys. Med. Biol.*, vol. 57, no. 7, pp. N65–81, Apr. 2012.
[86] F. Wang, Y. Shi, L. Lu, L. Liu, Y. Cai, H. Zheng, X. Liu, F. Yan, C. Zou, C. Sun, J. Shi, S. Lu, and Y. Chen, "Targeted delivery of GDNF through the blood-brain barrier by MRI-guided focused ultrasound," *PloS One*, vol. 7, no. 12, p. e52925, 2012.

[87] R. Alkins, A. Burgess, M. Ganguly, G. Francia, R. Kerbel, W. S. Wels, and K. Hynynen, “Focused ultrasound delivers targeted immune cells to metastatic brain tumors,” *Cancer Res.*, vol. 73, no. 6, pp. 1892–1899, Mar. 2013.
[88] A. Burgess, S. Dubey, S. Yeung, O. Hough, N. Eterman, I. Aubert, and K. Hynynen, “Alzheimer Disease in a Mouse Model: MR Imaging-guided Focused Ultrasound Targeted to the Hippocampus Opens the Blood-Brain Barrier and Improves Pathologic Abnormalities and Behavior,” *Radiology*, p. 140245, Sep. 2014.
[89] A. Alonso, E. Reinz, M. Fatar, M. G. Hennerici, and S. Meairs, “Clearance of albumin following ultrasound-induced blood-brain barrier opening is mediated by glial but not neuronal cells,” *Brain Res.*, vol. 1411, pp. 9–16, Sep. 2011.
[90] J. J. Choi, S. Wang, Y.-S. Tung, B. Morrison, and E. E. Konofagou, “Molecules of various pharmacologically-relevant sizes can cross the ultrasound-induced blood-brain barrier opening in vivo,” *Ultrasound Med. Biol.*, vol. 36, no. 1, pp. 58–67, Jan. 2010.
[91] K. Hynynen, N. McDannold, N. Vykhodtseva, S. Raymond, R. Weissleder, F. A. Jolesz, and N. Sheikov, “Focal disruption of the blood-brain barrier due to 260-kHz ultrasound bursts: a method for molecular imaging and targeted drug delivery,” *J. Neurosurg.*, vol. 105, no. 3, pp. 445–454, Sep. 2006.
[92] J. J. Choi, S. Wang, T. R. Brown, S. A. Small, K. E. K. Duff, and E. E. Konofagou, “Noninvasive and transient blood-brain barrier opening in the hippocampus of Alzheimer’s double transgenic mice using focused ultrasound,” *Ultrason. Imaging*, vol. 30, no. 3, pp. 189–200, Jul. 2008.
[93] N. McDannold, N. Vykhodtseva, and K. Hynynen, “Effects of acoustic parameters and ultrasound contrast agent dose on focused-ultrasound induced blood-brain barrier disruption,” *Ultrasound Med. Biol.*, vol. 34, no. 6, pp. 930–937, Jun. 2008.
[94] J. J. Choi, J. A. Feshitan, B. Baseri, S. Wang, Y.-S. Tung, M. A. Borden, and E. E. Konofagou, “Microbubble-size dependence of focused ultrasound-induced blood-brain barrier opening in mice in vivo,” *IEEE Trans. Biomed. Eng.*, vol. 57, no. 1, pp. 145–154, Jan. 2010.
[95] W. L. Nyborg, “Biological effects of ultrasound: development of safety guidelines. Part II: general review,” *Ultrasound Med. Biol.*, vol. 27, no. 3, pp. 301–333, Mar. 2001.
[96] O. P. Hamill, “Twenty odd years of stretch-sensitive channels,” *Pflüg. Arch. Eur. J. Physiol.*, vol. 453, no. 3, pp. 333–351, Dec. 2006.
[97] R. T. Mihran, F. S. Barnes, and H. Wachtel, “Transient modification of nerve excitability in vitro by single ultrasound pulses,” *Biomed. Sci. Instrum.*, vol. 26, pp. 235–246, 1990.
[98] P. Prentice, A. Cuschieri, K. Dholakia, M. Prausnitz, and P. Campbell, “Membrane disruption by optically controlled microbubble cavitation,” *Nat. Phys.*, vol. 1, no. 2, pp. 107–110, Oct. 2005.
[99] T. Kodama and Y. Tomita, “Cavitation bubble behavior and bubble-shock wave interaction near a gelatin surface as a study of in vivo bubble dynamics,” *Appl. Phys. B Lasers Opt.*, vol. 70, no. 1, pp. 139–149, Jan. 2000.
[100] N. McDannold, N. Vykhodtseva, and K. Hynynen, “Targeted disruption of the blood–brain barrier with focused ultrasound: association with cavitation activity,” *Phys. Med. Biol.*, vol. 51, no. 4, pp. 793–807, Feb. 2006.
[101] C. F. Caskey, S. M. Stieger, S. Qin, P. A. Dayton, and K. W. Ferrara, “Direct observations of ultrasound microbubble contrast agent interaction with the microvessel wall,” *J. Acoust. Soc. Am.*, vol. 122, no. 2, pp. 1191–1200, Aug. 2007.
[102] S. Qin and K. W. Ferrara, “The natural frequency of nonlinear oscillation of ultrasound contrast agents in microvessels,” *Ultrasound Med. Biol.*, vol. 33, no. 7, pp. 1140–1148, Jul. 2007.
[103] E. Sassaroli and K. Hynynen, “Resonance frequency of microbubbles in small blood vessels: a numerical study,” *Phys. Med. Biol.*, vol. 50, no. 22, pp. 5293–5305, Nov. 2005.
[104] J. E. Chomas, P. Dayton, D. May, and K. Ferrara, “Threshold of fragmentation for ultrasonic contrast agents,” *J. Biomed. Opt.*, vol. 6, no. 2, pp. 141–150, Apr. 2001.
[105] K. Hynynen, N. McDannold, H. Martin, F. A. Jolesz, and N. Vykhodtseva, “The threshold for brain damage in rabbits induced by bursts of ultrasound in the presence of an ultrasound contrast agent (Optison),” *Ultrasound Med. Biol.*, vol. 29, no. 3, pp. 473–481, Mar. 2003.

[106] J. A. Feshitan, C. C. Chen, J. J. Kwan, and M. A. Borden, “Microbubble size isolation by differential centrifugation,” *J. Colloid Interface Sci.*, vol. 329, no. 2, pp. 316–324, Jan. 2009.
[107] F. Vlachos, Y.-S. Tung, and E. Konofagou, “Permeability dependence study of the focused ultrasound-induced blood-brain barrier opening at distinct pressures and microbubble diameters using DCE-MRI,” *Magn. Reson. Med. Off. J. Soc. Magn. Reson. Med. Soc. Magn. Reson. Med.*, vol. 66, no. 3, pp. 821–830, Sep. 2011.
[108] S. Samuel, M. A. Cooper, J. L. Bull, J. B. Fowlkes, and D. L. Miller, “An ex vivo study of the correlation between acoustic emission and microvascular damage,” *Ultrasound Med. Biol.*, vol. 35, no. 9, pp. 1574–1586, Sep. 2009.
[109] S. Chen, R. V. Shohet, R. Bekeredjian, P. Frenkel, and P. A. Grayburn, “Optimization of ultrasound parameters for cardiac gene delivery of adenoviral or plasmid deoxyribonucleic acid by ultrasound-targeted microbubble destruction,” *J. Am. Coll. Cardiol.*, vol. 42, no. 2, pp. 301–308, Jul. 2003.
[110] E. Sassaroli and K. Hynynen, “Cavitation threshold of microbubbles in gel tunnels by focused ultrasound,” *Ultrasound Med. Biol.*, vol. 33, no. 10, pp. 1651–1660, Oct. 2007.
[111] B. Baseri, J. J. Choi, Y.-S. Tung, and E. E. Konofagou, “Multi-modality safety assessment of blood-brain barrier opening using focused ultrasound and definity microbubbles: a short-term study,” *Ultrasound Med. Biol.*, vol. 36, no. 9, pp. 1445–1459, Sep. 2010.
[112] J. J. Choi, K. Selert, Z. Gao, G. Samiotaki, B. Baseri, and E. E. Konofagou, “Noninvasive and localized blood-brain barrier disruption using focused ultrasound can be achieved at short pulse lengths and low pulse repetition frequencies,” *J. Cereb. Blood Flow Metab. Off. J. Int. Soc. Cereb. Blood Flow Metab.*, Sep. 2010.
[113] N. McDannold, N. Vykhodtseva, and K. Hynynen, “Blood-brain barrier disruption induced by focused ultrasound and circulating preformed microbubbles appears to be characterized by the mechanical index,” *Ultrasound Med. Biol.*, vol. 34, no. 5, pp. 834–840, May 2008.
[114] K. F. Bing, G. P. Howles, Y. Qi, M. L. Palmeri, and K. R. Nightingale, “Blood-brain barrier (BBB) disruption using a diagnostic ultrasound scanner and Definity in Mice,” *Ultrasound Med. Biol.*, vol. 35, no. 8, pp. 1298–1308, Aug. 2009.
[115] J. J. Choi, K. Selert, Z. Gao, G. Samiotaki, B. Baseri, and E. E. Konofagou, “Noninvasive and localized blood-brain barrier disruption using focused ultrasound can be achieved at short pulse lengths and low pulse repetition frequencies,” *J. Cereb. Blood Flow Metab. Off. J. Int. Soc. Cereb. Blood Flow Metab.*, vol. 31, no. 2, pp. 725–737, Feb. 2011.
[116] J. J. Choi, K. Selert, F. Vlachos, A. Wong, and E. E. Konofagou, “Noninvasive and localized neuronal delivery using short ultrasonic pulses and microbubbles,” *Proc. Natl. Acad. Sci. U. S. A.*, vol. 108, no. 40, pp. 16539–16544, Oct. 2011.
[117] R. Chopra, N. Vykhodtseva, and K. Hynynen, “Influence of exposure time and pressure amplitude on blood-brain-barrier opening using transcranial ultrasound exposures,” *ACS Chem. Neurosci.*, vol. 1, no. 5, pp. 391–398, May 2010.
[118] Y.-S. Tung, F. Vlachos, J. A. Feshitan, M. A. Borden, and E. E. Konofagou, “The mechanism of interaction between focused ultrasound and microbubbles in blood-brain barrier opening in mice,” *J. Acoust. Soc. Am.*, vol. 130, no. 5, pp. 3059–3067, Nov. 2011.
[119] M. A. O’Reilly, A. C. Waspe, M. Ganguly, and K. Hynynen, “Focused-ultrasound disruption of the blood-brain barrier using closely-timed short pulses: influence of sonication parameters and injection rate,” *Ultrasound Med. Biol.*, vol. 37, no. 4, pp. 587–594, Apr. 2011.
[120] D. E. Goertz, N. de Jong, and A. F. W. van der Steen, “Attenuation and size distribution measurements of Definity and manipulated Definity populations,” *Ultrasound Med. Biol.*, vol. 33, no. 9, pp. 1376–1388, Sep. 2007.
[121] S. Stapleton, H. Goodman, Y.-Q. Zhou, E. Cherin, R. M. Henkelman, P. N. Burns, and F. S. Foster, “Acoustic and kinetic behaviour of definity in mice exposed to high frequency ultrasound,” *Ultrasound Med. Biol.*, vol. 35, no. 2, pp. 296–307, Feb. 2009.
[122] J. J. Choi, M. Pernot, T. R. Brown, S. A. Small, and E. E. Konofagou, “Spatio-temporal analysis of molecular delivery through the blood-brain barrier using focused ultrasound,” *Phys. Med. Biol.*, vol. 52, no. 18, pp. 5509–5530, Sep. 2007.
[123] L. L. Rubin and J. M. Staddon, “THE CELL BIOLOGY OF THE BLOOD-BRAIN BARRIER,” *Annu. Rev. Neurosci.*, vol. 22, no. 1, pp. 11–28, Mar. 1999.

[124] K. Hynynen, N. McDannold, N. Vykhodtseva, and F. A. Jolesz, “Noninvasive MR imaging-guided focal opening of the blood-brain barrier in rabbits,” *Radiology*, vol. 220, no. 3, pp. 640–646, Sep. 2001.
[125] J. J. Choi, M. Pernot, S. A. Small, and E. E. Konofagou, “Noninvasive, transcranial and localized opening of the blood-brain barrier using focused ultrasound in mice,” *Ultrasound Med. Biol.*, vol. 33, no. 1, pp. 95–104, Jan. 2007.
[126] M. Kinoshita, N. McDannold, F. A. Jolesz, and K. Hynynen, “Noninvasive localized delivery of Herceptin to the mouse brain by MRI-guided focused ultrasound-induced blood-brain barrier disruption,” *Proc. Natl. Acad. Sci. U. S. A.*, vol. 103, no. 31, pp. 11719–11723, Aug. 2006.
[127] W. Dauer and S. Przedborski, “Parkinson’s disease: mechanisms and models,” *Neuron*, vol. 39, no. 6, pp. 889–909, Sep. 2003.
[128] P. Hadaczek, L. Johnston, J. Forsayeth, and K. S. Bankiewicz, “Pharmacokinetics and bioactivity of glial cell line-derived factor (GDNF) and neurturin (NTN) infused into the rat brain,” *Neuropharmacology*, vol. 58, no. 7, pp. 1114–1121, Jun. 2010.
[129] D. M. Gash, Z. Zhang, A. Ovadia, W. A. Cass, A. Yi, L. Simmerman, D. Russell, D. Martin, P. A. Lapchak, F. Collins, B. J. Hoffer, and G. A. Gerhardt, “Functional recovery in parkinsonian monkeys treated with GDNF,” *Nature*, vol. 380, no. 6571, pp. 252–255, Mar. 1996.
[130] J. H. Kordower, M. E. Emborg, J. Bloch, S. Y. Ma, Y. Chu, L. Leventhal, J. McBride, E. Y. Chen, S. Palfi, B. Z. Roitberg, W. D. Brown, J. E. Holden, R. Pyzalski, M. D. Taylor, P. Carvey, Z. Ling, D. Trono, P. Hantraye, N. Déglon, and P. Aebischer, “Neurodegeneration prevented by lentiviral vector delivery of GDNF in primate models of Parkinson’s disease,” *Science*, vol. 290, no. 5492, pp. 767–773, Oct. 2000.
[131] D. M. Gash, Z. Zhang, Y. Ai, R. Grondin, R. Coffey, and G. A. Gerhardt, “Trophic factor distribution predicts functional recovery in parkinsonian monkeys,” *Ann. Neurol.*, vol. 58, no. 2, pp. 224–233, Aug. 2005.
[132] R. Grondin, Z. Zhang, A. Yi, W. A. Cass, N. Maswood, A. H. Andersen, D. D. Elsberry, M. C. Klein, G. A. Gerhardt, and D. M. Gash, “Chronic, controlled GDNF infusion promotes structural and functional recovery in advanced parkinsonian monkeys,” *Brain J. Neurol.*, vol. 125, no. Pt 10, pp. 2191–2201, Oct. 2002.
[133] S. S. Gill, N. K. Patel, G. R. Hotton, K. O’Sullivan, R. McCarter, M. Bunnage, D. J. Brooks, C. N. Svendsen, and P. Heywood, “Direct brain infusion of glial cell line-derived neurotrophic factor in Parkinson disease,” *Nat. Med.*, vol. 9, no. 5, pp. 589–595, May 2003.
[134] N. K. Patel, M. Bunnage, P. Plaha, C. N. Svendsen, P. Heywood, and S. S. Gill, “Intraputamenal infusion of glial cell line-derived neurotrophic factor in PD: a two-year outcome study,” *Ann. Neurol.*, vol. 57, no. 2, pp. 298–302, Feb. 2005.
[135] J. T. Slevin, G. A. Gerhardt, C. D. Smith, D. M. Gash, R. Kryscio, and B. Young, “Improvement of bilateral motor functions in patients with Parkinson disease through the unilateral intraputaminal infusion of glial cell line-derived neurotrophic factor,” *J. Neurosurg.*, vol. 102, no. 2, pp. 216–222, Feb. 2005.
[136] J. G. Nutt, K. J. Burchiel, C. L. Comella, J. Jankovic, A. E. Lang, E. R. Laws Jr, A. M. Lozano, R. D. Penn, R. K. Simpson Jr, M. Stacy, G. F. Wooten, and ICV GDNF Study Group. Implanted intracerebroventricular. Glial cell line-derived neurotrophic factor, “Randomized, double-blind trial of glial cell line-derived neurotrophic factor (GDNF) in PD,” *Neurology*, vol. 60, no. 1, pp. 69–73, Jan. 2003.
[137] A. E. Lang, S. Gill, N. K. Patel, A. Lozano, J. G. Nutt, R. Penn, D. J. Brooks, G. Hotton, E. Moro, P. Heywood, M. A. Brodsky, K. Burchiel, P. Kelly, A. Dalvi, B. Scott, M. Stacy, D. Turner, V. G. F. Wooten, W. J. Elias, E. R. Laws, V. Dhawan, A. J. Stoessl, J. Matcham, R. J. Coffey, and M. Traub, “Randomized controlled trial of intraputamenal glial cell line-derived neurotrophic factor infusion in Parkinson disease,” *Ann. Neurol.*, vol. 59, no. 3, pp. 459–466, Mar. 2006.
[138] J. H. Kordower, C. D. Herzog, B. Dass, R. A. E. Bakay, J. Stansell 3rd, M. Gasmi, and R. T. Bartus, “Delivery of neurturin by AAV2 (CERE-120)-mediated gene transfer provides

structural and functional neuroprotection and neurorestoration in MPTP-treated monkeys," *Ann. Neurol.*, vol. 60, no. 6, pp. 706–715, Dec. 2006.
[139] R. T. Bartus, C. D. Herzog, Y. Chu, A. Wilson, L. Brown, J. Siffert, E. M. Johnson Jr, C. W. Olanow, E. J. Mufson, and J. H. Kordower, "Bioactivity of AAV2-neurturin gene therapy (CERE-120): differences between Parkinson's disease and nonhuman primate brains," *Mov. Disord. Off. J. Mov. Disord. Soc.*, vol. 26, no. 1, pp. 27–36, Jan. 2011.
[140] R. T. Bartus, T. L. Baumann, J. Siffert, C. D. Herzog, R. Alterman, N. Boulis, D. A. Turner, M. Stacy, A. E. Lang, A. M. Lozano, and C. W. Olanow, "Safety/feasibility of targeting the substantia nigra with AAV2-neurturin in Parkinson patients," *Neurology*, vol. 80, no. 18, pp. 1698–1701, Apr. 2013.
[141] S. Sirsi and M. Borden, "Microbubble Compositions, Properties and Biomedical Applications," *Bubble Sci. Eng. Technol.*, vol. 1, no. 1–2, pp. 3–17, Nov. 2009.
[142] P. S. Tofts and A. G. Kermode, "Measurement of the blood-brain barrier permeability and leakage space using dynamic MR imaging. 1. Fundamental concepts," *Magn. Reson. Med. Off. J. Soc. Magn. Reson. Med. Soc. Magn. Reson. Med.*, vol. 17, no. 2, pp. 357–367, Feb. 1991.
[143] A. C. Ruifrok and D. A. Johnston, "Quantification of histochemical staining by color deconvolution," *Anal. Quant. Cytol. Histol. Int. Acad. Cytol. Am. Soc. Cytol.*, vol. 23, no. 4, pp. 291–299, Aug. 2001.
[144] N. Maswood, R. Grondin, Z. Zhang, J. A. Stanford, S. P. Surgener, D. M. Gash, and G. A. Gerhardt, "Effects of chronic intraputamenal infusion of glial cell line-derived neurotrophic factor (GDNF) in aged Rhesus monkeys," *Neurobiol. Aging*, vol. 23, no. 5, pp. 881–889, Oct. 2002.
[145] B. Marty, B. Larrat, M. Van Landeghem, C. Robic, P. Robert, M. Port, D. Le Bihan, M. Pernot, M. Tanter, F. Lethimonnier, and S. Mériaux, "Dynamic study of blood-brain barrier closure after its disruption using ultrasound: a quantitative analysis," *J. Cereb. Blood Flow Metab. Off. J. Int. Soc. Cereb. Blood Flow Metab.*, vol. 32, no. 10, pp. 1948–1958, Oct. 2012.
[146] J. W. Langston, P. Ballard, J. W. Tetrud, and I. Irwin, "Chronic Parkinsonism in humans due to a product of meperidine-analog synthesis," *Science*, vol. 219, no. 4587, pp. 979–980, Feb. 1983.
[147] J. Bové, C. Zhou, V. Jackson-Lewis, J. Taylor, Y. Chu, H. J. Rideout, D.-C. Wu, J. H. Kordower, L. Petrucelli, and S. Przedborski, "Proteasome inhibition and Parkinson's disease modeling," *Ann. Neurol.*, vol. 60, no. 2, pp. 260–264, Aug. 2006.
[148] N. A. Tatton and S. J. Kish, "In situ detection of apoptotic nuclei in the substantia nigra compacta of 1-methyl-4-phenyl-1,2,3,6-tetrahydropyridine-treated mice using terminal deoxynucleotidyl transferase labelling and acridine orange staining," *Neuroscience*, vol. 77, no. 4, pp. 1037–1048, Apr. 1997.
[149] V. Jackson-Lewis and S. Przedborski, "Protocol for the MPTP mouse model of Parkinson's disease," *Nat. Protoc.*, vol. 2, no. 1, pp. 141–151, 2007.
[150] A. J. Harding, G. M. Halliday, and K. Cullen, "Practical considerations for the use of the optical disector in estimating neuronal number," *J. Neurosci. Methods*, vol. 51, no. 1, pp. 83–89, Jan. 1994.
[151] M. J. West, L. Slomianka, and H. J. Gundersen, "Unbiased stereological estimation of the total number of neurons in thesubdivisions of the rat hippocampus using the optical fractionator," *Anat. Rec.*, vol. 231, no. 4, pp. 482–497, Dec. 1991.
[152] G. Samiotaki, C. Acosta, S. Wang, and E. E. Konofagou, "Enhanced delivery and bioactivity of the neurturin neurotrophic factor through focused ultrasound-mediated blood-brain barrier opening in vivo," *J. Cereb. Blood Flow Metab. Off. J. Int. Soc. Cereb. Blood Flow Metab.*, Jan. 2015.
[153] Y.-S. Tung, F. Marquet, T. Teichert, V. Ferrera, and E. E. Konofagou, "Feasibility of noninvasive cavitation-guided blood-brain barrier opening using focused ultrasound and microbubbles in nonhuman primates," *Appl. Phys. Lett.*, vol. 98, no. 16, p. 163704, Apr. 2011.
[154] S.-Y. Wu, Y.-S. Tung, F. Marquet, M. Downs, C. Sanchez, C. Chen, V. Ferrera, and E. Konofagou, "Transcranial cavitation detection in primates during blood-brain barrier opening--

a performance assessment study," *IEEE Trans. Ultrason. Ferroelectr. Freq. Control*, vol. 61, no. 6, pp. 966–978, Jun. 2014.
[155] E. K. Fram, R. J. Herfkens, G. A. Johnson, G. H. Glover, J. P. Karis, A. Shimakawa, T. G. Perkins, and N. J. Pelc, "Rapid calculation of T1 using variable flip angle gradient refocused imaging," *Magn. Reson. Imaging*, vol. 5, no. 3, pp. 201–208, 1987.
[156] Y.-S. Tung, F. Marquet, T. Teichert, V. Ferrera, and E. E. Konofagou, "Feasibility of noninvasive cavitation-guided blood-brain barrier opening using focused ultrasound and microbubbles in nonhuman primates," *Appl. Phys. Lett.*, vol. 98, no. 16, p. 163704, Apr. 2011.
[157] Y. Zur, S. Stokar, and P. Bendel, "An analysis of fast imaging sequences with steady-state transverse magnetization refocusing," *Magn. Reson. Med. Off. J. Soc. Magn. Reson. Med. Soc. Magn. Reson. Med.*, vol. 6, no. 2, pp. 175–193, Feb. 1988.
[158] T. J. Swift and R. E. Connick, "NMR-Relaxation Mechanisms of O17 in Aqueous Solutions of Paramagnetic Cations and the Lifetime of Water Molecules in the First Coordination Sphere," *J. Chem. Phys.*, vol. 37, no. 2, pp. 307–320, Jul. 1962.
[159] P. S. Tofts, G. Brix, D. L. Buckley, J. L. Evelhoch, E. Henderson, M. V. Knopp, H. B. Larsson, T. Y. Lee, N. A. Mayr, G. J. Parker, R. E. Port, J. Taylor, and R. M. Weisskoff, "Estimating kinetic parameters from dynamic contrast-enhanced T(1)-weighted MRI of a diffusable tracer: standardized quantities and symbols," *J. Magn. Reson. Imaging JMRI*, vol. 10, no. 3, pp. 223–232, Sep. 1999.
[160] G. J. M. Parker and D. L. Buckley, "Tracer Kinetic Modelling for T1-Weighted DCE-MRI," in *Dynamic Contrast-Enhanced Magnetic Resonance Imaging in Oncology*, A. J. Mbc. (Hons), , FRCP FRCR, D. L. Buckley, and G. J. M. Parker, Eds. Springer Berlin Heidelberg, 2005, pp. 81–92.
[161] B. Kolb and I. Q. Whishaw, *Fundamentals of Human Neuropsychology*. Macmillan, 2009.